Title
An Investigation of the Effects of Black Carbon on Precipitation in the Western United States

Author
Tseng, Hsien-Liang Rose

Publication Date
2016

Peer reviewed|Thesis/dissertation

UNIVERSITY OF CALIFORNIA

Los Angeles

An Investigation of the Effects of Black Carbon on Precipitation in the Western United States

A dissertation submitted in partial satisfaction

of the requirements for the degree Doctor of Philosophy

in Atmospheric and Oceanic Sciences

by

Hsien-Liang Rose Tseng

2016

ABSTRACT OF THE DISSERTATION

An Investigation of the Effects of Black Carbon on Precipitation in the Western United States

by

Hsien-Liang Rose Tseng

Doctor of Philosophy in Atmospheric and Oceanic Sciences

University of California, Los Angeles, 2016

Professor Kuo-Nan Liou, Chair

Black carbon (BC), the byproduct of incomplete combustion, is considered to be the second most important anthropogenic climate forcing agent after carbon dioxide. BC warms the atmosphere by absorbing solar radiation (direct effect), alters cloud and precipitation formation by acting as cloud condensation nuclei (indirect effect), and modifies cloud distribution via cloud burn-off (semi-direct effect).

Currently, there are large discrepancies in general circulation model estimates of the influence of BC on precipitation. Even less known is how BC changes precipitation on regional scales. In the drought-stricken western United States (WUS), where BC emissions are known to affect the hydrological cycle, an investigation on how BC influences precipitation is warranted.

In this study, we employ the Weather Research and Forecasting-Chemistry (WRF-Chem) model (version 3.6.0) with the newly chemistry- and microphysics-coupled Fu-Liou-Gu radiation scheme to study how black carbon affects precipitation by separating BC-related effects into direct and semi-direct, and indirect effects. In this three-part study, we use a recent wet year (2005) to investigate black carbon effects. We first examine BC effects during a heavy wintertime heavy precipitation event (7–11 January 2005), a heavy summertime precipitation week for comparison to the wintertime event (20–24 July 2005), and finally, examine these same effects for the months of January to June 2005 to investigate month-long trends.

We find that BC suppresses precipitation, predominantly through its direct and semi-direct effects. The direct and semi-direct effects warm the air aloft, and cool the lower levels of the

atmosphere (surface dimming) through the reduction of downward shortwave radiation flux at the surface. These changes in vertical temperature increase the stability of the atmosphere and reduce convective precipitation. Convective precipitation reduction accounts for approximately 60–75% of the total precipitation reduction. Additionally, cooling in the lower levels reduces evaporation from the surface, which reduces the moisture needed for non-convective precipitation. Subsequently, reduced moisture in the atmosphere suppresses non-convective precipitation by approximately 10–40%. The indirect effects also reduce precipitation, but to a much smaller extent of 5-20%.

Although we use an atypical BC emission dataset is used in this study, the resulting reduction of the different types of precipitation sheds light on the physical mechanisms of BC-cloud-radiation interactions by which the reductions follow. In particular, our results highlight the importance of the cumulus and surface layer parameterizations that house the triggering mechanism and surface moisture flux parameterizations in future studies.

In this research we find the NEI 2005 emissions did not significantly change precipitation. This is likely due to the aggressive emission regulations that exist for the United States. Emission regulations, however, do not exist or are enforced equally across the globe. In the developing countries that rely on inefficient cook stoves and heating systems, the populations suffer the most due to black carbon emission. Along with respiratory and cardiovascular impacts from black carbon, they may suffer from reduced water resources from suppressed precipitation, as well. In a larger sense, findings from this research serve as a platform for understanding the wider-reaching effects of black carbon on regional precipitation and drought. In particular, in areas where there are no black carbon emission regulations, this would highlight health and potentially significant environmental benefits that could be achieved from a black carbon cap and trade.

The dissertation of Hsien-Liang Rose Tseng is approved.

Robert G. Fovell

Qinbin Li

William W. Yeh

Kuo-Nan Liou, Committee Chair

University of California, Los Angeles

2016

DEDICATION

to my father and mother,

who trailblazed

and to the Littles,

who will

Table of contents

List of figures

List of tables

ACKNOWLEDGMENTS

Keep away from people who try to belittle your ambitions. Small people always do that, but ***the really great make you feel that you, too, can become great****. — Mark Twain*

To the Really Greats, I offer my heartfelt gratitude:

Professors Kuo-Nan Liou, Robert Fovell, Qinbin Li, and William Yeh for sharing their passion for research with me; Professor Qinbin Li for sharing his ardor for teaching and presentation; Dr. Yu Gu for her invaluable assistance with WRF and the FLG radiation code; Dr. Longtao Wu (JPL), and Dr. Rajesh Kumar (UCAR) for their helpful assistance with black carbon emissions setup and with WRF-Chem; Carl Evans and Kara Leung for building and maintaining the computing cluster that was the workhorse for this research, and for reviving my laptop on more than one occasion. I would like to acknowledge high-performance computing support from Yellowstone (ark:/85065/d7wd3xhc) provided by NCAR's Computational and Information Systems Laboratory, sponsored by the National Science Foundation.

My fellow graduate students in AOS for their thoughtful discussions and who colored my time at UCLA with the most brilliant palette. Their show of support for each and all within the Department is astounding.

Dr. Robert T. Swanson, Jr., Colonel, US Air Force (Ret.) for showing me the avenues and turning me to PhD studies; Dr. Rebecca E. Stone, Captain, US Navy (Ret.), for her steadfast encouragement throughout the years and for inspiring me to possibilities of all sorts; and my friends and village for their unwavering support throughout this endeavor and so much more.

Rose Tseng

Los Angeles, California

August 2016

Hsien-Liang Rose Tseng

EDUCATION

Naval Postgraduate School, Monterey, CA

M.S. Meteorology — March 2010

M.S. Physical Oceanography — March 2010

University of California, Los Angeles, CA

B.S. Atmospheric, Oceanic, and Environmental Sciences — June 2004

FELLOWSHIPS AND AWARDS

NSF Research Experience for Undergraduates Fellowship in Mathematics (UCLA) Summer 2002

SELECTED PRESENTATIONS

Tseng, H.R., M.A. Schwartz, B.G. Langenbrunner 2016: Black Carbon: Its Role in Hastening Climate Change. University of California Climate Impacts Pitch Competition. Xerox PARC, Silicon Valley, CA. (Talk, Finalist)

Tseng, H.R. 2016c: Black Carbon: Can It Contribute to the Western United States Drought? 9th Annual Los Angeles Basin Earth and Planetary Space Science Student Research Symposium. UCLA, Los Angeles, CA. (Talk, 1st Place)

Tseng, H.R. 2016b: Black Carbon Reduction: A Key to Combating Global Warming? Los Angeles Policy Symposium. Pardee RAND Graduate School, Santa Monica, CA. (Talk)

Tseng, H.R. 2016a: Is Black Carbon a Culprit of the Severe Drought in the Western United States? UCLA Graduate Students Competitive Research Showcase. Los Angeles, CA. (Talk, Finalist)

Tseng, H.R., K.N. Liou, Y. Gu, R.G. Fovell, Q. Li, W. Yeh, 2015a: Investigating the effects of black carbon on precipitation in the western United States: A January 2005 case study. American Geophysical Union Fall Meeting. San Francisco, CA. (Poster)

Tseng, H.R., K.N. Liou, R.G. Fovell, Q. Li, W. Yeh, 2015b: Investigating the effects of black carbon on precipitation in the western United States: A January 2005 case study. Department of Atmospheric and Oceanic Sciences. Dec. 2, UCLA, Los Angeles, CA. (Talk)

Tseng, H.R., K.N. Liou, Y. Gu, R.G. Fovell, L. Wu, 2014: Investigation of black carbon effects on precipitation over the western United States using the new chemistry-coupled FLG Radiation scheme in WRF-Chem. American Geophysical Union Fall Meeting. San Francisco, CA. (Poster)

DEPARTMENTAL SERVICE AND LEADERSHIP

Chi Epsilon Pi, AOS Graduate Student Association (Secretary) 2014–2016

PROFESSIONAL ACTIVITIES

NASA Earth Obs Course: Using Satellite Observations to Advance Climate Models Summer 2015
California Institute of Technology, Pasadena, CA

Chapter 1

Introduction

This chapter serves to provide the motivation for this research, and the background on black carbon and its precipitation effects. Additionally, it discusses the 3-dimensional radiative transfer parameterization of the Fu-Liou-Gu radiation scheme.

1.1 Motivation

The 2012-2014 Exceptional Drought, defined by the US Drought Monitor, over the western United States is the worst drought over a century, with 2014 being the single driest year of the last 1,200 years (Griffin and Anchukaitis, 2014). With an estimated 410,000 acres fallowed due to extremely dry conditions, some 63 trillion gallons of groundwater were drawn for agriculture, human use, and energy production from the beginning of 2013 to August 2014 (Lin, 2015). In 2014 alone, drawing groundwater in California cost an estimated $450 million and increased energy costs by $800 million. Additionally, California lost 14,500 seasonal and full-time jobs and household income of $555 million; agricultural losses accounted for an $855 million decline in the state gross domestic product (California Farm Water Coalition, 2014).

The severity of this drought has been attributed to both warmer than average temperatures and anomalously low precipitation (Griffin and Anchukaitis, 2014). Current research, largely based on global models, shows that aerosols can both increase and decrease precipitation, with much variability along the temporal and spatial scales as well as across aerosol type (Griffin and Anchukaitis, 2014). A drought that poses environmental and economic destruction on this scale warrants in-depth investigation to improve prediction of its course. Note that other contributors to drought include water governance, population growth, and hydrological drought (Lauer, 2011),

although these are not addressed in this research.

1.2 Black Carbon

Black carbon is a carbonaceous material that is the byproduct of incomplete combustion of carbon-based fuels such as biofuel (e.g. wood, dung, crop residue), biomass (e.g. forests, crop residue), and fossil fuel (e.g. diesel, coal) (Bond et al., 2013; Ramanathan and Carmichael, 2008). While the dominant global source of black carbon is open burning that occurs in Africa and Latin America, the largest source of black carbon in North America is from energy-related combustion (Bond et al., 2013). Once emitted, black carbon can undergo regional and intercontinental transport at a height of three to five kilometers (km) above the surface, and has an approximate atmospheric lifetime of seven days, depending on the method of removal from the atmosphere (Bond et al., 2013; Ramanathan and Carmichael, 2008). Removal methods are dry and wet deposition. Dry deposition is deposition by the turbulent diffusion (collision due to random air movement or turbulent eddies) of gases and particles, or the sedimentation (settling due to gravity) of large particles based atmospheric and surface resistances described in Wesely (1989) (Lagzi et al., 2013).

Wet deposition, the more complex of the two major aerosol deposition methods, includes in-cloud scavenging (aerosols serve as cloud condensation nuclei, with or without collision) and below-cloud scavenging (falling precipitation collides with aerosols through interception, impaction or turbulent diffusion) of particles (Lagzi et al., 2013). The parameterization of wet deposition varies much more widely than that of dry deposition due to varying microphysical processes, and the interaction between wet deposition parameterization and other model physics parameterizations.

Black carbon has four main physical properties (Bond et al., 2013). First, it is refractory: it keeps its basic form up to its vaporization temperature of 400K. Second, it is insoluble in water, organic solvents, and other aerosols. Third, black carbon aggregates as small carbon spherules that are largely of Aitken (less than 0.1 micron) and accumulation modes (up to 1 micron) (Bond et al., 2013). Black carbon, therefore, can serve as cloud condensation nuclei (nucleation sites) for cloud droplet formation; but its activation depends on its size, composition, mixing states, and supersaturation (hygroscopicity) with respect to water vapor within the cloud (Bond et al., 2013). While particles that are larger, more soluble, lower in critical supersaturation, and more well mixed

with organic aerosols and gases are more likely to activate as a nucleation site, any particle can activate in extremely supersaturated air (Bond et al., 2013).

The fourth physical property of black carbon is that it strongly absorbs visible light, as it has a mass absorption cross section of at least 5 m2g-1 (Bond et al., 2013). Compared with organic aerosols and dust, black carbon is the highest absorber of incident solar radiation, making black carbon arguably the most influential amongst the aerosol species as shown in an idealized plot in Figure 1.1. Although this measurement does vary widely depending on the location and combustion source of black carbon, black carbon's absorption (imaginary) refractive index is the highest amongst the aerosols species (up to 0.79i compared with that of secondary organic carbon by a factor of 1000) (Bond and Bergstrom, 2006; Liu et al., 2013; Kandler et al., 2007). The high absorptivity of solar radiation of black carbon can also be due to the lensing effect in which black carbon particles, being well mixed with organic and hydrophilic aerosols, refract light toward the already absorptive black carbon core (Flanner et al., 2007).

The four physical properties of black carbon have broad implications for aerosol radiation-cloud interactions. The first three properties are the source of indirect and semi-direct effects; the fourth property alters the Earth's radiation budget by way of the direct effect (Figure 1). Directly, black carbon absorbs and scatters sunlight within the atmospheric column, which may otherwise have reached the surface (dimming), heating the atmosphere where black carbon is lofted (Bond et al., 2013). Indirectly, black carbon can serve as cloud condensation nuclei and increase the number of cloud droplets and consequently the overall albedo of the cloud (Twomey et al., 1984). As a result, these smaller cloud droplets can increase cloud liquid water, fractional cloudiness, liquid water path, and cloud lifetime, causing a suppression of drizzle (Albrecht, 1989; Liou and Ou, 1989; Peralta et al., 2007). Semi-directly, the additional heating due to the absorption of black carbon is thought to accelerate evaporation and stabilize the boundary layer, reducing cloudiness (Ackerman et al., 2000).

Despite its importance to radiation and microphysical processes, black carbon's emission data is sparse (Bond et al., 2013; Jacobson, 2001). The sparseness of the observations is largely due to the lack of a continuous temporal and spatial monitoring, which are especially needed due to its short lifetime (Devara and Manoj, 2013). Thus far, emission data is limited to ground-

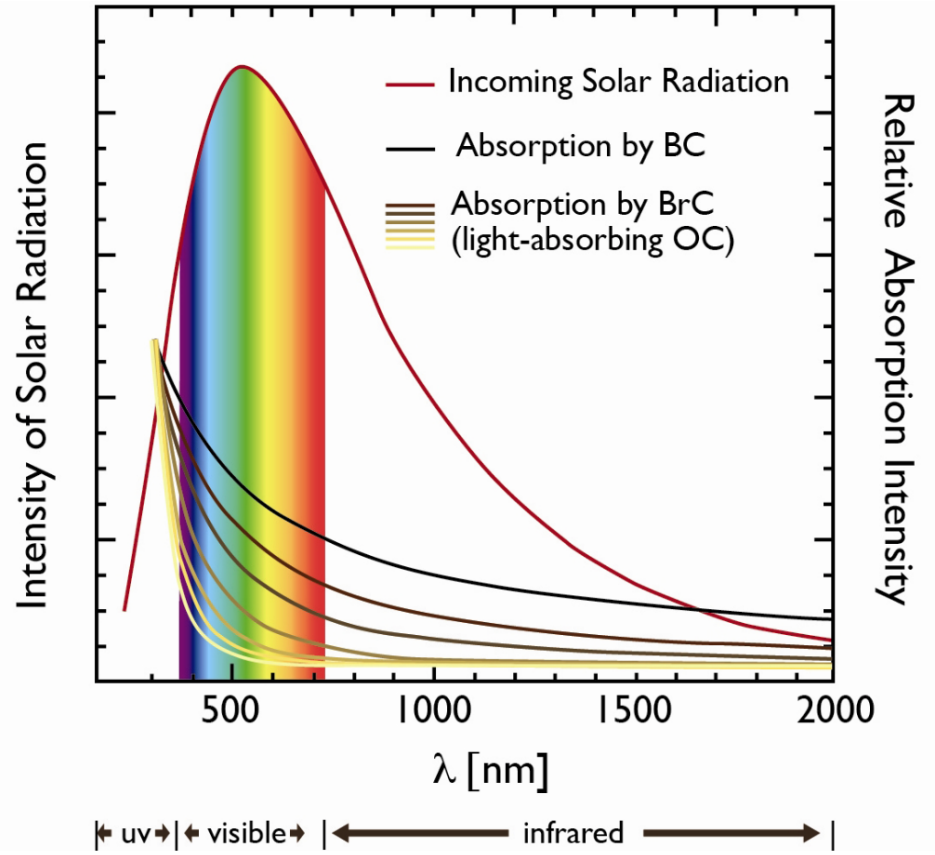

Figure 1.1: Light Absorption Comparison of Black Carbon, Brown Carbon, and Ambient Mixtures. Black carbon (black line) is the single most absorptive aerosol. When compared with the absorptivity of brown carbon and ambient mixtures (light-absorbing organic carbon, brown and yellow lines), it has the greatest relative absorption intensity, as shown in this idealization. Black carbon and brown carbon absorb higher in the shortwave wavelengths than in the longwave wavelengths. The incoming solar radiation (red) intensity, which begins at around 280 nm (UV-B), peaks in the mid-visible range, and drops off past 2800 nm (infrared) (Sasser, 2011).

based sensors such as the Aerosol Robotic Network, derived satellite information, and airborne observation instruments and campaigns.

1.3 Precipitation Effects Due to Black Carbon

Precipitation due to black carbon is complex as it can be influenced by a myriad of competing radiative and microphysical processes that generally decrease precipitation in place, but can influence circulation and precipitation across continents. Regional circulation and precipitation changes due to black carbon aerosol loadings; however, these effects remain uncertain (Bond et al., 2013; Shiogama et al., 2010). Research suggests both decreases in precipitation Shiogama et al. (2010); Ming et al. (2010); Andrews et al. (2010) and increases in precipitation due to black carbon (Roberts, 2004; Devara and Manoj, 2013). Other research has shown a spatial change in precipitation patterns (Pendergrass and Hartmann, 2012).

Shiogama et al. (2010) used the Model for Interdisciplinary Research On Climate Version 3.2 to show that precipitation due to black carbon is sensitive to the moisture to precipitation conversion. Precipitation decreased with black carbon concentration due to the high absorptivity of solar radiation of the black carbon and black carbon's dimming effect at the surface, leading to a reduction in evaporation. Similarly, Ming et al. (2010) used the Geophysical Fluid Dynamics Laboratory AM2.1 atmosphere general circulation model and demonstrated that atmospheric heating could outweigh surface warming to reduce precipitation by 0.4%. Andrews et al. (2010) used the Hadley Center Global Environmental Model Version1, and found that black carbon forcing decreases precipitation as part of a fast atmospheric response to radiative forcing, rather than a slow response to global surface temperature. Moreover, Tosca et al. (2010), through the Community Atmosphere Model Version 3.1, found a positive feedback cycle such that the El Nino-induced drought in Equatorial Asia increased deforestation fires. Fire-emitted aerosols increased heating aloft and cooled temperatures at the surface over land and water, suppressing convection and precipitation by 10%, which further intensified the drought.

Conversely, Roberts (2004) used an older version of the Hadley Center climate model (HadSM4) and found a small increase in black carbon forcing, which resulted in a global mean precipitation increase of 0.53% (0.015 mm/day). Here, he noted that the outgoing longwave ra-

diation from cloudiness reduction (semi-direct effect) at the black carbon level outweighed the increased shortwave radiation. Black carbon can also alter wind circulations that facilitate increased precipitation. Devara and Manoj (2013) showed that amplified heating caused by black carbon forcing over central India induces an atmospheric heating gradient that led to large-scale convergence of moisture flux and low-level uplift necessary for convection. Moreover, the moisture flux could enhance the moist static instability also needed for initiating convection. The results from Devara and Manoj (2013) are consistent with the findings of Ramanathan and Carmichael (2008), though, the latter cautions that the magnitude of this convection is highly uncertain.

Additionally, current research shows that large black carbon loadings can bring about extraordinarily large spatial changes to the precipitation pattern in areas where black carbon is not generated. For example, in response to black carbon forcing, Bond et al. (2013) described a northward shift of the Inter-Tropical Convergence Zone as the Hadley cell strengthens in the Northern Hemisphere and weakens in the Southern Hemisphere. Through the use of the Community Earth Systems Model Version 1, Tosca et al. (2010) found that enhanced tropospheric heating and reduced surface temperatures (the direct effect of black carbon forcing) generated an increase in equatorial subsidence and a weakened Hadley circulation, reducing precipitation over tropical forests in South America. Similarly, Wang et al. (2009) indicated a northward shift in rainfall during the Indian summer monsoon. Rotstayn et al. (2007) used the Commonwealth Scientific and Industrial Research Organisation Mark 3.6 General Circulation Model and found that the anthropogenic aerosols over Asia changed the meridional temperature and pressure gradients over the tropical Indian Ocean, increasing the tendency for monsoonal winds to flow toward Australia and associated rainfall and cloudiness to increase. In this same study, surface dimming produced surface temperature changes akin to that of La Niña.

Existing studies have largely been accomplished using general circulation and global models, with an emphasis on broad spatial precipitation impacts due to black carbon sources from Asia. The magnitude of precipitation change from this research, thus far, has been inconclusive. There is little doubt that it is difficult to predict the net effect of black carbon on global rainfall (Ramanathan and Carmichael, 2008). However, investigating precipitation at a regional scale with greater attention on a finer horizontal resolution using a 3-dimensional radiative transfer parameterization could alter

the black carbon-radiation-precipitation interaction to produce insight to precipitation changes.

1.4 3-Dimensional Radiative Transfer Parameterization

In current regional climate and global models, the conventional one-dimensional radiative transfer scheme assumes an unobstructed horizontal surface when computing solar fluxes (Lee et al., 2011). In order to incorporate detailed information about topography, Lee et al. (2011) used a set of simple regression equations to develop a radiation scheme that parameterizes solar flux differences between the presence of mountains and a flat horizontal surface. This 3-dimensional radiative transfer parameterization calculates 1) direct-reflected flux; 2) diffuse-reflected flux; and 3) coupled flux elevation, in addition to the 4) direct flux and 5) diffuse flux from the plane-parallel radiation scheme, using solar incident angle, sky view factor, terrain configuration, terrain elevation and skewness of terrain (Figure 2).

Gu et al. (2012) implemented this 3-dimensional radiative transfer parameterization into the Fu-Liou-Gu radiation scheme (FLG3D) in WRF and found overall decreases in surface temperature and solar fluxes in the Sierra Nevada. The Sierra Nevada received more solar insolation in the early morning and late afternoon, which enhanced surface temperatures, as well as upward sensible and latent heat fluxes from the surface (Gu et al., 2012).

Subsequently, Liou et al. (2013) found an 18% increase in snow water equivalent (SWE) at the lowest elevation at the surface and a decrease of 8% at the elevations above 3 km when investigating surface hydrology using this 3-dimensional radiation parameterization scheme. These findings aid in the understanding and modeling of terrain effects on surface hydrology; they are critically important as approximately 60-90% of water resources originate from mountain regions (Liou et al., 2013).

1.5 Organization of Dissertation

This research aims to investigate and ascertain the pathways by which black carbon affects precipitation, and to determine the relative significance of each of these pathways at a regional level from an online, coupled meteorology-chemistry approach. To accomplish this, we use the

Weather Research and Forecasting with Chemistry model (WRF-Chem) with a newly chemistry- and microphysics-coupled Fu-Liou-Gu (FLG) radiation scheme. In this three-part study, we first examine black carbon-specific effects on precipitation during a heavy wintertime precipitation event (7–11 January 2005), during a heavy summertime precipitation event (20–24 July 2005), and finally, during the months of January to June 2005.

Additionally, using WRF-Chem setup described above, we also employ in the 7–11 January 2005 case the 3-dimensional (3D) version of the Fu-Liou-Gu radiation scheme, which parameterizes radiative transfer 3-dimensionally (versus the conventional plane-parallel radiative transfer parameterization). We compare the precipitation change from this 3D radiative parameterization to the precipitation change from various black carbon emission datasets.

This dissertation is outlined as follows: Chapter 2 describes in detail the model, experiment setup, and model's physics parameterizations. Chapter 3 describes in detail the model code modifications made in order to obtain aerosol effect-specific precipitation. Chapter 4 presents and discusses the results from the 7–11 January 2005 case study. Chapter 5 presents and the discusses the results from the 7–11 January 2005 case study using a 3D FLG radiation parameterization. Chapter 6 presents the results from a summertime rain event from the 20–24 July 2005. Chapter 7 presents and discusses the results from the monthly long simulations of January to June 2005. Chapter 8 contains concluding remarks and presents future work.

Chapter 2

Experiment Setup

This chapter describes the model used in this research and the selected physics parameterizations. Additionally, it provides a physics-based characterization of the Fu-Liou-Gu radiation parameterization.

2.1 Model: Weather Research and Forecasting (WRF) Model and WRF-Chemistry

Weather Research and Forecasting model with the Advanced Research WRF (WRF-ARW) core (hereafter referred to as WRF) simulated with and without the online coupled meteorology-chemistry model (WRF-Chem and WRF) version 3.6.0 is employed for simulations (Skamarock et al., 2008; Grell et al., 2005). WRF is a 3-dimensional, fully compressible, non-hydrostatic terrain-following model. It has the capability to conduct research at the mesoscale. The meteorology boundary conditions are from the National Center for Environmental Prediction Final Operational Global Analysis data (National Centers for Environmental Prediction, National Weather Service, NOAA, U.S. Department of Commerce, 2000). The main area of interest is the western United States: the model domain is bounded by 31.34°N and 46.79°N, and 99°W and 124.46°W with a horizontal spatial resolution of 30 km by 30 km (Figure 2.1), a resolution that is both computationally efficient and effective at resolving precipitation for the goals of our investigation. Model timestep is 180 seconds, and output is every three hours. Detailed descriptions of the simulation year, black carbon emission inventory, aerosol scheme, and physics parameterizations in this Chapter's sections below.

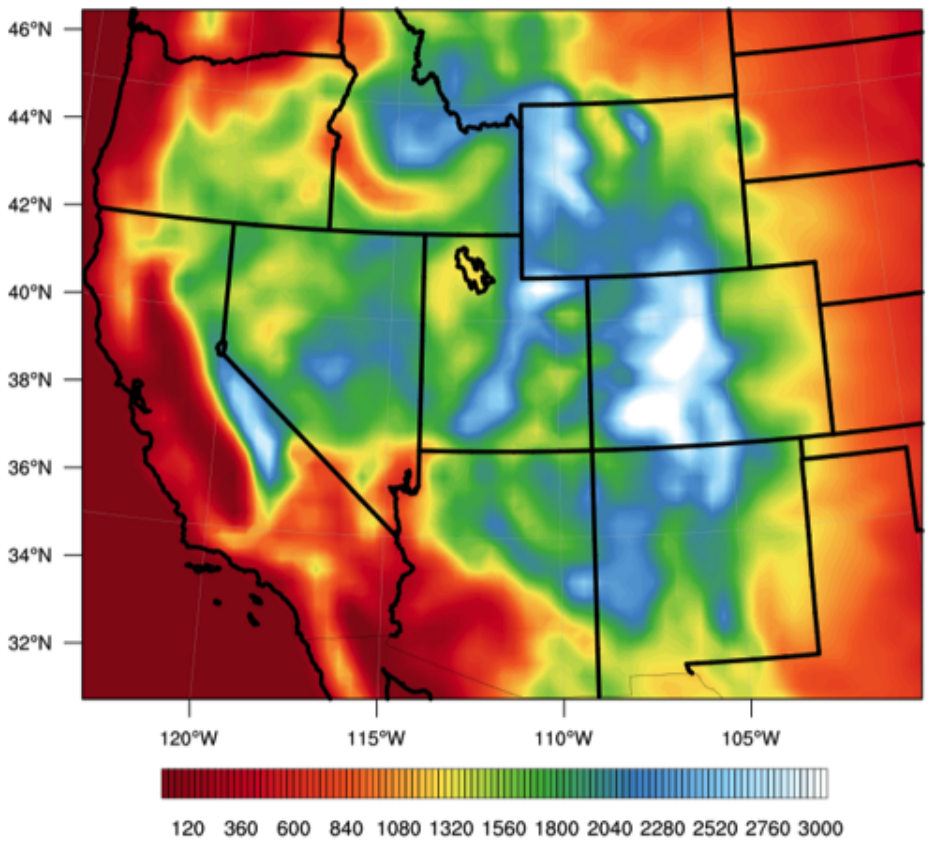

Figure 2.1: Experiment Domain: Western United States Domain. Shown here is the western United States domain at 30 km by 30 km horizontal resolution, as simulated in WRF-Chem. The western United States includes a variety of terrain features, with valleys such as the California Central Valley and mountains such as the Sierra Nevada and the Rocky Mountains. The height of mountains extends as high as 4420 m in the Rocky Mountains. (National Geodetic Survey, 1995).

2.2 Simulation Year: 2005

January to June 2005 exhibited an array of weather conditions suitable for our study. From 1 January through 30 June, there are 80 days of rain in the Sierra Nevada and the Rocky Mountains. Within these 80 days there are heavy rain events as well as relatively lighter rain events along with areas with dry periods. Specific time periods of interests are defined by specific rain events (5-days) and by the springtime precipitation period (months). The rain events are 7–11 January 2005 in which an atmospheric river brought heavy precipitation to California (CA) and 20–24 July 2005 in which a widespread summertime rain event occurred over the Sierra Nevada and Rocky Mountains. We will also investigate January to June 2005 as whole, discrete months to study trends that encompass wintertime and springtime rain.

2.3 Meteorology Boundary Conditions: National Centers for Environmental Prediction (NCEP) Final (FNL) Operational Global Analysis

The NCEP FNL Operational Global Analysis data is a 6-hourly 1-degree by 1-degree dataset produced from the Global Data Assimilation System that combines observational data and data from the Global Forecast System model. The Analyses is available at the surface, at 26 levels from 1000 mb to 10 mb, in the surface boundary layer, at some sigma layers, and at the tropopause. The Analyses has 56 meteorological parameters including air temperature, convection, surface and upper level winds, potential temperature, humidity, precipitable water, and pressure (National Centers for Environmental Prediction, National Weather Service, NOAA, U.S. Department of Commerce, 2000). This meteorological data is extracted and horizontally interpolated across the domain at the 30 km by 30 km horizontal resolution.

2.4 Black Carbon Emissions: National Emissions Inventory (NEI)

The National Emissions Inventory (NEI) supplies the black carbon loadings in our experiment. The NEI is a comprehensive inventory created by the Environmental Protection Agency (EPA) Emission Inventory and Analysis Group in Research Triangle Park, North Carolina. NEI includes all criteria air pollutants and hazardous air pollutants for all areas of the United States

(Eastern Research Group, Inc., 2008). South of 52°N, the inventory includes Canadian point, area and mobile source emissions, and north of 24°N, the inventory includes emission estimates from Mexico gathered from the Big Bend Regional Aerosol and Visibility Observational study (Kuhns and Vukovich, 2003).

NEI is representative of a typical summer day averaged over both weekday and weekend days, "as derived by temporal allocation factors specific to each source classification code provided by the EPA" (Peckham, 2012). It includes 41 volatile organic compounds, five PM2.5 aerosol species, and seven primary species, which are then divided into 24 average hourly emissions. All fire-related emissions from the United States, Canada, and Mexico have been removed. The data has a relatively high horizontal data resolution of 4 km. Point emissions have associated latitude and longitude and stack parameter information to allow for plume-rise calculations (Peckham, 2012).

To accomplish this research, we employ the National Emissions Inventory for the year 2005 to match our simulation year. The goal of this research is to understand trends of precipitation changes and how these changes occur by way of aerosol effects (e.g. direct, indirect, and semi-direct effects). As such, rather than employing the 2005 NEI inventory, we employ a black carbon emission dataset that uniformly emits black carbon at all grid points, horizontally and vertically. This removes any dependencies on the location of black carbon, and allows the meteorological dynamics and thermodynamics to advect the black carbon. Further justification for the usage of a uniform black carbon emission dataset is described in Section 6.6.

2.5 Aerosol Scheme: Modal Aerosol Dynamics for Europe (MADE)

The Modal Aerosol Dynamics for Europe (MADE) aerosol module is used to parameterize aerosol transport and deposition (Ackermann et al., 1998). Utilizing the chemistry module in addition to WRF increases computational expense 10 fold; however, current comparisons of computational efficiency between a modal treatment of aerosols and a sectional treatment of aerosols is not definitive and varies by test case (Zaveri et al., 2008). MADE is arguably the most complete aerosol module with a reasonable computational expense. MADE accounts for all aerosol size groups: Aitken, accumulation, and coarse modes; black carbon is represented in each of the

size groups. It produces both the direct and indirect effects (first) via radiation and microphysics schemes, in which the aerosol number determines the cloud drop number and size. (Note: The indirect effects are only true to resolved clouds.) MADE also contains aqueous chemistry, accounting for wet scavenging of aerosols, although currently this is only applicable to SO4 and NO3 aerosols (Kazil, 2014). Dry deposition is proportional to the sum of aerodynamic resistance, sublayer resistance, and surface resistance, where surface resistance is derived from the resistances of soil and plants according to WRF land use data and seasons as parameterized according to Wesely (1989) (Peckham, 2012).

The cloud droplet number source is determined by aerosol activation. The cloud droplet number and cloud water mixing ratio is used to compute the effective cloud water and cloud ice radii to be used to calculate optical depth, single scattering albedo, and expansion coefficients of the phase function (1, 2, 3, 4) resulting from the Mie scattering of water clouds (Fu, 1991; Fu et al., 2015). The droplet number mixing ratio tendency is defined by

$$\frac{\partial N_k}{\partial t} = -(V \bullet \nabla N)_k + D_k - C_k - E_k + S_k, \tag{2.1}$$

where N_k is the grid cell mean droplet number mixing ratio in layer k, V is velocity, D_k is vertical diffusion, C_k is droplet loss due to collision, coalescence and collection, E_k is droplet loss due to evaporation, and S_k is droplet source due to nucleation. Moreover, the droplet number mixing ratio is a function of supersaturation and hygroscopicity (Abdul-Razzak and Ghan, 2000).

The droplet source due to nucleation is proportional to the cloud fraction and the aerosol molar mixing ratio. The droplet source is not time integrated but parameterized (diagnostic) while the droplet number mixing ratio is prognostic as it is integrated with time.

Within the aerosol scheme, the hygroscopicity of black carbon is 10^{-5} to represent black carbon's hydrophobic nature, and the imaginary part of the refractive index of black carbon is set to 0.79i to represent its high absorptivity of solar radiation. The hygroscopic value is in line with Petters and Kreidenweis (2007) and the refractive index is consistent with Bond et al. (2013).

Simulations										
			Year 2005							
			7–11 Jan	20–24 Jul	Jan	Feb	Mar	Apr	May	Jun
WRF-Chem	D + S + I	BC 0	x	x	x	x	x	x	x	x
		BC Uni	x	x	x	x	x	x	x	x
		BC NEI		x						
		BC Uni Sfc		x						
		BC Uni Sfc-3km		x						
	D + S	BC Uni	x	x	x	x	x	x	x	x
	I	BC Uni	x	x	x	x	x	x	x	x
WRF	FLG	n/a	x							
	FLG 3D	n/a	x							

Table 2.1: Simulations. This table lists the simulations used in this research. WRF-Chem denotes the WRF model with the chemistry package. WRF-Chem is used to investigate the direct (D) and semi-direct (S), and indirect (I) effects of black carbon (BC). The D+S+I effects are simulated using the fully coupled chemistry (black carbon), Fu-Liou-Gu (FLG) radiation, and Morrison microphysics. Direct and semi-directs are simulated using the fully coupled model, subtract the indirect effects coupled model in Figure 3.2. Indirect effects are simulated using the fully coupled model subtract the direct + semi-direct effects coupled model in Figure 3.3. The emission dataset used in this research is primarily uniform black carbon emissions from the surface to 19km. Values for each grid point in the x, y, z directions are the highest black carbon concentration values of the National Emissions Inventory (NEI) 2005 (0.01μg/kg-dry air of Aitken mode black carbon and 0.04 μg/kg-dry air of accumulation mode black carbon). Other emission datasets used in the 20–24 July summertime case are NEI 2005 (variable, with highest concentrations in metropolitan areas such as Los Angeles and San Francisco), uniform black carbon values at the surface, and uniform black carbon values from the surface to 3 km. The time periods used are two wet 5-day events, one in January (cold) and one in July (warm) of 2005, as well January to June 2005. The January case is also used to employ FLG and 3-dimensional FLG (3D FLG) in a WRF environment (without the chemistry module) to compare the differences in precipitation from black carbon and from a 3D radiation parameterization (Lee et al., 2011; Gu et al., 2012; Liou et al., 2013).

2.6 Simulations

Time periods of interest are defined by wet periods (5 days) and by the seasonal precipitation period (months). The rain events are 7–11 January 2005, in which an atmospheric river brought heavy precipitation to California, and 20–24 July 2005, when a spatially summertime precipitation occurred over the Sierra Nevada and Rocky Mountains. We also investigate January to June 2005 as whole, discrete months, during which the western United States underwent various precipitation events. A summary of simulations is in Table 2.1.

2.7 Physics Parameterizations

Because this research relies on the coupling between the microphysics, radiation, and cumulus parameterizations, it is worthwhile to discuss in detail the specific schemes chosen for use in this investigation.

2.7.1 Radiation Parameterization: Fu-Liou-Gu (FLG)

The Fu-Liou-Gu (FLG) radiation scheme, created by the original architects of the correlated k-distribution method (Liou et al., 1988; Fu and Liou, 1992), is used in this research. Thus far, Tseng et al. (2014) coupled the FLG plane-parallel radiation scheme to accept aerosol optical depth, single scattering albedo, and forward scattering parameters for each aerosol type in the shortwave and longwave at each time step (FLGchem) from WRF-Chem. The four shortwave and sixteen longwave bands are interpolated into the original six shortwave and twelve longwave Fu-Liou bands (Fu and Liou, 1993). To investigate the elevation dependency of precipitation changes from black carbon emissions, FLGchem is modified into a 3-dimensioned parameterized radiation scheme (FLGchem3D).

2.7.2 Microphysics Parameterization: Morrison Two-Moment

Compatibility of a microphysics parameterization requires the parameterization to be a double-moment type to allow for greater flexibility in representing rain drop size and microphysical process rates (e.g. evaporation) (Morrison, 2010). This means that the microphysics scheme, in addition to predicting mixing ratios for each hydrometeor required of a single-moment scheme, also predicts an additional quantity for each hydrometeor such as number concentration that is dependent on aerosol input (Wang et al., 2014). Compatible with WRF-Chem is the Lin microphysics parameterization (Lin et al., 1983) and the Morrison Two-Moment microphysics parameterization (Morrison et al., 2009). Both parameterization treat cloud droplet number as prognostic as it has a time integration component (Chapman et al., 2009; Peckham et al., 2014), and neither use predicted particulate e.g. black carbon as ice nuclei (Chapman et al., 2009; Morrison et al., 2009).

The Lin parameterization, when used in WRF, is a single-moment parameterization, but

when used in WRF-Chem, it initiates the autoconversion of cloud droplets to rain droplets that is dependent on the droplet number using the Liu and Penner (2005) parameterization, converting it into a double-moment parameterization (Chapman et al., 2009; Peckham et al., 2014). The Morrison microphysics parameterization is a double-moment parameterization, calculating mass and number concentration of hydrometeors as well as effective cloud water and effective cloud ice radii. The main difference between the Lin and Morrison parameterizations is that Lin expresses cloud droplet distribution as an exponential distribution, whereas Morrison expresses the same as a gamma distribution (Baró et al., 2015; Morrison et al., 2009).

The Lin parameterization also differs from the Morrison parameterization in terms of coupling a microphysics scheme to a radiation scheme in WRF-Chem. The Lin parameterization relies on the radiation scheme to calculate the effective cloud water and cloud ice radii. In WRF-Chem version 3.6.0, the Lin microphysics parameterization passes the cloud droplet number concentration information into the Goddard shortwave radiation scheme, where it calculates effective cloud water and effective cloud ice radii (Chapman et al., 2009). On the other hand, the Morrison microphysics scheme calculates cloud water and cloud ice effective radii within its own scheme. The choice for the radiation parameterization in this investigation is the Fu-Liou-Gu radiation scheme, which, without coupling to a microphysics parameterization, calculates radiation parameters based on prescribed and constant effective cloud water and cloud ice radii. To capture the indirect effects between a microphysics scheme and the Fu-Liou-Gu radiation scheme, only effective cloud water and effective cloud ice radii from a microphysics scheme are needed. Therefore, in the most direct way to capture the indirect effects of black carbon in the Fu-Liou-Gu radiation parameterization, we incorporate the already calculated effective cloud water and cloud ice radii from the Morrison parameterization. In an in-depth comparison of the Lin and Morrison microphysics parameterizations, Baró et al. (2015) found no significant benefits from the selection of either microphysical scheme.

Morrison Two-Moment microphysics scheme parameterizes rain, snow, graupel, cloud water, and cloud ice hydrometeors in mass and number concentration (Morrison et al., 2009). It parameterizes key liquid microphysical conversion processes such as accretion of droplets by existing rain and autoconversion of droplets to form rain, and ice microphysical processes such as homo- and heterogenous freezing of cloud droplets and rain to form cloud ice (Morrison et al., 2009).

Additionally, Morrison microphysics scheme also parameterizes droplet activation from aerosol, and ice nucleation from freezing of aerosol (Morrison et al., 2009). An additional note is made in Section 3.4. Tendencies for cloud droplets, cloud ice, snow, rain, and graupel based on number concentration are described in Morrison et al. (2009).

2.7.3 Cumulus Parameterization: Grell-Freitas (GF)

There are a number of cumulus schemes available for use with WRF-Chem. Amongst them are two that are able to capture the cumulus-radiation feedback (radiation will see parameterized clouds): G3 (Grell and Dévényi, 2002) or Grell-Freitas (GF) cumulus parameterizations (Grell and Freitas, 2014; Peckham et al., 2014). Because GF is the updated version of G3, we will employ the GF as the cumulus (convective) scheme.

GF is an ensemble cumulus parameterization based on Grell and Dévényi (2002) in which multiple cumulus schemes (Brown, 1979; Frank and Cohen, 1985; Krishnamurti et al., 1980; Fritsch and Chappell, 1980; Kain and Fritsch, 1993; Arakawa and Schubert, 1974) are employed and results of which are averaged as feedback to the model (Skamarock et al., 2008). All of the internal schemes are mass-flux type schemes, and differed by updraft and downdraft entrainment and detrainment parameters, and precipitation efficiencies (Skamarock et al., 2008). The method of determining cloud mass flux is determined by static and dynamic controls (Skamarock et al., 2008). The closure mechanism (dynamic) in GF are Convective Available Potential Energy, low-level vertical velocity, or moisture convergence, in which CAPE is relaxed and the moisture convergence returns the cloud rainfall to the integrated vertical advection of moisture (Skamarock et al., 2008). The trigger mechanism that permits convection is determined by the maximum cap strength (difference between environmental temperature and parcel temperature), essentially instability, in which a weak cap in the presence of positive CAPE will initiate the cumulus scheme (Skamarock et al., 2008; Haby, 2016b).

Unlike the Morrison microphysics scheme, GF does not ingest cloud droplet number mixing ratio from the chemistry (black carbon) package. Instead GF assumes a cloud condensation nuclei number of 250 per cm^3. This means GF does not account for the indirect effects of black carbon.

2.7.4 Other Parameterizations

Parameterizations are also needed to describe the land surface (LSM), the surface layer (SL), and the planetary boundary layer (PBL). The LSM uses atmospheric information from the surface layer scheme, radiative forcing from the radiation scheme, and precipitation forcing from the microphysics and convective schemes along with the land's state variables and land-surface properties to provide heat and moisture fluxes over land points (Skamarock et al., 2008). The SL schemes calculates friction velocities and exchange coefficients for the calculation of surface heat and moisture fluxes by the land-surface models and surface stress in the planetary boundary scheme (Skamarock et al., 2008). The planetary boundary layer (PBL) calculates vertical sub-grid scale fluxes due to eddy transports in the whole atmospheric column including the boundary layer. It determines the flux profiles within the well mixed boundary layer and the stable layer and gives the atmospheric tendencies of temperature, moisture, and horizontal momentum (Skamarock et al., 2008). In our research setup, we have chosen the NOAH land-surface model parameterization (LSM) (Hong et al., 2006) and MM5 Monin-Obukhov surface layer parameterization (SL) (Paulson, 1970; Dyer and Hicks, 1970), and the Yonsei University planetary boundary layer parameterization (PBL) (Hong and Lim, 2006), which are consistent with research using the Fu-Liou-Gu radiation parameterization.

Chapter 3

Model Modifications

The core of this research examines not only the precipitation change, but also the type of precipitation—convective, and non-convective—that are associated with black carbon's direct and semi-direct, and indirect effects. The default WRF-Chem configuration outputs precipitation in these two categories—convective and non-convective—that reflects only the total aerosol effects. This precipitation, however, does not reflect the black carbon-specific effects. This means that the FLG radiation parameterization, by default, is not connected to the chemistry module, where the black carbon emission data is ingested and its optical properties calculated; nor is it connected to a microphysics scheme.

In order to obtain precipitation information specific to the direct, semi-direct, and the indirect effects, the chemistry module, FLG radiation parameterization and Morrison microphysics parameterization must all be in communication with each other. Therefore, the Fortran codes within the physics (phys) including microphysics and radiation, dynamics (dynamics em core), and Registry areas are amended. We note here that the results of this research groups direct and semi-direct effects of black carbon together. This is further explained in Section 3.4.

3.1 Fu-Liou-Gu Radiation Code Modifications

FLG radiation parameterization (Liou et al., 1988; Fu and Liou, 1992, 1993; Gu et al., 2010, 2011) is based on eleven aerosol species data optical properties of which are calculated internally within the parameterization. In particular, there is a constant aerosol optical depth (AOD) for each grid point, which is then vertically distributed based on the relative humidity from meteorological input. Additionally, the AOD is distributed spectrally across six shortwave bands, and twelve

longwave bands using look-up tables internal to the parameterization. Similarly, forward scattering (G) and single scattering albedo (SSA) are also based on internal look-up tables.

In this research, we take full advantage of black carbon emissions data and microphysics calculations. Black carbon emissions data is fed into the chemistry module, which then calculates the AOD, SSA, and G optical properties by substituting the FLG-internal calculations for calculations that are based on the chemistry module. Note: WRF-Chem calculates aerosol optical properties based at four wavelengths: 400 nm, 600 nm, 800 nm, and 999 nm. Additionally, the FLG radiation also ingests the effective cloud water radius and effective ice water radius that the Morrison microphysics scheme calculates. In connecting the FLG radiation scheme to the chemistry module and microphysics scheme, the fully coupled radiation-chemistry-microphysics model is a self-contained and physically consistent model with realistic aerosol fields and meteorological effects.

3.2 A Schematic of the Modifications to Attain Direct, Semi-Direct, and Indirect Effects

The coupling of the FLG radiation parameterization to the Morrison microphysics parameterization and chemistry module gives us total—direct, semi-direct, and indirect effects. The following sections describe in detail how these effects can be separated from one another.

3.2.1 Direct and Semi-direct, and Indirect effects

The FLG radiation scheme is first connected to the chemistry module and Morrison microphysics scheme. As a result of these connections, the FLG radiation scheme is able to ingest the aerosol optical properties of AOD, W, and G at 300 nm, 400 nm, 600 nm, and 999 nm from the chemistry module, and effective cloud water radius (EFFCS) and effective ice water radius (EFFIS) from the microphysics scheme, making this the fully coupled online chemistry-radiation-microphysics model. The precipitation from simulations using this configuration is the result of direct, semi-direct, and indirect black carbon effects (Figure 3.1).

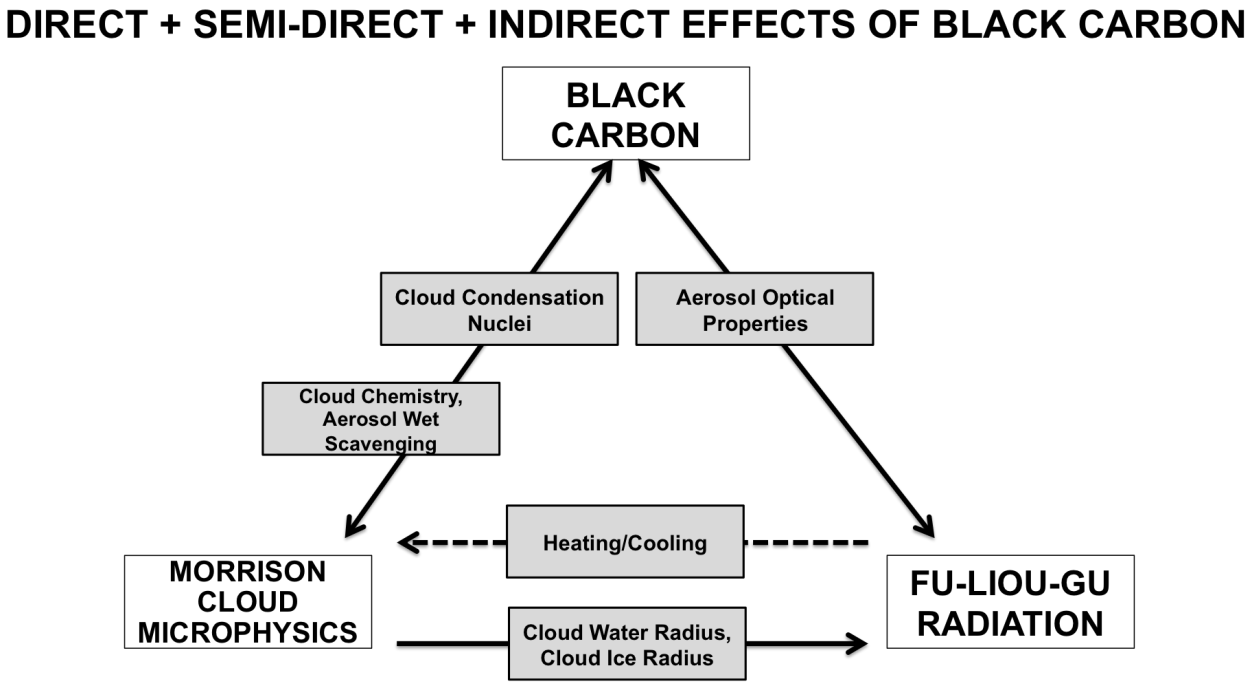

Figure 3.1: Simulation of Direct, Semi-Direct, and Indirect Effects of Black Carbon within WRF-Chem. Shown here is the setup of the fully coupled chemistry-radiation-microphysics interaction within WRF-Chem that is capable of producing the direct, semi-direct, and indirect effects of black carbon. The direct effect is captured by the connection between the black carbon emissions (chemistry module) and the Fu-Liou-Gu radiation parameterization. Semi-direct effect is captured with the direct effect and the connection between Morrison microphysics and Fu-Liou-Gu radiation parameterizations. The indirect effects are captured by the black carbon emissions and Morrison microphysics parameterization connection, and by the Morrison microphysics parameterization connection with Fu-Liou-Gu radiation parameterizations. Parameters that are passed between the chemistry module, radiation parameterization, and microphysics parameterization are further described in Section 3.2.1.

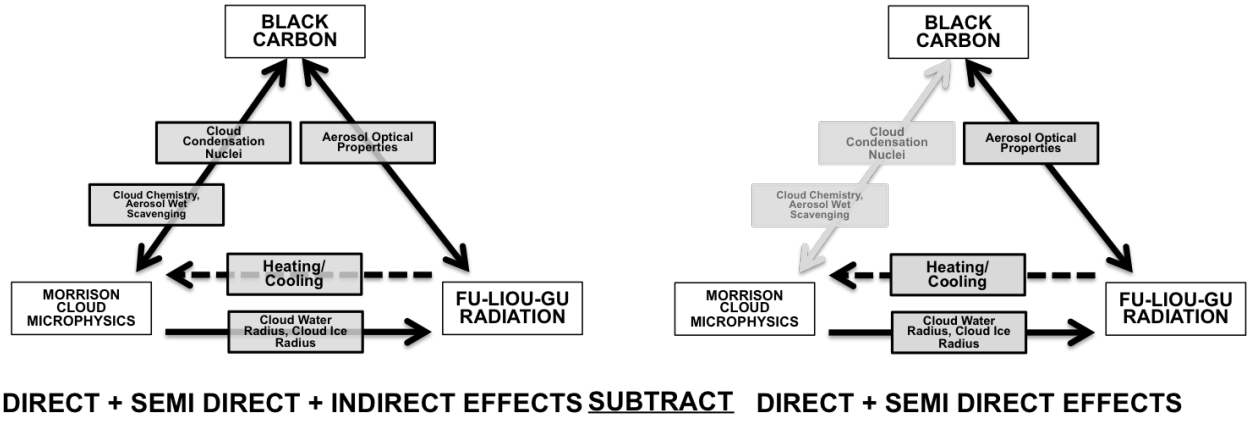

Figure 3.2: Simulation of Indirect Effects within WRF-Chem. Indirect effects within WRF-Chem are obtained by subtracting the direct and semi-direct effects from the fully coupled chemistry-radiation-microphysics interaction created in Figure 3.1.

3.2.2 Indirect Effects

The direct effect is captured within WRF-Chem when the optical properties from chemistry are passed into the radiation scheme. The semi-direct effect is captured when these optical properties are passed to the microphysics scheme by way of the radiation scheme; meaning the heating and/or cooling from black carbon is passed into the microphysics scheme where it can then calculate cloud water and cloud ice effective radii. In order to isolate these effects (i.e. remove the indirect effects), we alter the Morrison microphysics parameterization such that it does not ingest cloud condensation nuclei information from the chemistry module, while leaving the connection between chemistry and radiation, and radiation and microphysics unchanged. In these cases, cloud formation is dependent on condensation of water vapor (Morrison et al., 2009). Then, by subtracting this altered model with only the direct and semi-direct effects from the fully coupled chemistry-radiation-microphysics model, what remains is the calculation of meteorological output of the indirect effects (Figure 3.2).

3.2.3 Direct and Semi-Direct Effects

The indirect effects are captured within WRF-Chem when the cloud condensation nuclei information is passed from the chemistry module to the microphysics scheme; meaning cloud formation is directly dependent on the quantity of aerosols from the emissions scheme. In order to isolate these effects (e.g. remove the direct and semi-direct effects), we alter the FLG radiation parameterization such that it neither ingests optical properties calculated from the chemistry module nor does it internally calculate aerosol optical properties based on its attached lookup tables, while leaving the connection between chemistry and microphysics unchanged. Then, by subtracting this altered model with only the indirect effects from the fully coupled chemistry-radiation-microphysics model, what remains is the calculation of meteorological output of direct effects (Figure 3.3).

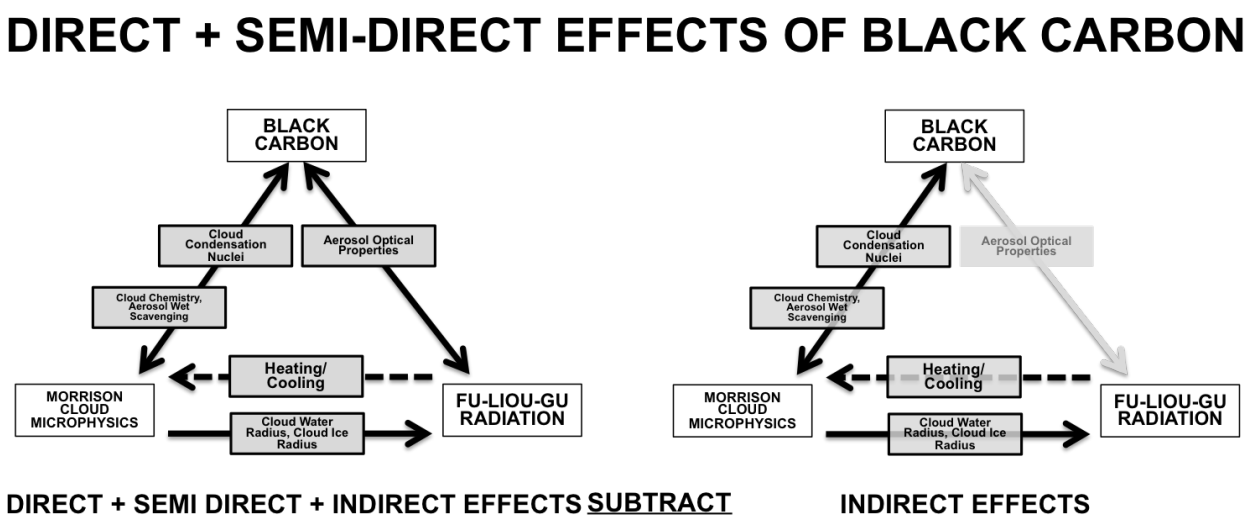

Figure 3.3: Simulation of Direct and Semi-Direct Effects within WRF-Chem. Direct and semi-direct effects are obtained by subtracting the indirect effects from the fully coupled chemistry-radiation-microphysics interaction created in Figure 3.1.

3.3 Simulation Types for Analysis

In analyzing how black carbon affects precipitation, four simulations are used: fully coupled simulation with black carbon; fully coupled simulation without black carbon; indirect effects only simulation; and direct and semi-direct effects simulation. Precipitation differences between the simulation without black carbon and the simulation with black carbon are studied. Novel to this

research is this particular method of obtaining the indirect, and direct and semi-direct effects, as well as the further separation of precipitation to the convective and non-convective categories. Simulations types are included in Table 2.1 in Section 2.6.

3.4 A Note About the Semi-Direct Effect

In order for semi-direct effect to be isolated, we must be able to separate the effects of the radiation and microphysics schemes from each other. The current state of WRF-Chem, however, does not allow us to isolate the semi-direct effect, because the radiation and microphysics scheme are inherently bounded by its inseparable communication of heating and/or cooling. Radiation parameters that are calculated within the FLG parameterization is passed to Morrison microphysics not directly but indirectly, by way of temperature, wind, and pressure, and cannot be separated. As such, the results in this research show semi-direct and direct effects together.

3.5 A Note About the Indirect Effects on Ice Clouds

In Section 2.7.2, we noted that the Morrison microphysics scheme parameterizes droplet activation from aerosol and ice nucleation from the freezing of aerosol and that the effective cloud ice radius is passed from the microphysics scheme to the radiation scheme. This gives the impression that this model setup dependably models the indirect effects on ice clouds. However, there is only a cloud water droplet number concentration that is passed from the chemistry module to the cloud fields in the microphysics scheme (i.e. "QNDROP" is passed to "nc1d", "nc3d"). Once in the Morrison microphysics parameterization, the freezing of cloud droplets is achieved if the cloud water number meets a threshold and the temperature is less than 269K (Morrison, 2014). Because there are cloud water number and temperature requirements, there is no direct ice nucleation due to black carbon in this research. Therefore, the indirect effects on cloud ice are not dependably modeled. Additionally, large uncertainties remain in basic understanding of physical processes of ice particles including nucleation (Morrison, 2010).

3.6 Assumptions of Linearity

The way that are investigating aerosol effects—by subtracting specific effects from total aerosol effects—assumes that the direct and semi-direct, and indirect effects are linear processes relative to each other and to the fully coupled chemistry-radiation-microphysics model. Research has shown that indirect and direct effects are, in fact, weakly non-linear (Lohmann and Feichter, 2001). It is, therefore, important to spot trends in behavior to precipitation with the inclusion of black carbon, rather than focus on specific values.

Chapter 4

Effects of Black Carbon in a Heavy Wintertime Precipitation Event: 7–11 January 2005

4.1 Synoptic Background and Goals

We start with a heavy wintertime precipitation event: the 7–11 January 2005 atmospheric river event. During this event, the western United States was under the influence of an atmospheric river that brought heavy precipitation to the west coast states, particularly to California (CA). Colloquially, this rain event is known as a "Pineapple Express" in which the subtropical jet brings moisture-laden air directly from the tropics, over the Hawaiian Islands, and onto the west coast of the US as depicted in Figure 4.1. In CA, accumulated precipitation registered as high as 800 mm in some regions. In southern California, this storm caused $100 million in damages and 20 deaths across southern CA.

The goals for this case study are: 1) to achieve a proof of concept that our model setup produces black carbon aerosol effects, and 2) to have an initial gauge of the significance of precipitation behavior due to black carbon in a heavy wintertime precipitation event that largely produce non-convective precipitation.

4.2 Proof of Concept: Modeling Black Carbon Effects in WRF-Chem

Section 1.2 defines the how the direct and indirect effects of black carbon alter the atmosphere and Section 3.2 describes the model modifications to obtain the direct, semi-direct, and indirect effects. This Section uses the wintertime case to check the direct and indirect effects from the model output. Missing from these proof of concept checks on black carbon effects is the check

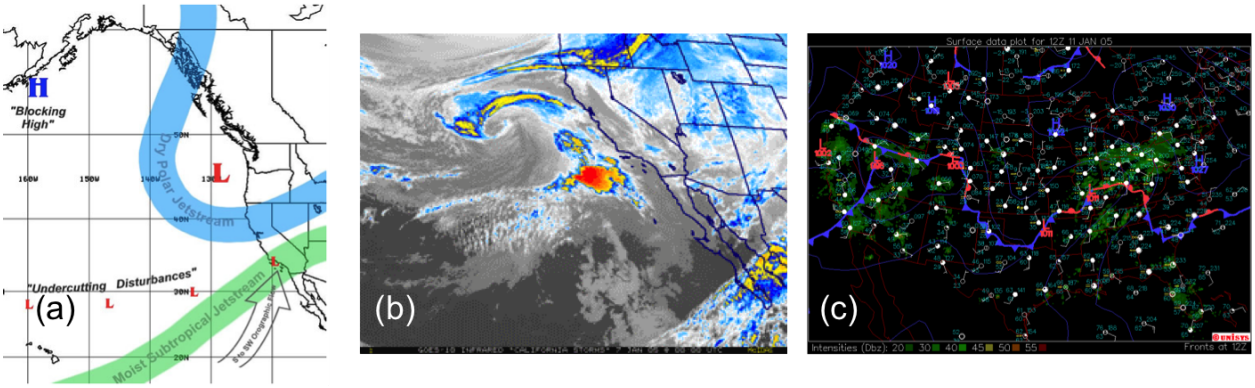

Figure 4.1: Wintertime Case (7–11 January 2005): A Synoptic Outlook. Synoptic conditions during 7–11 January 2005 in (a) a typical "Pineapple Express" schematic, (b) infrared satellite imagery, and (c) surface analysis on 11 January 2005 at 1200Z. (a) In a typical Pineapple Express event, a subtropical jet (green jet) brings moisture-laden air directly from the tropics onto the west coast of the United States. (b) At the surface this disturbance is a low pressure centered off of the west coast. During this atmospheric river event, the surface received rainfall as high as 800 mm in some regions in California (c) with the cold fronts bringing a moist airmass over the western United States (California Nevada River Forecast Center, 2016; UNISYS Weather, 2016).

for semi-direct effects of black carbon, reason for which is described in Section 3.4.

4.2.1 Direct Effects

Because the direct effect of black carbon warms the atmosphere, we expect the temperature to increase in direct effect—which is what happens. In Figure 4.2, the domain average temperature time series plot increases in the direct effect, while temperatures in the indirect effects exhibit a slight decrease. This decrease can be due to the formation of cloud droplets, which inhibits incoming solar radiation and cools the atmosphere below the cloud levels. In looking at the domain average vertical profile, the temperature increase is localized to the midlevels, between 6 and 9 km (Figure 4.2). Comparing this to the domain average vertical profile of black carbon, the maximum heat increase is not at the surface where there is the maximum black carbon concentration. In fact, there is cooling at the surface, where there is maximum black carbon concentration. This suggests that black carbon that has been lofted from the emission source (surface) to the midlevels absorbs the majority incoming solar radiation, pointing to the existence of surface dimming. This is consistent with Samset et al. (2013), who showed that more than 40% of the total radiative forcing absorbed by black carbon is exerted above 5 km, even with the majority of the black carbon being in the lower levels of the atmosphere.

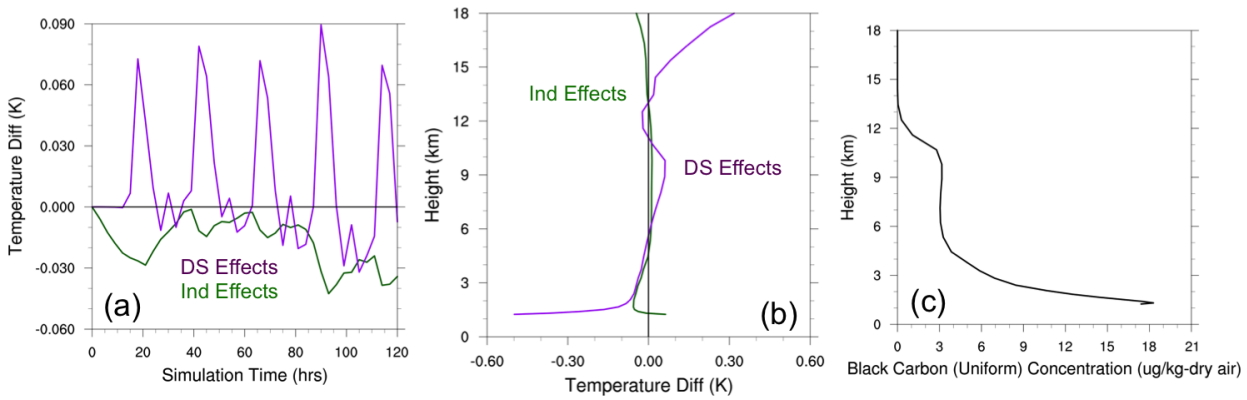

Figure 4.2: Wintertime Case: Direct Effect of Black Carbon. (a) The direct effect of black carbon on temperature (purple) renders an increase to the average domain temperature up to 0.9K during the 7–11 January 2005 simulation, as shown in a domain average temperature time series plot. Additionally, black carbon exhibits a diurnal variation in its heating of the atmosphere as it absorbs highly at the shortwave lengths that are received during the day. There is also diurnal variation from the indirect effects (green) on temperature, with slight cooling from an increased cloud amount. This warming, however, is unevenly distributed throughout the vertical column. (b) The domain averaged vertical temperature profile shows that vertical distribution of heating due to the direct effect of black carbon, which is an increase of approximately 0.10K at 9 km and a cooling of 0.5K at the surface. This points to surface dimming. By contrast, the indirect effects of black carbon on temperature (green) remain relatively unchanged. (c) The domain averaged vertical black carbon profile is shown for reference. Note that the warming occurs where incoming solar radiation reaches black carbon lofted into the middle of the atmosphere, leaving a decreased amount of solar radiation at the surface, which leads to the surface dimming.

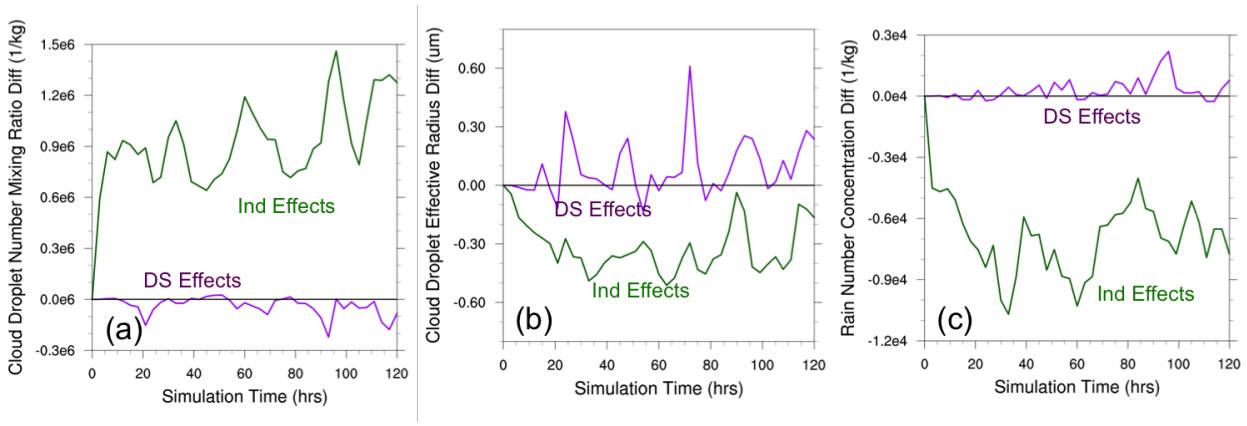

Figure 4.3: Wintertime Case: Indirect Effects of Black Carbon. The indirect effects of black carbon (green) are threefold: (a) more cloud droplets, (b) smaller cloud droplets, and (c) less rainfall. (a) Depicts the cloud droplet number increase of approximately 600,000 to 1.5 million droplets per kg within the domain during the simulation period. (b) The cloud droplet effective radii decrease by approximately 0.5 micron. (c) The rain number concentration decreases by approximately 6,000 to 10,000 per kg. By contrast, the direct and semi-direct effects on the same parameters (purple) remain relatively unchanged, as expected.

4.2.2 Indirect Effects

In order for indirect effects to be accurately modeled, the simulations should produce a greater quantity of smaller cloud droplet and potentially less rain droplets. Figure 4.3 shows precisely these characteristics by way of a cloud droplet number mixing ratio increase, a cloud droplet effective radius decrease, and a decrease in rain droplet mixing ratio.

4.3 Accumulated Precipitation Difference Due to Black Carbon

The domain accumulated precipitation amounted to 88,694 mm and the domain accumulated precipitation with black carbon amounted to 88,035 mm. Due to black carbon inclusion, the negative difference of 659 mm is approximately 0.7% decrease (Figure 4.4). This is within the global estimation range of precipitation decrease due to black carbon of 0.4-10% (Ming et al., 2010; Shiogama et al., 2010; Tosca et al., 2010). This small decrease may be due the nature of this precipitation event. In particular, this atmospheric river generated a large quantity of rain, and any change in precipitation due to black carbon is potentially dwarfed by precipitation without black carbon.

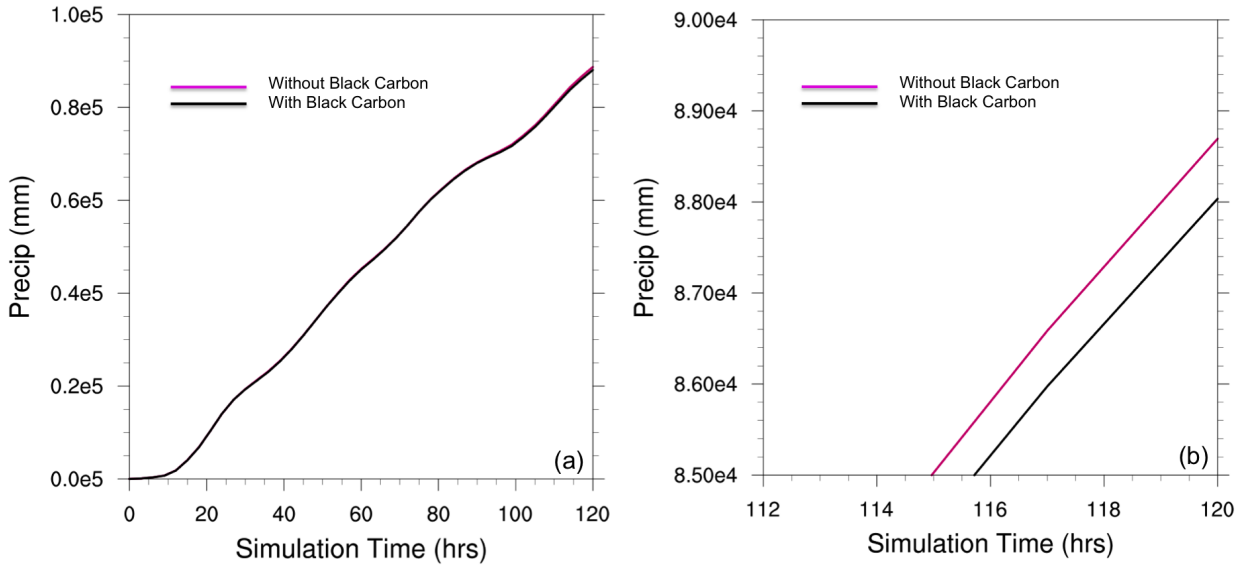

Figure 4.4: Wintertime Case: Domain Averaged Time Series of Accumulated Precipitation Simulated with and without Black Carbon (mm). Accumulated precipitation with (black) and without (pink) black carbon show little difference from one another during the 7–11 January 2005 simulation. In all, black carbon generated a decrease of 659 mm (0.7%) across the domain. Although this value is small, it is within the global estimate for precipitation decrease due to black carbon of 0.4-10% (Ming et al., 2010; Shiogama et al., 2010; Tosca et al., 2010). Precipitation at the end of the simulation in (a) is enlarged in (b).

4.4 Black Carbon Effects-Based Precipitation Difference

Breaking this up this precipitation into its black carbon-based effects, we can make several observations (Figure 4.5). 1) The total precipitation accumulation trend resembles that of the direct and semi-direct effects with indirect effects changing the magnitude of precipitation difference, 2) Both the precipitation responses to the direct and semi-direct effects of black carbon, and the indirect effects of black carbon are decreasing, 3) The direct and semi-direct effects on precipitation has near zero difference in precipitation followed by a marked decrease in precipitation after the 72nd simulation hour, while the indirect effects on precipitation maintains a steady decrease throughout the simulation.

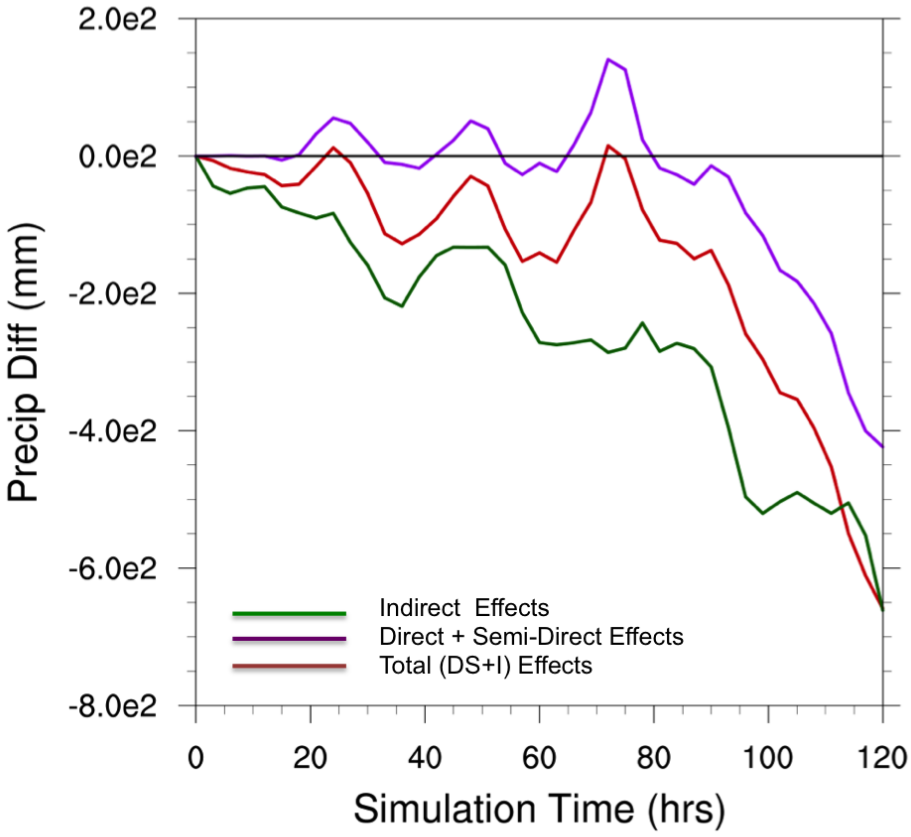

Figure 4.5: Wintertime Case: Domain Averaged Time Series of Black Carbon Effects-Based Precipitation (mm). Precipitation difference due to black carbon (red) is obtained by subtracting the time series in black from the time series in pink in Figure 4.4. The precipitation can also be divided into direct and semi-direct effects (purple) on precipitation and indirect effects (green) on precipitation, as described in Sections 3.2.3 and 3.2.2, respectively. The addition of the direct and semi-direct effects on precipitation (purple) and the indirect effects on precipitation (green) do not add up to the total difference (red) due to the non-linearity nature of the simulations due to the nonlinearity of the model. This nonlinearity between indirect and direct effects are also observed in Lohmann and Feichter (2001), where they find the nonlinearity to be weak but present.

4.5 Non-Convective and Convective Precipitation Differences Due to Black Carbon

Further understanding these trends entails separating the precipitation response to black carbon into non-convective and convective precipitation. In models, microphysics parameterization models non-convective precipitation, where clouds and their associated processes are represented directly on the model grid; this is known as explicit precipitation (Stensrud, 2009). These processes include cloud development and evolution and are modeled explicitly by incorporating additional equations that represent various water substance phases and cloud particle types (Stensrud, 2009). Conversely, cumulus parameterizations model convective precipitation, where only the cumulative effects of clouds are represented on the grid; this is known as implicit parameterization (Stensrud, 2009). While only a microphysics parameterization is needed to produce non-convective precipitation, both microphysics and cumulus (convective) parameterizations are needed to model convective precipitation with models at 10-40 km. This is because sub-grid scale (convective) precipitation requires deep convection activation prior to water vapor saturation at a grid point, while resolvable grid scales model equations develop appropriate precipitation (non-convection).

The following sections look at the precipitation in two categories: non-convective and convective precipitation.

4.5.1 Non-Convective Precipitation

The non-convective precipitation generated from black carbon indirect effects varies more significantly compared with that of convective precipitation. Accumulated convective precipitation from black carbon indirect effects straddles zero, meaning the indirect effects had little to no effect in producing convective precipitation. This is as expected, as the precipitation response to the indirect effects is sensitive to the microphysics scheme, while the precipitation response to convective precipitation is sensitive to the radiation scheme (Figure 4.6). These two schemes are directly connected to each other by way of water and ice cloud effective radii only. On the other hand, non-convective precipitation due to indirect effects shows a marked decline. This result makes sense, as the indirect effects mean that the available black carbon particles activate as cloud condensation nuclei (CCN). As new cloud droplets form using black carbon as CCN, the cloud droplets that are

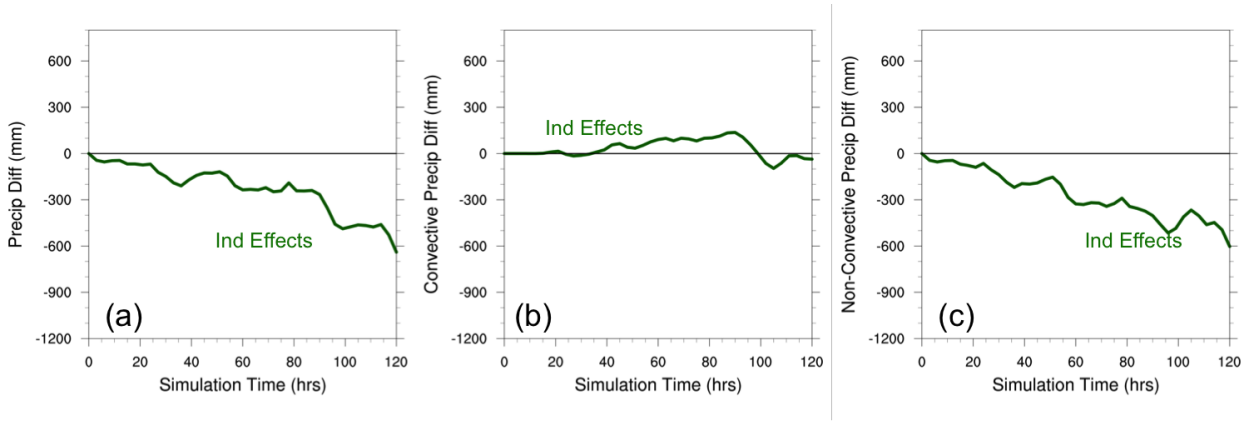

Figure 4.6: Wintertime Case: Domain Averaged Time Series of Indirect Effects on Convective and Non-Convective Precipitation (mm). Focusing on the indirect effects on precipitation in Figure 4.5, (a) the indirect effects reduces precipitation by approximately 600 nm, most of which comes from the (c) non-convective precipitation while the (b) convective precipitation remains at approximately zero. This is as expected, as the cloud condensation nuclei are passed from the chemistry part of the model into the microphysics scheme and not via the cumulus parameterization.

vying for the same water vapor are smaller in size (cloud water radii). Because rain droplets are grown from cloud droplets (Stensrud, 2009) to obtain raindrop fall speeds (on the order of m/s) (Cotton and Anthes, 1989), less rain is formed with the indirect effect. Small cloud droplets tend to advect with the airflow around the larger drops, reducing collection efficiency. Moreover, with small cloud droplets, the collision efficiency (efficiency of cloud drops that collide) and the coalescence efficiency (efficiency of cloud drops that collide and remain together) are reduced, thereby reducing collection efficiency (collision and coalescence efficiencies) (Stensrud, 2009). Ultimately, a lower collection efficiency leads to reduced precipitation formation (Stensrud, 2009).

4.5.2 Convective Precipitation

What commands added attention is the precipitation generated from the direct and semi-direct effects. From these effects, both non-convective and convective precipitation types assume interesting characteristics that warrant more in-depth investigation. Overall, accumulated precipitation remains near zero (unchanged) until approximately 72 hours into the simulations, at which point the precipitation response decreases (Figure 4.7). To understand this, we look at the non-convective precipitation and convective precipitation together and then separately. The non-convective and convective precipitation difference, up to 72 hours, both increase and decrease at the

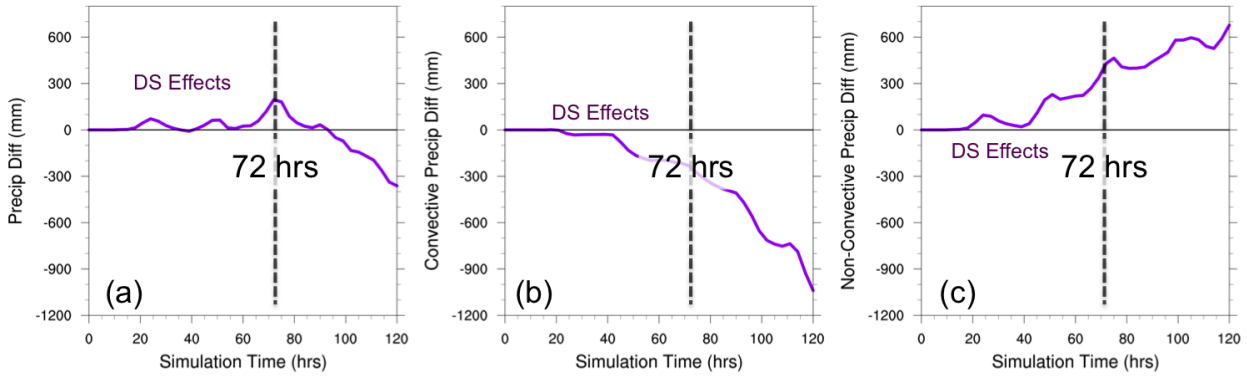

Figure 4.7: Wintertime Case: Domain Averaged Time Series of Direct and Semi-Direct Effects on Convective and Non-Convective Precipitation (mm). Focusing on the direct and semi-direct effects on precipitation in Figure 4.5, (a) the direct and semi-direct effects reduce precipitation overall, but not in as straightforward of a pattern as the indirect effects exhibit in Figure 4.6. (b) With the increased stability due to temperature increase aloft and cooling at the surface, direct and semi-direct effects reduce non-convective precipitation, which requires instability. (c) Because non-convective precipitation does not rely on column stability, non-convective precipitation increases.

same rate, giving the total precipitation difference its near zero value. After 72 hours, convective precipitation declines sharply compared with that of non-convective precipitation, which is still increasing, but at a slower rate than that of convective precipitation. The domain average relative humidity (RH) vertical profile and domain average RH time series both indicate an increase, which is consistent with the increase in non-convective precipitation, as increased relative humidity points to the available condensate that is necessary for non-convective precipitation. Simultaneously, the domain average vertical temperature profile indicates a strengthening of warming in the midlevels and cooling in lower levels, a phenomenon called surface dimming. The domain average temperature time series shows this increase, while the domain average surface temperature time series decreases markedly after 72 hours into the simulation (Figure 4.8). Altogether, the decrease in convective precipitation outweighs the increase in non-convective precipitation, rendering a total decrease to direct and semi-direct precipitation.

4.6 Discussion

From this initial five-day case study, we observe the following. Our simulation set up, using model coupling and decoupling, renders black carbon effects-based precipitation, as expected

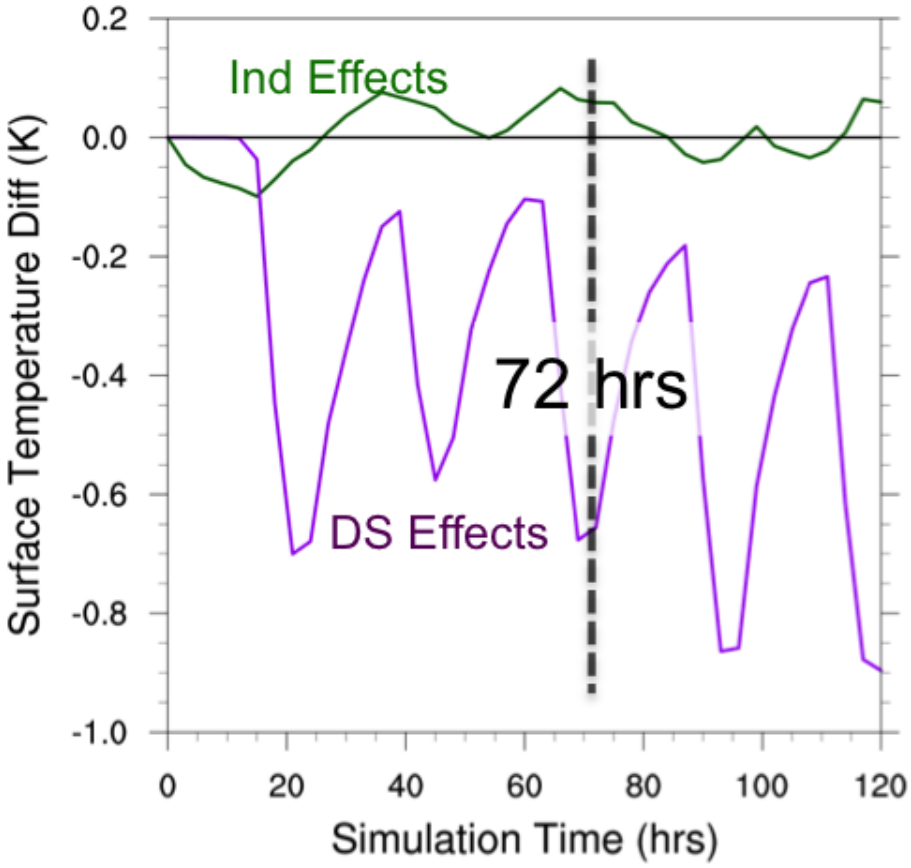

Figure 4.8: Wintertime Case: Domain Averaged Time Series of Black Carbon Effects-Based Surface Temperature (K). The surface temperature time series due to the direct and semi-direct effects of black carbon (purple) reveals the timing of surface dimming strengthening. At the 80^{th} hour point, the surface temperature maximum (diurnal variation) is -0.2 K, whereas the maximum surface temperature on previous days is -0.1 K. This surface temperature drop does not recover to the first day's surface temperature for the remainder of the simulation. The minimum surface temperature experiences similar changes and, as such, the strengthening of the surface dimming is approximated at the 72^{nd} hour. This corresponds well to the accelerated decrease of convective precipitation. This result is reasonable, as surface dimming contributes to atmospheric stability, and with greater stability comes a decrease in convective precipitation. Effectively, the timing of precipitation decrease is marked by the timing of the strengthening of surface dimming. The indirect effects on surface temperature (green) indicate a slight diurnal cycle from the increased cloud, although basically causes no change to the surface temperature.

according to our definition of those effects. These results, along with the assumption of the weak nonlinearity between the direct and indirect effects, allow us to proceed with longer simulations. Black carbon can increase and decrease precipitation within the domain depending on the contributions of its effects. In this case, black carbon decreases precipitation by 0.7%, which is within the range of global studies (Tosca et al., 2010; Ming et al., 2010). The indirect effects produce more numerous but smaller cloud droplets, which inhibits the formation of non-convective precipitation and left convective precipitation relatively unchanged. The direct and semi-direct effects strengthened surface dimming, which stabilized the atmosphere. The consequence of this stabilization effect is that it reduces formation of convective precipitation. Furthermore, the timing of surface dimming strengthening corresponds with the sharp drop in convective precipitation. As such, sufficient attention should be given to the timing of surface temperature drops and possibly domain temperature increases to time the accelerated decrease in convective precipitation, which can potentially dictate the timing of precipitation decrease.

Chapter 5

Effects of the 3-Dimensional Fu-Liou-Gu Radiation Parameterization (3D FLG) in a Heavy Wintertime Precipitation Event: 7-11 January 2005

5.1 3D FLG Background and Goals

From the results in Chapter 4, we know that direct and semi-direct effects of black carbon play an important role in altering precipitation accumulation behavior, more pronounced than that of the indirect effects. From Gu et al. (2012) and Liou et al. (2013), we also know the range of effects a 3-dimensional radiation parameterization can have on surface temperature, solar fluxes, and snow water equivalence. Combining these two ideas together in this chapter, we explore how the 3-dimensional FLG radiation parameterization (3D FLG) affects precipitation in a heavy precipitation event. Figure 5.1 describes the 3-dimensional FLG radiation parameterization schematic (1.4).

The goal for this case study is to compare the precipitation behavior due to the 3D FLG with the precipitation behavior due to black carbon for the same heavy wintertime precipitation event as described in Chapter 4.

5.2 Inclusion of 3-Dimensional Fu-Liou-Gu Radiation Parameterization

Including a 3-dimensional parameterization of the FLG radiation scheme generates a decrease in accumulated precipitation of approximately 80 mm. This is a 0.09% decrease to the accumulated precipitation from the basic simulation. To understand this precipitation decrease, we separate the precipitation according to height (Figure 5.2): precipitation between 1000 m and 2000 m, between 2000 m and 3000 m, and above 3000 m. Of the 80 mm, most of the precipitation

θ_i = angle between the incident solar beam and slope's normal vector of a target point; is a function of solar zenith and azimuthal angles, mountain slope, slope orientation

V_d = sky view factor; represents the shadow effect of mountains on direct and diffuse solar fluxes reaching target point

C_t = terrain configuration; area of surrounding mountains visible to the target point which determines the solar fluxes reflected to the target point from the surrounding mountains; affected direct-reflected, diffuse-reflected, and coupled flux

h = terrain elevation

γ = skewness of terrain elevation

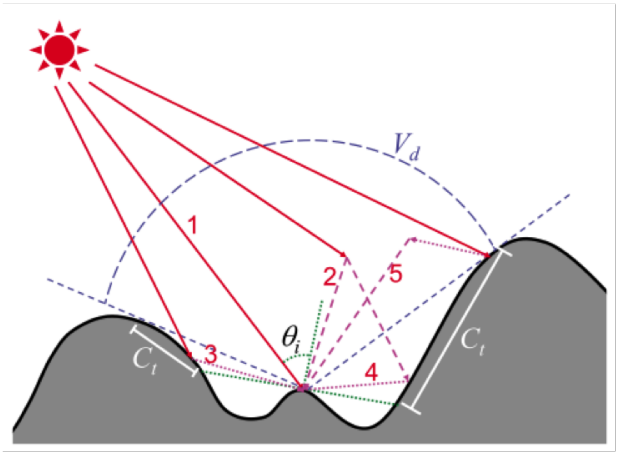

Lee et al. (2011), *JGR*

		Air Molecule Collision (scattering)	Surface/Terrain Collision (reflectance)	Surface/Terrain Collision (no reflectance)
(1) F*dir	Direct Flux			
(2) F*dif	Diffuse Flux			
(3) F*rdir	Direct-reflected Flux			
(4) F*rdif	Diffuse-reflected Flux	1	2	
(5) F*coup	Coupled Flux	2	1,2	

Figure 5.1: 3-Dimensional Fu-Liou-Gu Radiation Parameterization: Description. The 3-dimensional Fu-Liou-Gu radiation parameterization (3D FLG) is described by multiple linear regression that defines five fluxes (direct, diffuse, direct-reflected, diffuse-reflected, and coupled) based on five parameters (the angle between the incident solar beam and slope's normal vector of the target point, the sky view factor, the terrain configuration, terrain elevation, and skewedness of terrain elevation). The direct flux is where the incident solar radiation collides with the surface or terrain without reflectance. The diffuse flux is where the incident solar radiation collides with air molecules, scattering the sunlight. The direct-reflected flux is where the incident solar radiation collides with the surface or terrain with reflectance. The diffuse-reflected flux is where the incident solar radiation first scatters off of air molecules and then reflects off of the surface or terrain. The coupled flux is where incident solar radiation first reflects against a surface or terrain followed by further reflectance against a surface or terrain, or scatters against air molecules (Lee et al., 2011).

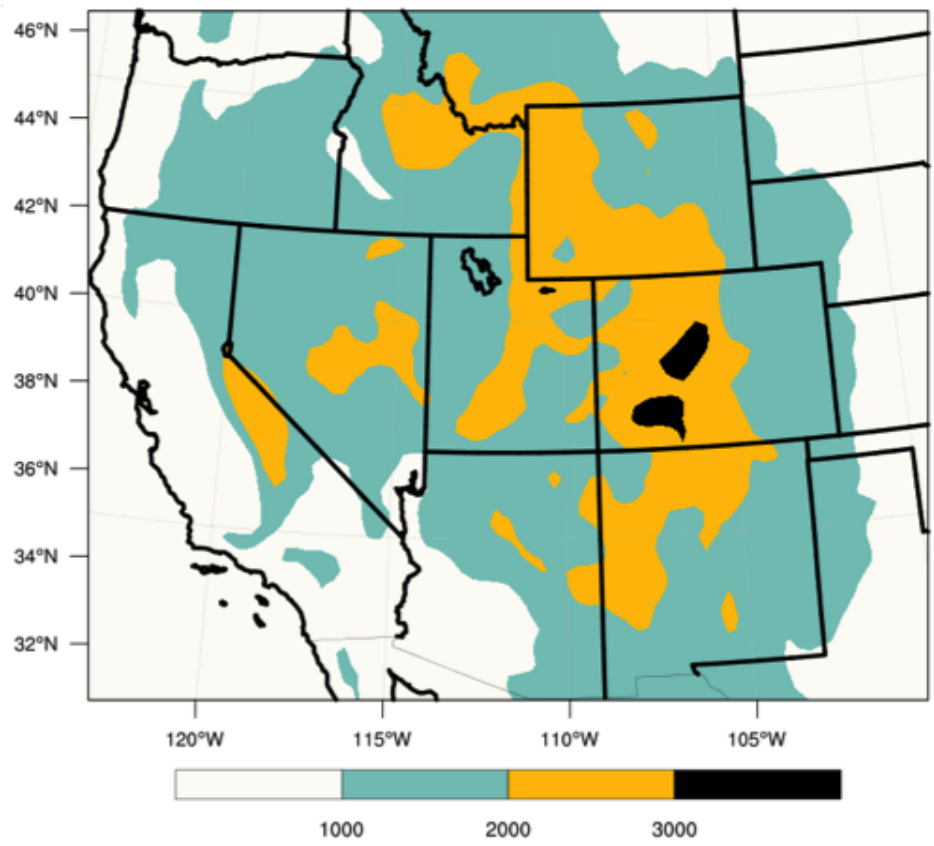

Figure 5.2: 3-Dimensional Fu-Liou-Gu (3D FLG) Radiation Parameterization: Terrain Height (m) Categories for Precipitation Analysis. Just as the precipitation generated by black carbon is analyzed by separating into black carbon-based effects, we separate the precipitation difference generated by 3-dimensional Fu-Liou-Gu radiation parameterization into elevation ranges. Here, we separate precipitation into three elevation categories: elevation between 1000 m and 2000 m (teal), elevation between 2000 m and 3000 m (orange), and elevation greater than 3000 m (black).

reduction is in the lower levels, where the shading effect dominates compared with any additional radiative fluxes from the 3D FLG, which is a stabilizing effect. In the midlevels, precipitation increased due to minor enhanced convection due to additional radiative fluxes, which is a destabilizing effect. With a decreasing number of neighboring points available for scattering of radiation fluxes, 3-dimensional radiative fluxes become increasingly closer to that of plane-parallel radiative fluxes.

5.3 Comparison of Precipitation Behavior Between Black Carbon Inclusion and 3D Radiation Parameterization Inclusion

We include black carbon emissions in our experiment and, in a separate experiment, include a 3-dimensional radiation parameterization (without black carbon). Here, we compare the precipitation behavior of the 7–11 January 2005 case due to black carbon and the precipitation behavior due to the 3D radiation parameterization. Figure 5.3 shows the precipitation accumulation due to NEI black carbon (yellow), the 3D FLG (blue), uniform black carbon at the surface (orange), uniform black carbon from the surface to 3 km (brown), and uniform black carbon from the surface to 19 km (red). Both black carbon and the 3D radiation parameterization decrease precipitation, with the 3D radiation parameterization reducing precipitation by 80 mm. This value sits between the 23 mm decrease from black carbon NEI and the 117 mm decrease from uniform black carbon at the surface. This suggests that both black carbon and a more realistic parameterization of radiation are important in understanding the changes they cause to precipitation. The results here are for a heavy wintertime precipitation event that that produced mostly non-convective precipitation. More simulations of various precipitation events are needed to elucidate this research.

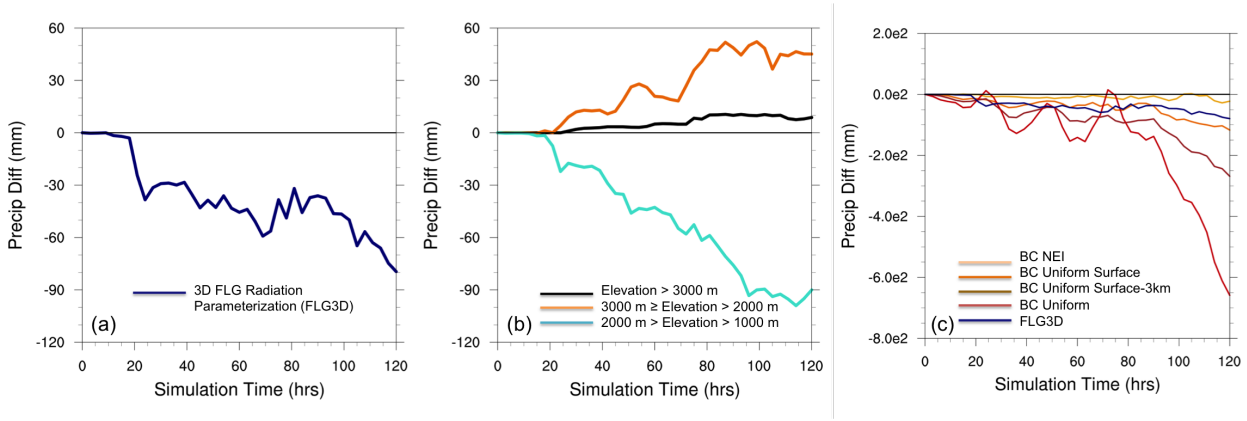

Figure 5.3: 3-Dimensional Fu-Liou-Gu Radiation Parameterization: Domain Averaged Time Series of Accumulated Precipitation (mm). (a) Accumulated precipitation due to 3-Dimensional Fu-Liou-Gu radiation parameterization (3D FLG) is 80 mm throughout the 7–11 January 2005 period. (b) Precipitation separated by elevation category. Most of the precipitation reduction is in the lower elevations of the topography (teal) where shading effect (stabilization) dominates to any additional radiative fluxes from the 3D FLG inclusion. In the midlevels of the topography (orange), precipitation increases due to minor enhanced convective precipitation from additional radiative fluxes (destabilizing). With a decreasing number of neighboring points in the highest elevations (black), available for scattering of radiation fluxes, the 3D radiative fluxes become increasingly closer to that of plane parallel. (c) Precipitation accumulation due to NEI black carbon (yellow), the 3D FLG (blue), uniform black carbon at the surface (orange), uniform black carbon from the surface to 3 km (brown), and uniform black carbon from the surface to 19 km (red). Both black carbon and the 3D radiation parameterization decrease precipitation, with the 3D radiation parameterization reducing precipitation by 80 mm. The reduction in precipitation due to the 3D FLG is between the precipitation reduction generated by NEI (23 mm) and by uniform black carbon at the surface (117 mm). This suggests that both black carbon and a more realistic parameterization of radiation are important in understanding the changes they cause to precipitation.

Chapter 6

Effects of Black Carbon in a Heavy Summertime Precipitation Event: 20–24 July 2005

6.1 Synoptic Background and Goals

In addition to a heavy precipitation event in the winter, we also investigate how black carbon changes precipitation in a relatively heavy summertime rain event. Unlike the 7–11 January 2005 Pineapple Express, the 20–24 July 2005 rain event was largely due to thermal (heat) lows over the western United States. Heat lows are warm core low pressures that form due to the increased warming at the surface, compared with horizontally adjacent locations. Often intensified in dry conditions that lack evaporative cooling, the heating lowers the pressure at the surface while leaving upper pressure unchanged (Figure 6.1). Heating at the surface that generates instability couples with moisture influx from the Gulf of Mexico and the Gulf of California, making the atmosphere conducive for localized convective precipitation (Haby, 2016c).

The goals for this case study are: 1) to study the precipitation behavior due to black carbon in a summertime precipitation event that produced largely convective precipitation, and 2) to compare the atmospheric patterns between the summertime precipitation event that largely produced convective precipitation with the heavy wintertime precipitation event produced largely produced non-convective precipitation.

6.2 Accumulated Precipitation Difference Due to Black Carbon

The domain accumulated precipitation amounts to 20386 mm; domain accumulated precipitation with black carbon uniform amounts to 9820 mm (black). Due to black carbon inclusion,

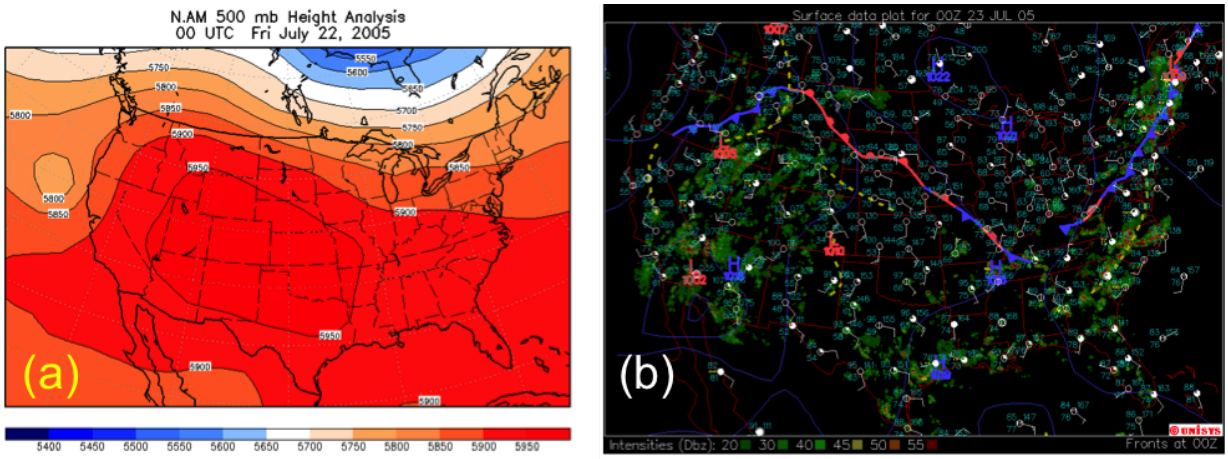

Figure 6.1: Summertime Case (20–24 July 2005): A Synoptic Outlook. (a) The 500 mb height analysis show moisture influx from the Gulf of Mexico in the midlevels of the atmosphere. (b) This moisture influx coupled with the instability at the surface creates convective precipitation. Non-convective precipitation is largely from the northwest brought about the cold front over Oregon and Idaho (NOAA National Centers for Environmental Information, 2016; UNISYS Weather, 2016).

the negative difference of 10566 mm equates to a 52% decrease (Figure 6.2). Because thermal low pressures are horizontally dependent on temperature differences, the low-pressure centers exhibit a diurnal cycle. Black carbon also exhibits a diurnal cycle, with the highest absorption in the daytime, particularly in this case where clouds do not inhibit incoming solar radiation. Therefore, precipitation accumulation also exhibits a diurnal cycle with periods of decelerated accumulation.

6.3 Black Carbon Effects-Based Precipitation Difference

Separating the precipitation into its black carbon-based effects, we can make several observations (Figure 6.3): 1) The total precipitation accumulation from black carbon is from the direct and semi-direct effects with negligible contribution from the indirect effect, 2) The direct and semi-direct effects on precipitation nears zero difference in precipitation followed by a marked decrease in precipitation after the 60^{th} simulation hour. This is different from the wintertime case where the precipitation response to black carbon resembles all three effects of black carbon.

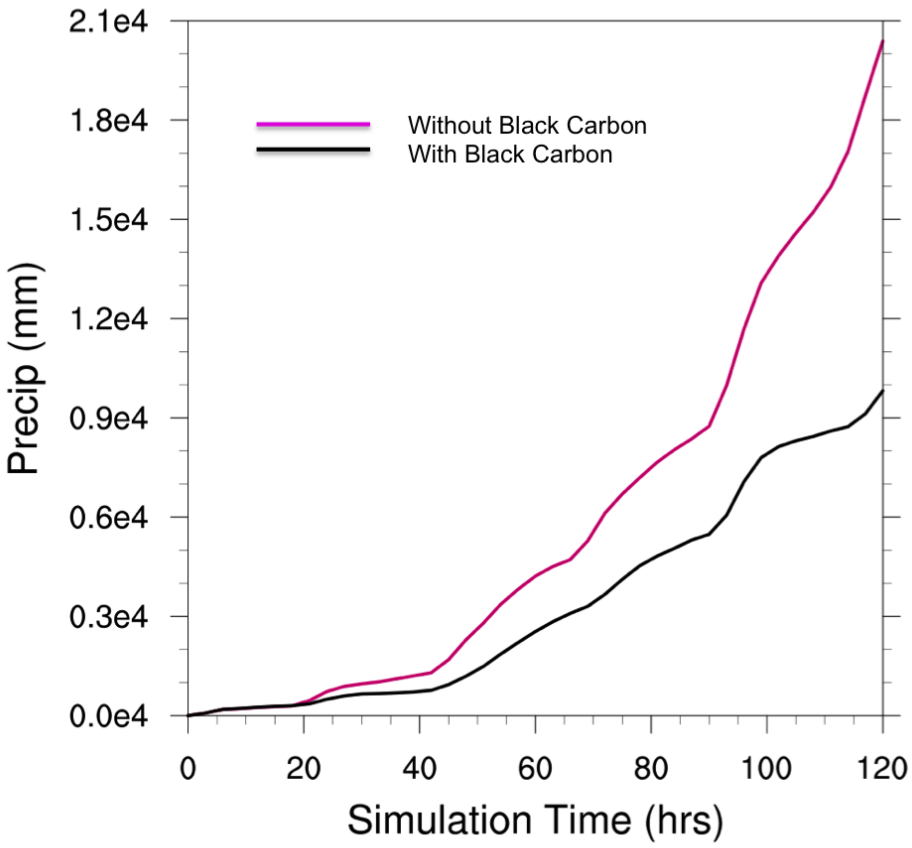

Figure 6.2: Summertime Case: Domain Averaged Time Series of Accumulated Precipitation (mm) Simulated with and without Black Carbon. Accumulated precipitation with (black) and without (pink) black carbon show a significant difference from one another compared with the wintertime case as shown in Figure 4.4. In all, black carbon generates a decrease of 10566 mm (52%) across the domain. The marked changes from the precipitation reduced by black carbon in the wintertime case and the summertime case suggest a trend that is further explored in Chapter 7.

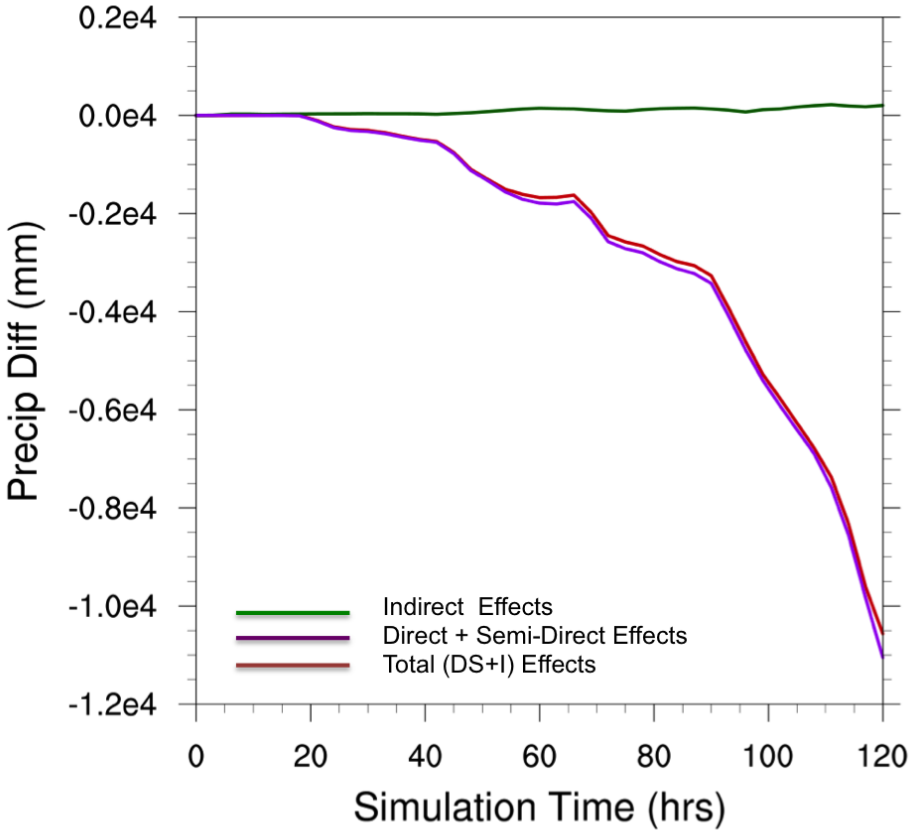

Figure 6.3: Summertime Case: Domain Averaged Time Series of Black Carbon Effects-Based Precipitation (mm). Precipitation difference due to black carbon (red) is obtained by subtracting the time series in black from the time series in pink in Figure 6.2. The precipitation can also be separated into direct and semi-direct effects (purple) on precipitation and indirect effects (green) on precipitation. Contrary to the wintertime case, the total precipitation difference sides very closely with that of direct and semi-direct effects, while the indirect effects on precipitation remain relatively unchanged. This marked change from the wintertime case further suggests a seasonal trend which is discussed in Chapter 7.

6.4 Non-Convective and Convective Precipitation Differences Due to Black Carbon

The following sections look at precipitation in two categories—convective and non-convective precipitation—as described in Section 4.5.

6.4.1 Convective Precipitation

Nearly all of the 40% of the precipitation decrease is from the direct and semi-direct effects of black carbon (Figure 6.4a). Precipitation due to the direct and semi-direct effects start to decrease markedly at the 60^{th} hour, and, like the 7–11 January 2005 case, this starts at the same time as the maximum surface temperature decrease (Figure 6.4b). We also note that the decrease in surface temperature is stronger during the summertime case (2 K) compared with the wintertime case (0.5K) as shown in Figure 4.8. This surface temperature decrease is observed in the domain averaged vertical temperature profile (Figure 6.5). By contrast, the indirect effects of black carbon show essentially no changes to surface temperature, foregoing even the diurnal effects. This lack of diurnal variation from the indirect effects suggests that the over indirect effects is weaker in the summertime case than in the wintertime case due to the lowered amount of water vapor available to form clouds. The domain averaged vertical temperature profile also exhibits warming in the midlevels of the atmosphere. Because of the strengthened column stability, we also observe a decrease in convective precipitation, as the Grell-Freitas convective scheme depends on column stability (greater the cap, the less convection scheme is used) (Grell and Freitas, 2014). Throughout the time period, there is also a decrease in the potential temperature tendency from the cumulus scheme (Figure 6.4c), which is expected from a decrease in convective precipitation.

6.4.2 Non-Convective Precipitation

Non-convective precipitation due to black carbon in both the indirect, and direct and semi-direct effects varies, but changes by two orders of magnitude less than that of convective precipitation. Different from the wintertime rain event, the summertime rain event shows an increase in non-convective precipitation. (Figure 6.6).

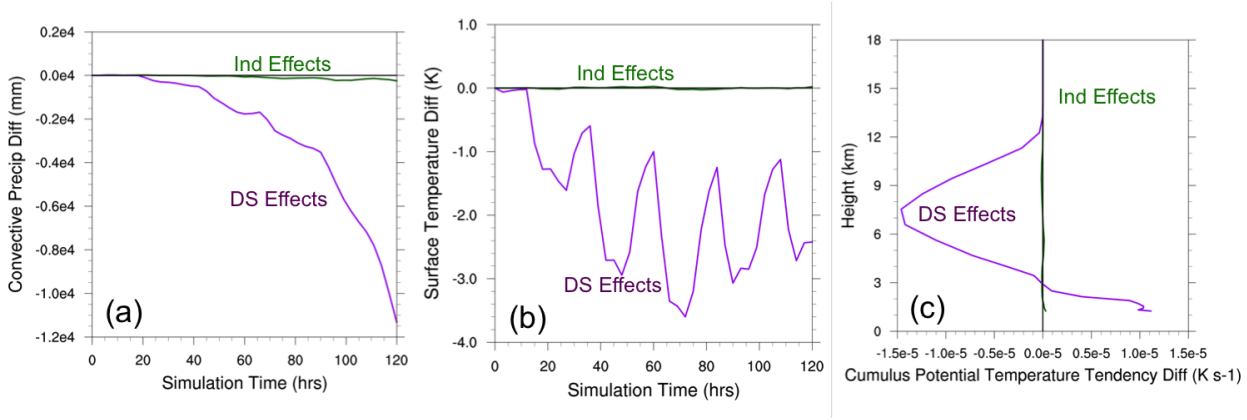

Figure 6.4: Summertime Case: Domain Averaged Time Series of Black Carbon Effects-Based Convective Precipitation (mm), Surface Temperature (K); and Domain Averaged Vertical Profile of Black Carbon Effects-Based Cumulus Potential Temperature Tendency (K/s^{-1}). (a) Convective precipitation in the summertime case closely reflects that of the overall behavior of the precipitation decrease due to black carbon (red) in Figure 6.3, where the bulk of the precipitation decrease is due the direct and semi-direct effects (purple) of black carbon. Indirect effects (green) of black carbon changes precipitation is very small. (b) The precipitation decrease also exhibits a similar acceleration with the strengthening in surface dimming—at approximately the 60^{th} hour with the direct and semi-direct effects (purple) of black carbon. The decrease in surface temperature is stronger during the summertime case (0.5 K) compared with the wintertime case (0.1 K) as shown in Figure 4.8. This enhanced stability is due to the strengthened warming aloft from solar radiation absorption from decreased cloud availability (cloud formation from heat lows rather than a mesoscale low pressure frontal system) in the direct and semi-direct mechanism, making the atmosphere more stable in the summertime case. By contrast, the indirect effects (green) of black carbon show essentially no changes to surface temperature, foregoing even the diurnal effects. This lack in diurnal variation form the indirect effects suggests that the over indirect effects is weaker in the summertime case than in the wintertime case due to the lowered amount of available water vapor to form clouds. (c) This stability from the direct and semi-direct effects (purple) from black carbon reduces the potential temperature tendency from cumulus scheme, but causes no changes to the same by the indirect effects (green).

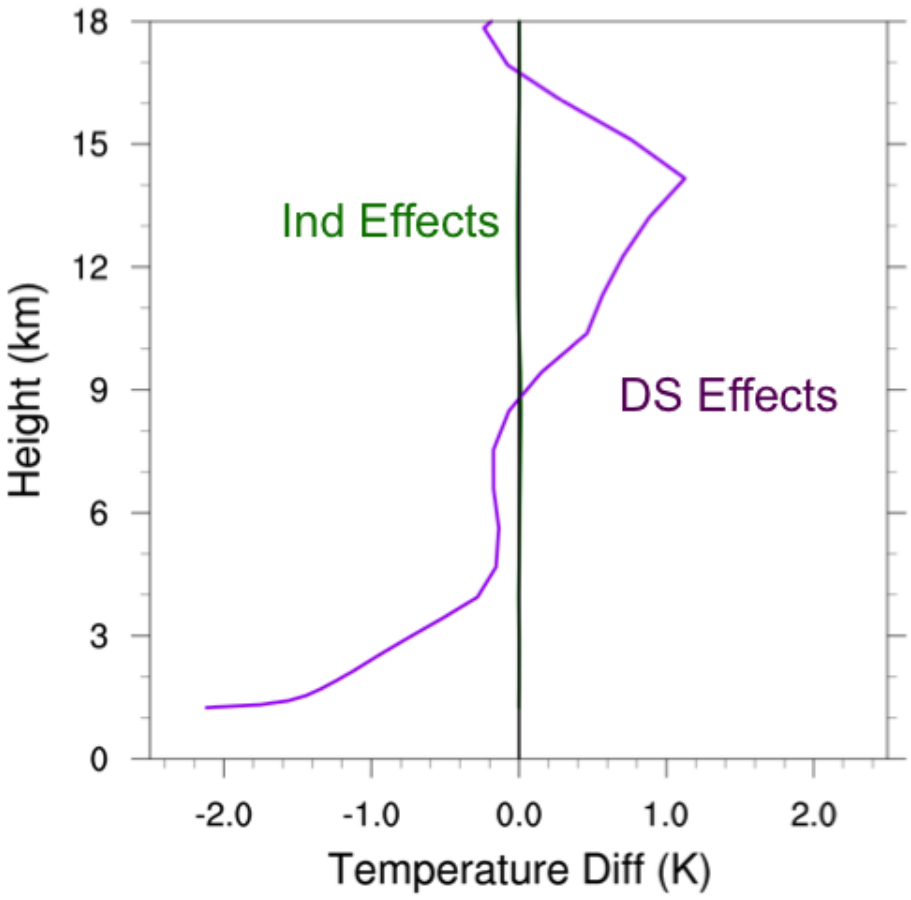

Figure 6.5: Summertime Case: Domain Averaged Vertical Profile of Black Carbon Effects-Based Temperature (K). This vertical temperature profile shows warming aloft by approximately 1 K and surface temperature cooling below by over 2 K due to the direct and semi-direct effects (purple). Little to no change is caused by the indirect effects on temperature (green).

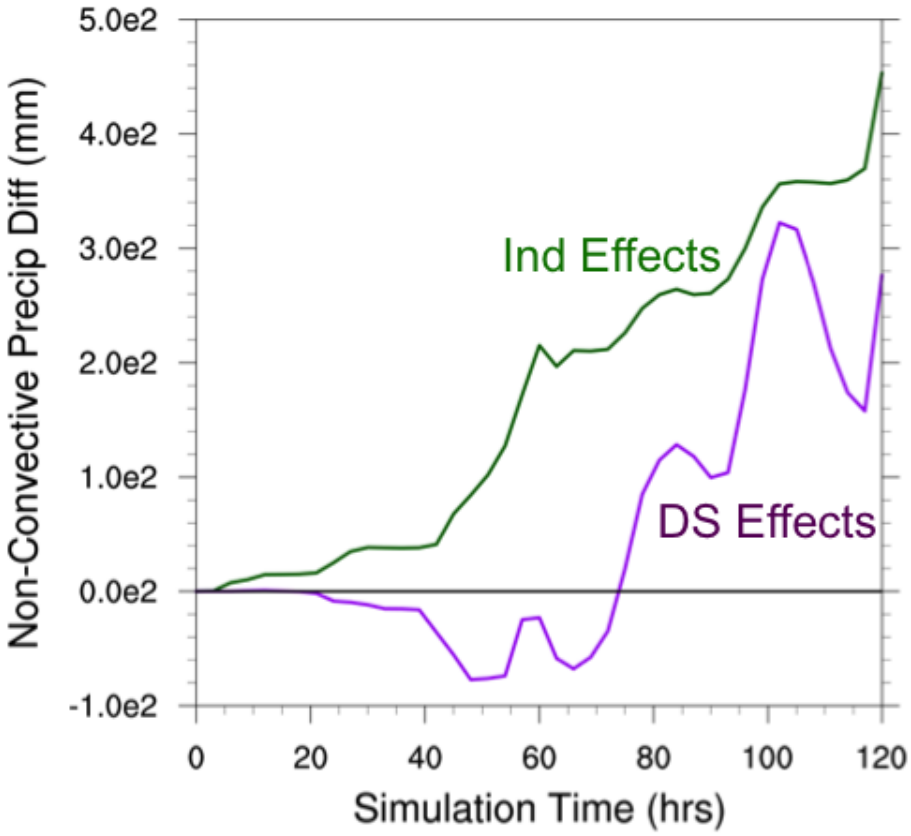

Figure 6.6: Summertime Case: Domain Averaged Times Series of Black Carbon Effects-Based Non-Convective Precipitation (mm). Non-convective precipitation shows an increase in precipitation due to direct and semi-direct effects (purple) of black carbon of two orders less than that of the decrease in convective precipitation shown in Figure 6.4a. Opposite to the wintertime case, non-convective precipitation due to indirect effects (green) of black carbon shows an increase.

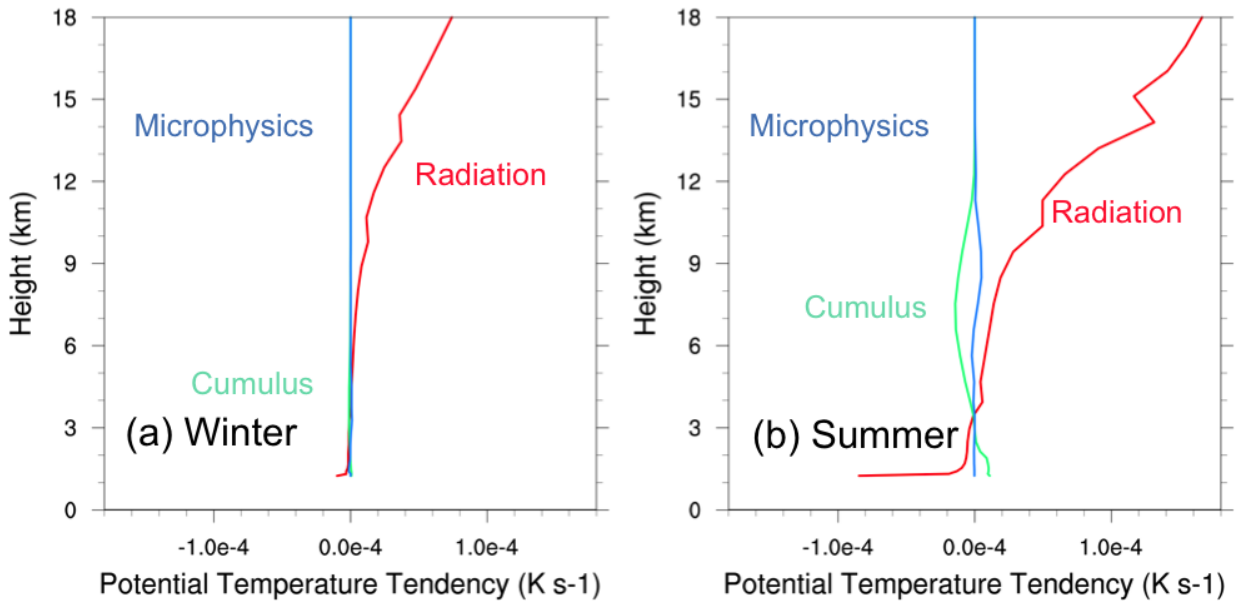

Figure 6.7: Summertime and Wintertime Cases: Domain Averaged Vertical Profile of Black Carbon Effects-Based Microphysics, Cumulus, Radiation Potential Temperature Tendencies (K/s^{-1}). The domain averaged vertical microphysics (blue), cumulus (teal), and radiation (red) potential temperature tendencies due to the direct and semi-direct, and indirect effects of black carbon in the (a) wintertime and (b) summertime show a marked increase in radiation potential temperature tendency. In both the wintertime and summertime Cases, incoming solar radiation is absorbed near the top of the atmosphere where black carbon is lofted. However, in the summertime case, the incoming solar radiation is stronger owing to an increased amount of daylight and reduced cloud, as described in Section 7.2. As such, the atmosphere is more stable, which cools the potential temperature tendency from the cumulus scheme. The potential temperature tendency from the microphysics scheme has no significant changes in either the wintertime or summertime cases.

6.5 Discussion

Thus far, black carbon has decreased precipitation in both a wintertime rain event of a synoptic-scale low-pressure system and a summertime warm core low rain event of localized low-pressure centers. In both the wintertime non-convective and the summertime convective rain event, it is the convective rainfall of the direct and semi-direct effects that is reduced to black carbon. This indicates the importance of the convection scheme used, and in this research, the importance of the stability layer. Moreover, in both cases, the timing of the surface temperature reduction marks the strengthening of the surface dimming, and well corresponds to the timing of accelerated precipitation decrease. Furthermore, the results also indicate the large role of the incoming solar radiation, as depicted by the comparison between the potential temperature tendency changes due to radiation, convection, and microphysics (Figure 6.7).

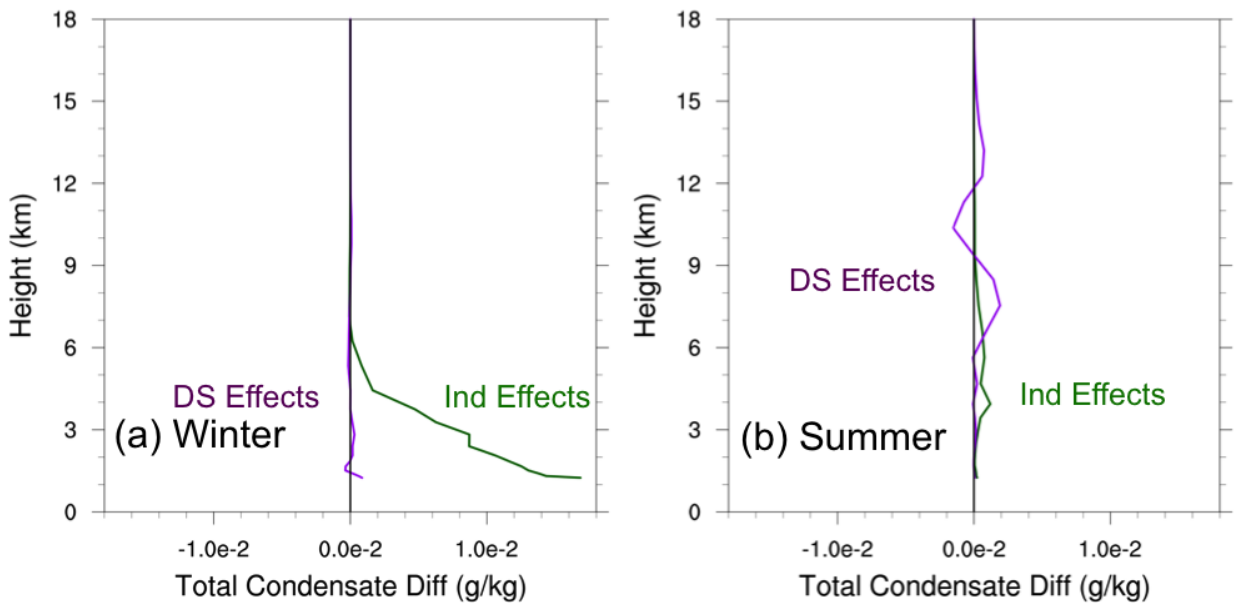

Figure 6.8: Summertime and Wintertime Cases: Domain Averaged Vertical Profile Black Carbon Effects-Based Condensate (g/kg). (a) The domain averaged vertical profiles of condensate (sum of rain, water, graupel, ice, snow mixing ratios) due to black carbon in the wintertime case show an increase in condensate largely due to the increase in water mixing ratio from the indirect effects (green) of black carbon, which uses black carbon as a cloud condensation nuclei to create more, smaller cloud droplets. The direct and semi-direct effects (purple) of black carbon contribute an insignificant amount to total condensate. (b) In the summertime case, the indirect effects (green) of black carbon creates more cloud, which contributes to the small increase in condensate. The direct and semi-direct effects (purple) of black carbon show an increase in condensate in the midlevels of the atmosphere with ice multiplication (Medrano, 2008). Overall, neither the indirect effects (green) nor the direct and semi-direct effects (purple) of black carbon causes significant change in condensate.

A difference between the wintertime case and the summertime case is the behavior of the precipitation due to the indirect effects in the non-convective rainfall. In the wintertime case, the indirect effects lead to a decrease in precipitation, while in the summertime case, the indirect effects lead to an increase in precipitation. The wintertime decrease fits the definition of the indirect effects where there is an increase in cloud drop number contributing to more condensate (Figure 6.8) and a decrease in cloud water effective radius (Figure 4.3). The increase in non-convective precipitation from the indirect effects summertime rain event are not associated with an increase in condensate, suggesting that this precipitation is insignificant.

6.6 A Note About the Black Carbon Emissions Dataset

The summertime case with black carbon inclusion produces a deviation in precipitation from the simulation without black carbon that is large enough (52%) decrease is large enough to study precipitation behavior based on varying black carbon emission. The current black carbon emission is a uniform emission at all horizontal and vertical grid points of 0.01 μg/kg-dry air Aitken mode black carbon and 0.04 μg/kg-dry air accumulation mode black carbon. Additionally, we used black carbon emission from the National Emissions Inventory (NEI) 2005, uniform black carbon at the surface, and uniform black carbon from the surface to 3 km.

From simulations using these black carbon emissions, we find that whether emissions are lofted from the surface or already lofted higher into the atmosphere, the black carbon generates a decrease in precipitation with the exception of the NEI emissions, which generate a 0.1% increase in precipitation. This increase is small and is likely due to uncertainty within the model. Uniform black carbon at the surface decreases precipitation by 4%, uniform black carbon up to 3 km reduces precipitation by 33% (Figure 6.9).

The potential temperature tendency from total radiation responds in a similar fashion, as there is a large response toward the top of the atmosphere compared to potential temperature tendency changes from the cumulus and microphysics schemes. This signifies the absorption of incoming solar radiation at the very top where black has been vertically mixed and lofted (Figure 6.10). The response from NEI is generates output too small for comparison.

The behavior of the potential temperature tendency from radiation translates into warming in the upper levels and cooling at the surface for all black carbon emission variations other than NEI. The increase in temperature is similar to that of Chen et al. (2016) (Figure 6.11). Therefore, while black carbon emission used in this research is not representative of current black carbon emissions, it does present clearest affects of black carbon for interpretation to achieve our goals in understanding how the atmosphere responds to black carbon.

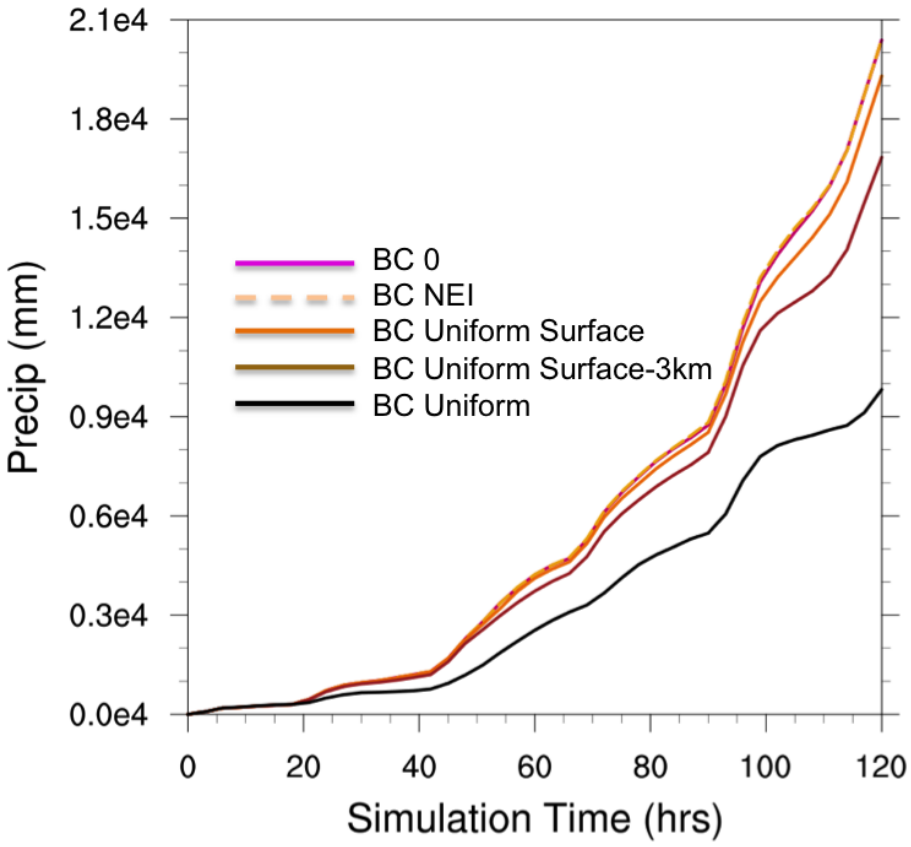

Figure 6.9: Summertime Case: Accumulated Precipitation (mm) with Varying Black Carbon Emissions. Accumulated precipitation from various black carbon emissions (yellow dotted, yellow, orange, brown, black) and without black carbon (pink) show a significant difference between each emission. In all, uniform black carbon generates a decrease of 10566 mm (52%) decrease across the domain (percentage difference of the black line from pink line). The domain accumulated precipitation with NEI black carbon amounts to 20408 mm (0.1% increase, dotted yellow); domain accumulated precipitation with uniform black carbon at the surface amounts to 19548 mm (4% decrease, orange); and domain accumulated precipitation with uniform black carbon at the surface amounts to 13572 mm (33% decrease, brown).

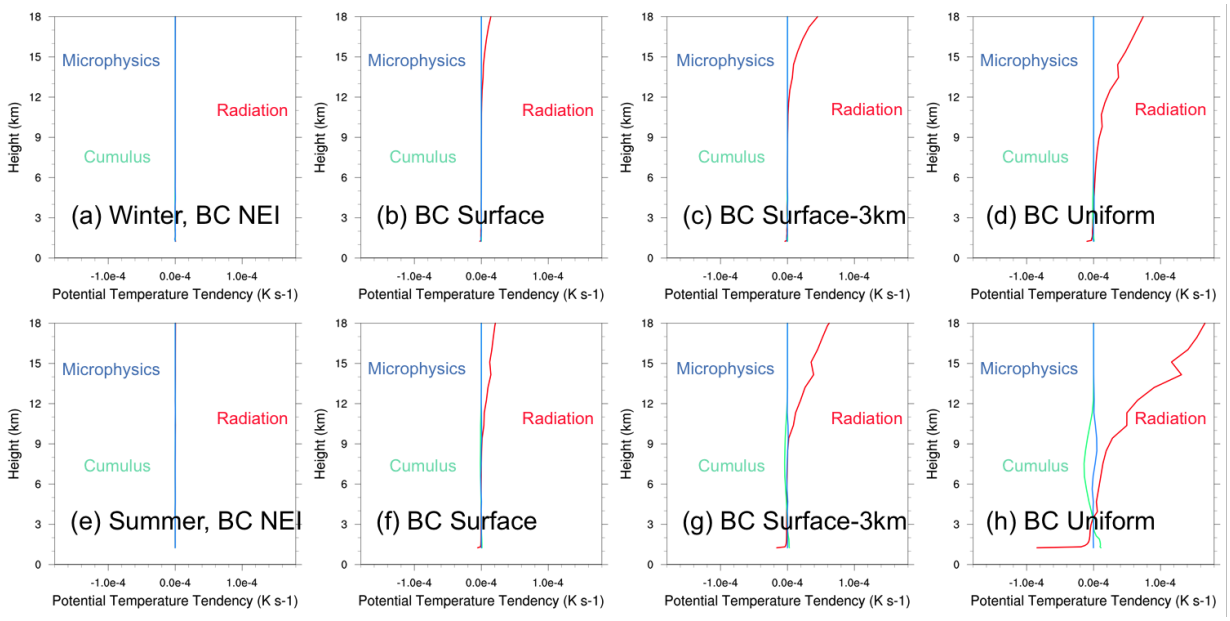

Figure 6.10: Summertime and Wintertime Cases: Domain Averaged Vertical Profile of Black Carbon Effects-Based Microphysics, Cumulus, Radiation Potential Temperature Tendencies (K/s^{-1}) for Varying Black Carbon Emissions. The domain averaged vertical profiles of microphysics (blue), cumulus (teal), and radiation (red) potential temperature tendencies due to indirect, and direct and semi-direct effects of black carbon in the wintertime (a–d) case and (e-h) summertime case for various black carbon emissions: (a,e) National Emissions Inventory 2005; (b,f) uniform black carbon at the surface; (c,g) uniform black carbon from the surface to 3 km; and (d,h) uniform black carbon emissions. Black carbon emissions, whether emitted at the surface or higher in the atmosphere, all show an increase in potential temperature tendency from radiation in the highest level. This indicates that warming begins where black carbon is lofted into the highest levels, regardless of the black carbon's level of emission. Because we are focused on investigating how black carbon influences precipitation by way of changes in the atmosphere, we focus on the results generated from (d,h) uniform black carbon emissions, which show the most drastic black carbon changes.

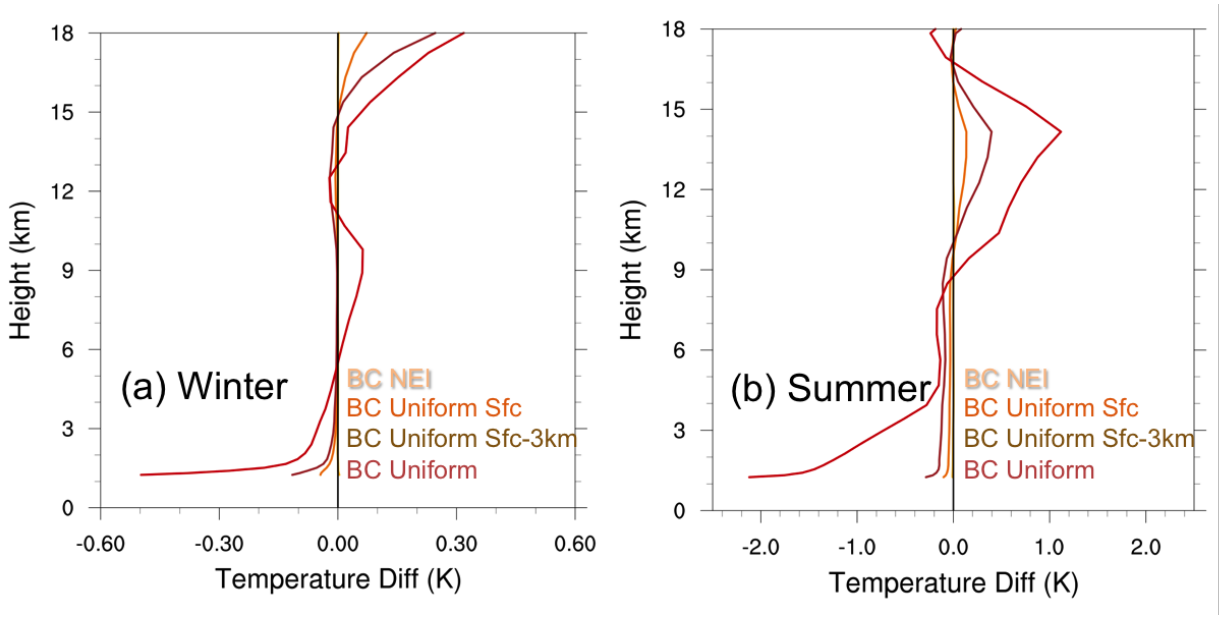

Figure 6.11: Summertime and Wintertime Cases: Domain Averaged Vertical Profile of Black Carbon Effects-Based Temperature (K) for Varying Black Carbon Emissions. The domain averaged vertical temperature in the (a) wintertime and (b) summertime cases due for various black carbon emissions are shown here. Varying emissions are as follows: National Emissions Inventory 2005 (yellow), uniform black carbon at the surface (orange), uniform black carbon from the surface to 3 km (brown) and uniform black carbon emissions (red). Black carbon emissions, whether emitted at the surface or higher in the atmosphere, all show a similar trend in temperature—warming in the upper levels and cooling in the lower levels—that stabilizes the atmosphere. As such, we look at the results generated from uniform black carbon emissions (red). These profiles are of total black carbon effects: direct, semi-direct, and indirect effects.

Chapter 7

Effects of Black Carbon on Precipitation on Month-Long Timescales: January to June 2005

7.1 Synoptic Background and Goals

To take full advantage of investigating black carbon effects, we also studied black carbon effects on the month-long time scale for the months of January to June 2005. Each month is treated as a discrete month, with the simulated month starting from last day of the previous month and ending on the 00Z hour of the first day of the following month. A general synopsis of the weather pattern for each month is given in Figure 7.1. Monthly rainfall amounts simulated with and without black carbon are listed in Table 7.1.

The goals for this case study are: 1) to study the precipitation behavior due to black carbon on month-long timescales, 2) to map out the pathways by which black carbon changes precipitation, and 3) to determine the relative significance of each pathway.

In January, there are multiple low-pressure systems in transit from the Pacific to the western United States. It is during this time that the 7–11 January 2005 Pineapple Express event occurs. During the middle of the month, a strong high pressure strengthens to 1037 mb, keeping precipitation at bay for nearly half of the month. Toward the end of the month, the high pressure weakens and low-pressure centers are allowed to move inland before an area of high pressure builds once again.

The pattern in February is generally stable in the first half of the month, as a high pressure center provides subsidence for much of the western United States. In the second half, however, a stationary boundary provides the instability that generates precipitation.

The pattern in March is similar to that of February, where the first half of the month is relatively stable. Once the high pressure weakens, a series of low pressure centers and their associated fronts make their way over the western United States, bringing with them about as much precipitation as in February.

The pattern in April is largely unstable. Multiple fast-progressing low pressure centers and frontal systems move through western United States during this spring month.

In May, the synoptic pattern shows general instability for much of the month. The multiple low pressure centers and frontal system provide the instability needed for ample precipitation generated during this spring month.

This instability continues throughout June, when heat lows begin to be the source of localized precipitation. The precipitation total for this month is less than that for May, and the precipitation itself happens more in the inland states rather than California.

7.2 Accumulated Precipitation Difference Due to Black Carbon

Figure 7.2 and Table 7.1 show the accumulated precipitation at 00Z on the day after the previous month for the entire domain, with and without black carbon. All months saw a reduction in precipitation from the inclusion of black carbon, strengthening with a general decrease from the winter months (January to March) to the spring months (April to June). Because the months vary with meteorology (black carbon emissions remain the same), the increase in percentage difference in precipitation due to black carbon is attributed to variation in month meteorology itself. This is particularly evident when comparing January and May results. Both January and May accumulate approximately the same amount of precipitation across the domain, but black carbon reduces the precipitation in January by just 4% and in May by 40%, an order of magnitude of difference.

Therefore, it is important to discuss the difference between January and May. The standout difference is the number of daylight hours. January has approximately 10-10.5 daylight hours each day, whereas May has approximately 13.5-14 daylight hours each day (United States Naval Observatory, 2016) (Figure 7.3). This additional 35% increase in daylight hours has a remarkable effect on the meteorology over the western United States. Additional daylight heating means additional shortwave radiation availability, which, in the presence of black carbon, translates into

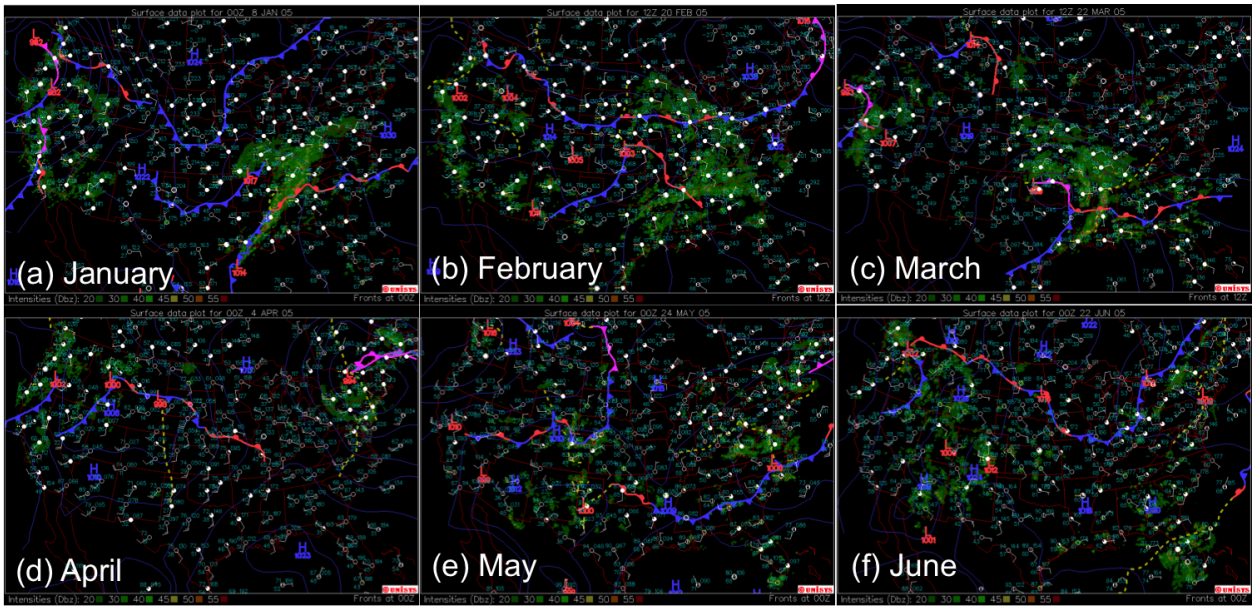

Figure 7.1: Monthly Cases (January to June 2005): A Synoptic Outlook for January–June. The typical synoptic pattern for (a) January through (e) June 2005 of the simulation as analyzed by the surface analysis (UNISYS Weather, 2016). (a) In January, the synoptic pattern is one that has multiple low-pressure systems transiting from the Pacific to the western United States. (b) February is generally stable in the first half of the month as a high pressure provides subsidence for much of the western United States. In the second half of the month, however, a stationary boundary provides the instability that generates precipitation. (c) March is like February, where the first half is relatively stable and the second half sees a series of low pressure centers and its associated fronts. (d) April is largely unstable with multiple fast-progressing low pressure centers and frontal systems. (e) In May, the synoptic pattern shows general instability for much of the month. This instability continues throughout June (f), when heat lows begin to be the source of localized precipitation.

	No BC (mm)	BC Uni (mm)	BC Uni - BC0	%
Jan	222741	213653	-9087	-4%
Feb	155930	135279	-20651	-13%
Mar	154664	136917	-17747	-11%
Apr	139922	99126	-40796	-29%
May	224990	134150	-90840	-40%
Jun	165365	78824	-86541	-52%

Table 7.1: Monthly Cases: Accumulated Precipitation Totals (mm) Simulated with and without Black Carbon. Accumulated precipitation totals for January to June 2005. The months with the highest precipitation are January and May, although the percentage differences due to black carbon differ by one order of magnitude with January decrease due to black carbon being -4% and May decrease being -40%. All months saw a decrease in precipitation due to black carbon, with a steady increase from 4% in January to 52% in June signifying a trend.

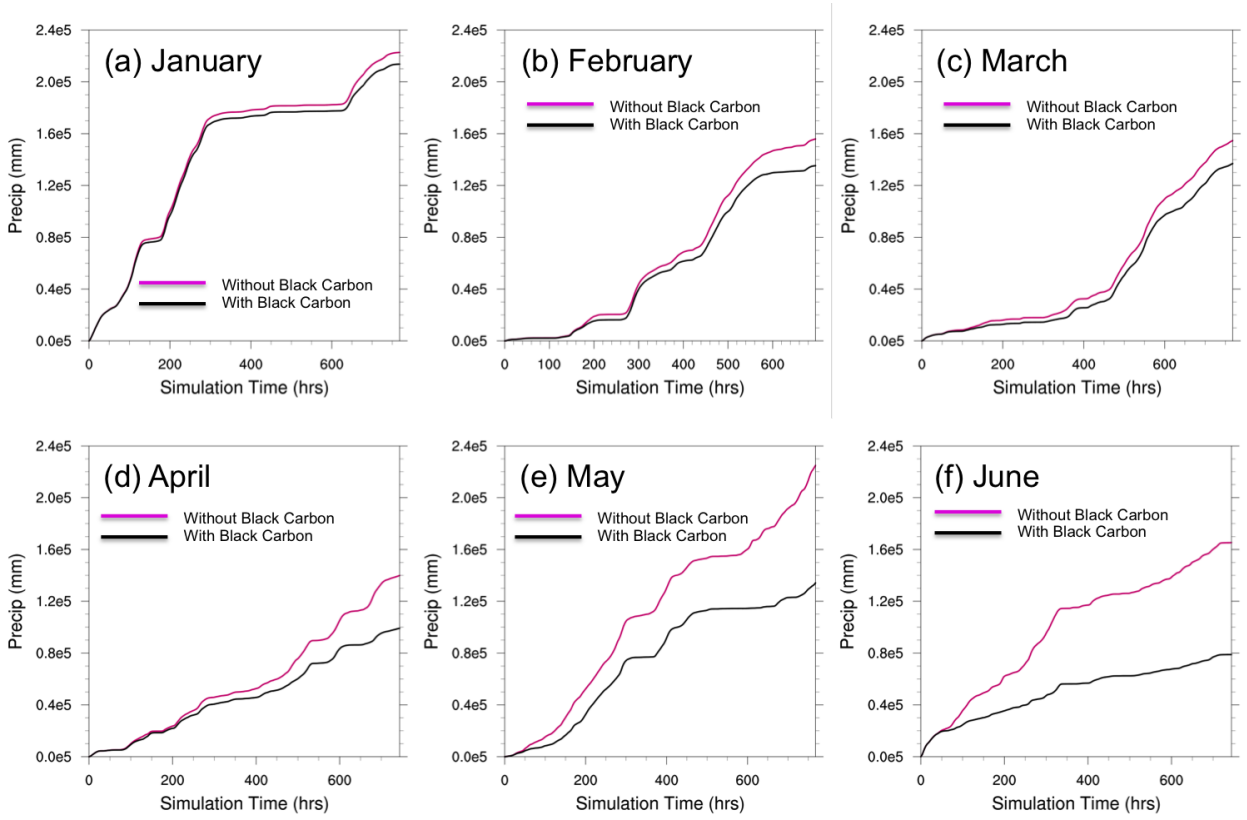

Figure 7.2: Monthly Cases: Domain Averaged Time Series of Accumulated Precipitation (mm) Simulated with and without Black Carbon for January–June. Accumulated precipitation with (black) and without (pink) black carbon from (a–f) January to June 2005 show the monthly precipitation trend where black carbon reduces more precipitation in the spring months of (d–e) April to June than in the winter months of (a–c) January to March. The months with the highest precipitation without black carbon are (a) January and (e) May, although the percentage differences due to black carbon differ by one order of magnitude with January decrease due to black carbon of -4% and May decrease of -40%. All months saw a decrease in precipitation due to black carbon with a steady decrease from -4% in January to -52% in June, signifying a trend that is discussed later in this Chapter.

Location: W118 22, N34 05 (o , o ,)

LOS ANGELES, CALIFORNIA
Pacific Standard Time

Astronomical Applications Dept.
U. S. Naval Observatory
Washington, DC 20392-5420

Duration of Daylight for 2005

Day	Jan.	Feb.	Mar.	Apr.	May	June	July	Aug.	Sep.	Oct.	Nov.	Dec.
	h m	h m	h m	h m	h m	h m	h m	h m	h m	h m	h m	h m
01	09:56	10:34	11:28	12:34	13:34	14:17	14:23	13:49	12:52	11:49	10:47	10:03
02	09:57	10:36	11:30	12:36	13:35	14:18	14:23	13:48	12:50	11:47	10:45	10:02
03	09:57	10:37	11:32	12:38	13:37	14:19	14:22	13:46	12:48	11:45	10:43	10:01
04	09:58	10:39	11:35	12:40	13:39	14:19	14:21	13:44	12:46	11:43	10:41	10:00
05	09:59	10:41	11:37	12:42	13:41	14:20	14:21	13:43	12:44	11:41	10:40	09:59
06	10:00	10:43	11:39	12:45	13:42	14:21	14:20	13:41	12:41	11:39	10:38	09:59
07	10:00	10:44	11:41	12:47	13:44	14:21	14:19	13:39	12:39	11:37	10:36	09:58
08	10:01	10:46	11:43	12:49	13:46	14:22	14:19	13:38	12:37	11:35	10:35	09:57
09	10:02	10:48	11:45	12:51	13:47	14:23	14:18	13:36	12:35	11:32	10:33	09:57
10	10:03	10:50	11:47	12:53	13:49	14:23	14:17	13:34	12:33	11:30	10:31	09:56
11	10:04	10:52	11:49	12:55	13:51	14:24	14:16	13:32	12:31	11:28	10:29	09:55
12	10:05	10:54	11:51	12:57	13:52	14:24	14:15	13:30	12:29	11:26	10:28	09:55
13	10:06	10:56	11:54	12:59	13:54	14:24	14:14	13:29	12:27	11:24	10:26	09:55
14	10:08	10:58	11:56	13:01	13:55	14:25	14:13	13:27	12:25	11:22	10:25	09:54
15	10:09	11:00	11:58	13:03	13:57	14:25	14:12	13:25	12:23	11:20	10:23	09:54
16	10:10	11:02	12:00	13:05	13:58	14:25	14:11	13:23	12:21	11:18	10:22	09:54
17	10:11	11:04	12:02	13:07	14:00	14:25	14:10	13:21	12:19	11:16	10:20	09:53
18	10:12	11:06	12:04	13:09	14:01	14:26	14:09	13:19	12:16	11:14	10:19	09:53
19	10:14	11:08	12:06	13:11	14:02	14:26	14:07	13:17	12:14	11:12	10:17	09:53
20	10:15	11:10	12:09	13:13	14:04	14:26	14:06	13:16	12:12	11:10	10:16	09:53
21	10:17	11:12	12:11	13:15	14:05	14:26	14:05	13:14	12:10	11:08	10:14	09:53
22	10:18	11:14	12:13	13:17	14:06	14:26	14:04	13:12	12:08	11:06	10:13	09:53
23	10:19	11:16	12:15	13:19	14:07	14:26	14:02	13:10	12:06	11:04	10:12	09:53
24	10:21	11:18	12:17	13:21	14:09	14:25	14:01	13:08	12:04	11:02	10:11	09:53
25	10:22	11:20	12:19	13:23	14:10	14:25	14:00	13:06	12:02	11:00	10:09	09:53
26	10:24	11:22	12:21	13:24	14:11	14:25	13:58	13:04	12:00	10:58	10:08	09:54
27	10:26	11:24	12:23	13:26	14:12	14:25	13:57	13:02	11:58	10:56	10:07	09:54
28	10:27	11:26	12:26	13:28	14:13	14:24	13:55	13:00	11:55	10:54	10:06	09:54
29	10:29		12:28	13:30	14:14	14:24	13:54	12:58	11:53	10:53	10:05	09:55
30	10:30		12:30	13:32	14:15	14:24	13:52	12:56	11:51	10:51	10:04	09:55
31	10:32		12:32		14:16		13:51	12:54		10:49		09:56

Figure 7.3: Duration of Daylight for the Year 2005. The length of daylight hours is critical to understanding how black carbon changes accumulated precipitation. In 2005, January 2005 has 10 to 10.5 hours of daylight hours. This time lengthens to 13.5 to 14 hours in May and to 14 to 14.5 hours in June (United States Naval Observatory, 2016).

heating aloft and cooling at the surface (surface dimming). The result of the heating and surface dimming Figure 7.4 is a more stabilized atmosphere, in January and even more enhanced in May. This heating also renders a decrease in total condensate (largely due to the decrease in snow mixing ratio, not shown) in May, as depicted in Figure 7.5b. A decrease in condensate would further allow incoming solar radiation to be absorbed by the black carbon aloft (Figure 7.6), which further reduces surface temperature. In January, there is an increase in condensate, largely due to the indirect effects of black carbon, creating an increased number of cloud droplets (Figure 7.5a).

7.3 Black Carbon Effects-Based Precipitation Difference

Separating the precipitation decrease into black carbon effects-based precipitation, as shown in Figure 7.7 and Table 7.2, we see the precipitation decrease is mainly due to the direct and semi-direct effects on precipitation. The contribution from the indirect effects is minimal. Also, the total

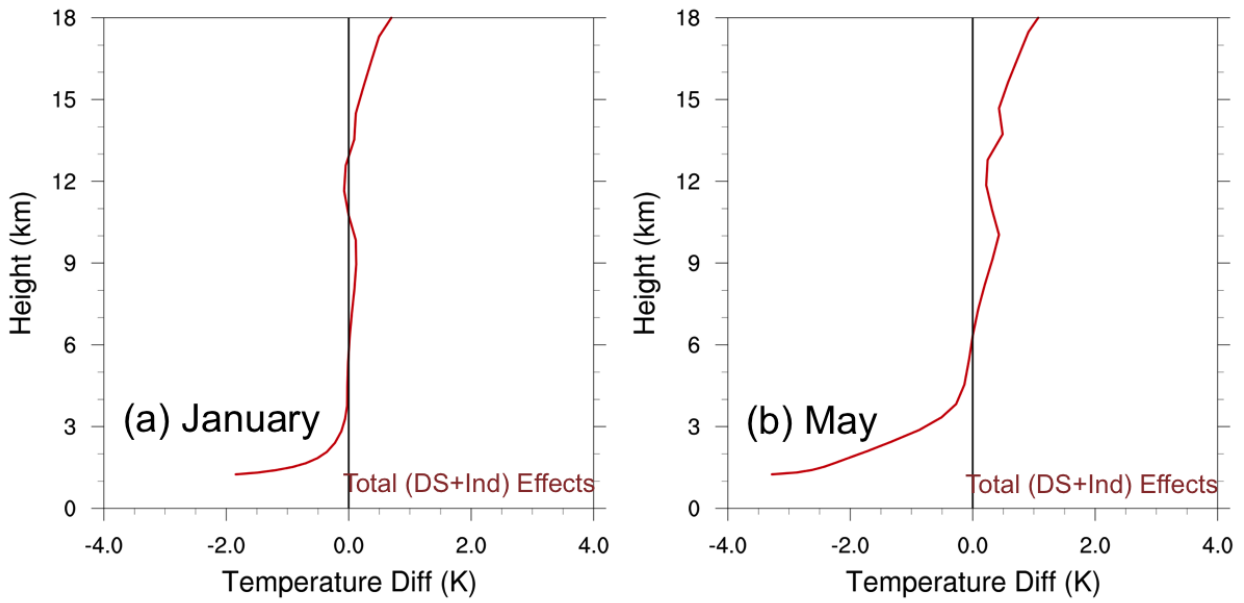

Figure 7.4: Monthly Cases: Domain Averaged Vertical Profile of Black Carbon Effects-Based Temperature (K) due to Black Carbon for January and May. The domain averaged vertical temperature profiles due to indirect, and direct and semi-direct effects of black carbon in (a) January and (b) May show heating aloft and cooling at the surface, more enhanced in May than in January. This is the result of the additional available daylight hours (7.3 that allows more incoming shortwave radiation for absorption by black carbon. This heating and surface dimming stabilizes the atmosphere.

precipitation decrease closely matches the timing of the strengthening of the surface temperature decrease (Figure 7.8), just as it did in the wintertime and summertime cases, signifying the role column stability has in precipitation reduction. These times are approximately: (a) January: 648$^{\text{th}}$ hour, (b) February: 498$^{\text{th}}$ hour, (c) March: 198$^{\text{th}}$ hour, (d) April: 501$^{\text{st}}$ hour, (e) May: 15$^{\text{th}}$ and 561$^{\text{st}}$ hours, (f) June: 15$^{\text{th}}$ hour.

7.4 Non-Convective and Convective Precipitation Differences Due to Black Carbon

The following sections look at precipitation in two categories—convective and non-convective precipitation—as described in Section 4.5.

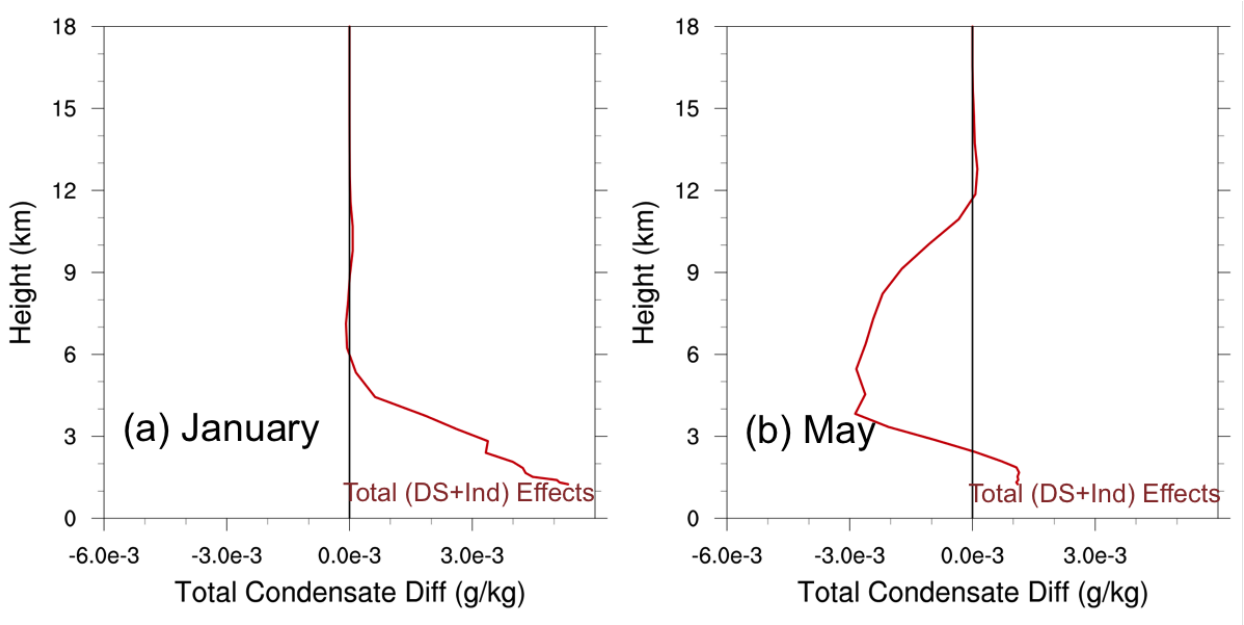

Figure 7.5: Monthly Cases: Domain Averaged Vertical Profile of Black Carbon Effects-Based Total Condensate (g/kg) due to Black Carbon for January and May. The domain averaged vertical condensate profile due to indirect, and direct and semi-direct effects of black carbon in (a) January and (b) May show an increase in condensate in January and a decrease in condensate in May. This increase in condensate in January is largely due to the increase in cloud water mixing ratio (not shown). The decrease in condensate in May is largely due to the decrease in rain and cloud water mixing ratios (not shown) from enhanced heating (drying).

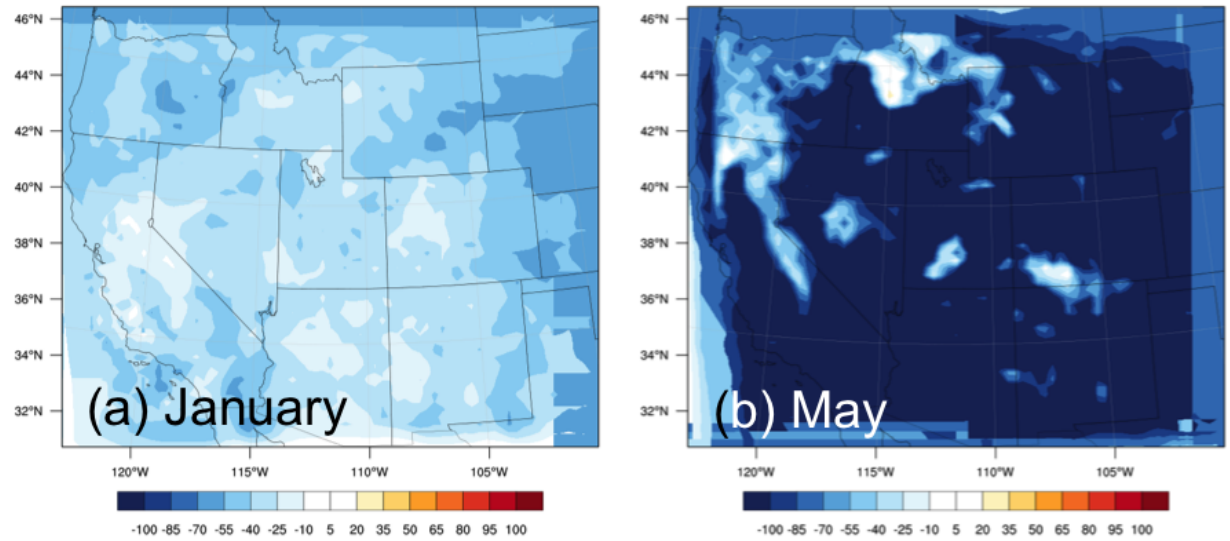

Figure 7.6: Monthly Cases: Month-Long Time Averaged Downward Shortwave Flux at the Surface (W/m^2) due to Black Carbon for January and May. The month-long time averaged shortwave radiation at the surface due to direct, semi-direct, and indirect effects of black carbon in (a) January and (b) May indicate the decrease of shortwave radiation reaching the surface in May compared with January. This is indicative of the surface dimming strengthening that occurs in May compared with January in Figure 7.4.

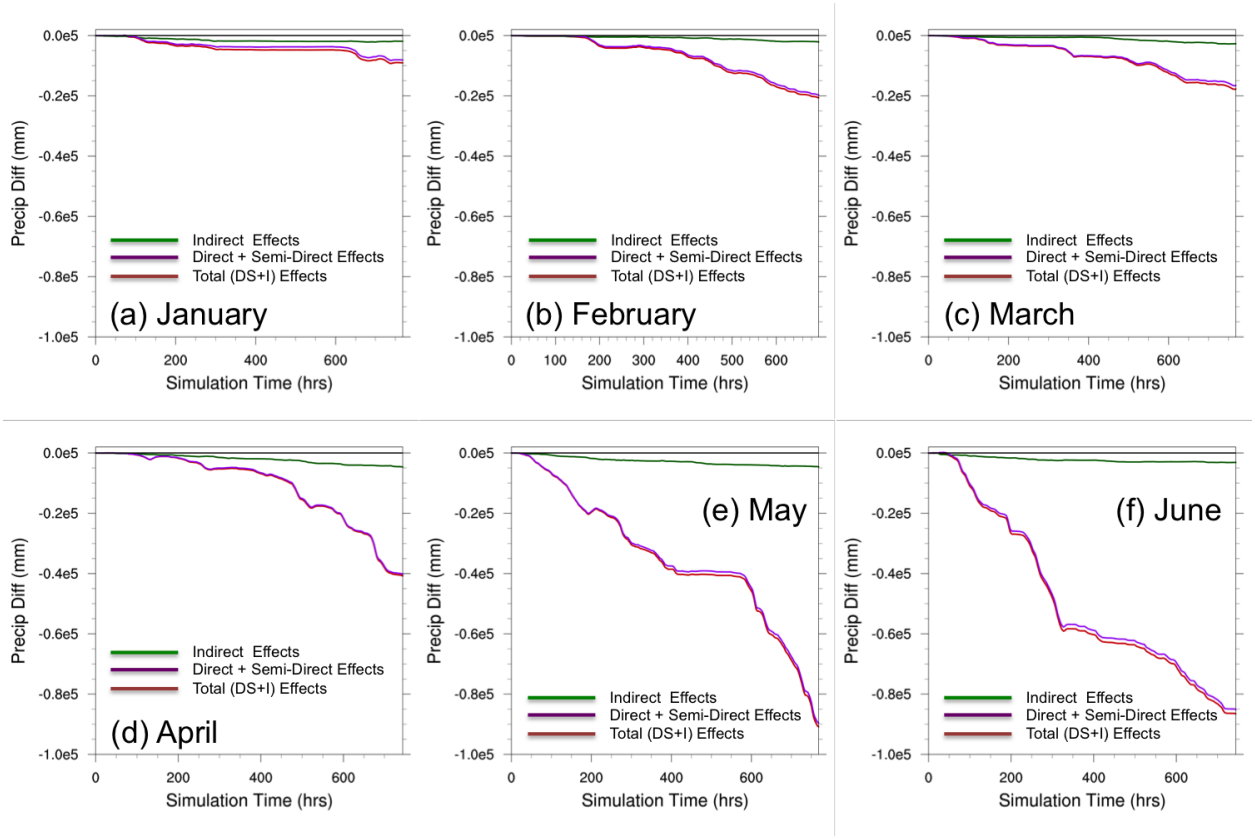

Figure 7.7: Monthly Cases: Domain Averaged Time Series of Black Carbon Effects-Based Precipitation (mm) for January–June. Black carbon effects-based precipitation difference in (a) January through (f) June show the decrease in precipitation being mostly due to the direct and semi-direct effects (purple), hence, the nearly indistinguishable lines between total black carbon effects (red) and direct and semi-direct effects (purple) of black carbon. Indirect effects (green) precipitation is a minor contributor to the overall precipitation decrease when compared with the total precipitation decrease due to black carbon (red). Amount of precipitation decrease due to the each of the effects of black carbon is given in Table 7.2. Percentage of decrease from simulations without black carbon are given in Table 7.1.

	Indirect		Direct + Semi-Direct		DS NC to C Ratio
	Conv (mm)	Non-Conv (mm)	Conv (mm)	Non-Conv (mm)	
Jan	-669	-1233	-6994	-1117	16%
Feb	-768	-1323	-12358	-7392	60%
Mar	-998	-1704	-11911	-4673	39%
Apr	-1462	-3152	-23470	-16805	72%
May	-2790	-1790	-59177	-30403	51%
Jun	-2433	-701	-62590	-22498	36%

Table 7.2: Monthly Cases: Black Carbon Effects-Based Convective and Non-Convective Precipitation (mm) Totals. Black carbon effects-based precipitation difference from January to June shows the amount of precipitation decrease due to each of the black carbon effects. The decrease in precipitation is mostly due to the direct and semi-direct effects of black carbon on precipitation. Indirect effects (green) on precipitation make minor contributions to the overall precipitation decrease. The far right column gives the ratio of precipitation decrease due to non-convective and convective precipitation from the direct and semi-direct effects.

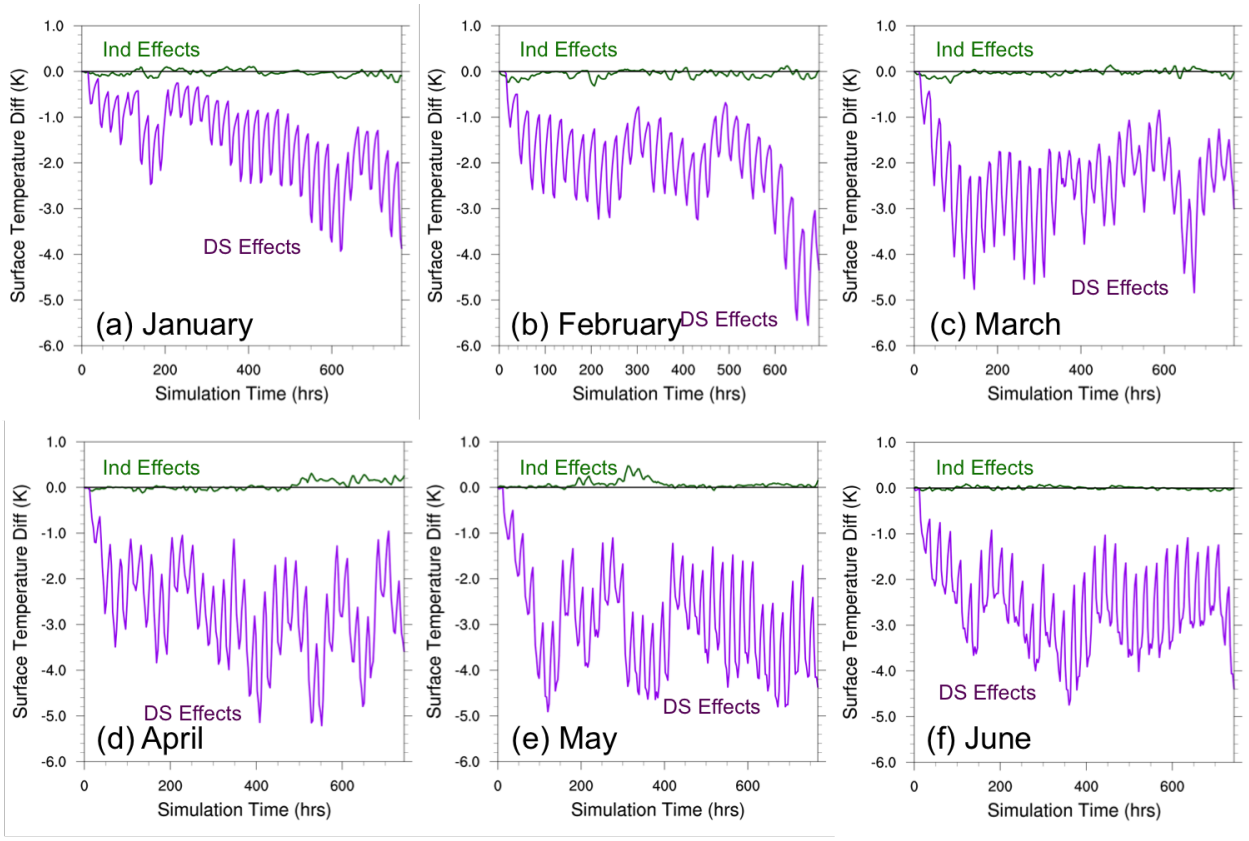

Figure 7.8: Monthly Cases: Domain Averaged Time Series of Black Carbon Effects-Based Surface Temperature (K) for January–June. As in the wintertime and summertime cases, the month-long surface temperature time series due to the direct and semi-direct effects (purple) of black carbon reveals the timing of surface timing strengthening, which well corresponds to the precipitation decrease in Figure 7.7. These times are approximately: (a) January: 648^{th} hour; (b) February: 498^{th} hour; (c) March: 198^{th} hour; (d) April: 501^{st} hour; (e) May: 15^{th} and 561^{st} hours; and (f) June: 15^{th} hour. Although with greater magnitude variation in the month-long simulations, the timing of rapid precipitation decrease is marked by the timing of the strengthening of surface dimming as in the case in the wintertime and summertime cases. In all cases, the indirect effects (green) on precipitation offer a negligible contribution to the variation in surface temperature compared with the contribution from the direct and semi-direct effects (purple) of black carbon.

7.4.1 Convective Precipitation

Convective precipitation, fueled by more daylight hours and incoming solar energy, steadily decreases with black carbon emissions, from January to June (Figure 7.9). Black carbon absorbs the incoming solar radiation and warms the upper levels of the atmosphere. With this warming in the upper levels, there is cooling at the lower levels, which works together to stabilize the atmosphere through the direct and semi-direct effects process, and gives the warming aloft and cooling below temperature profile. Black carbon warms the upper levels and cools the lower throughout this time period (Figure 7.10). The heating aloft and cooling below due to black carbon is also evident in the potential temperature tendency warming from total radiation in the upper levels as shown in Figure 7.11. Temperatures in the lower levels cool as little as 2 K in January and as much as nearly 3.5 K in May. Convective precipitation driven by the indirect effects decreases, but is small in the overall trend.

This decrease in convective precipitation is evident in the cooling of domain-averaged potential temperature tendency from the cumulus scheme in Figure 7.12. Recall that the GF cumulus scheme is triggered by atmospheric instability (Section 2.7.3). With the increased atmospheric stability due to black carbon, the cumulus scheme is triggered less often than without black carbon. This is the case in January and more enhanced in May. We can use the timing of the cooling of the cumulus potential temperature to our advantage: by coupling it with the surface temperature decrease, we are able to time rapid decrease in precipitation.

7.4.2 Non-Convective Precipitation

Like the convective precipitation trend, the non-convective precipitation decreases become more pronounced from January to June (Figure 7.13). The decrease is largely attributed to the direct and semi-direct effect, although not to the extent of the convective precipitation. This is because the Grell-Freitas convective precipitation depends on atmospheric instability as a trigger, whereas the Morrison microphysics parameterization does not have a trigger; rather it is dependent on availability of moisture (Grell and Freitas, 2014; Morrison et al., 2009).

Results show that the direct and semi-direct effects of black carbon reduce specific humidity

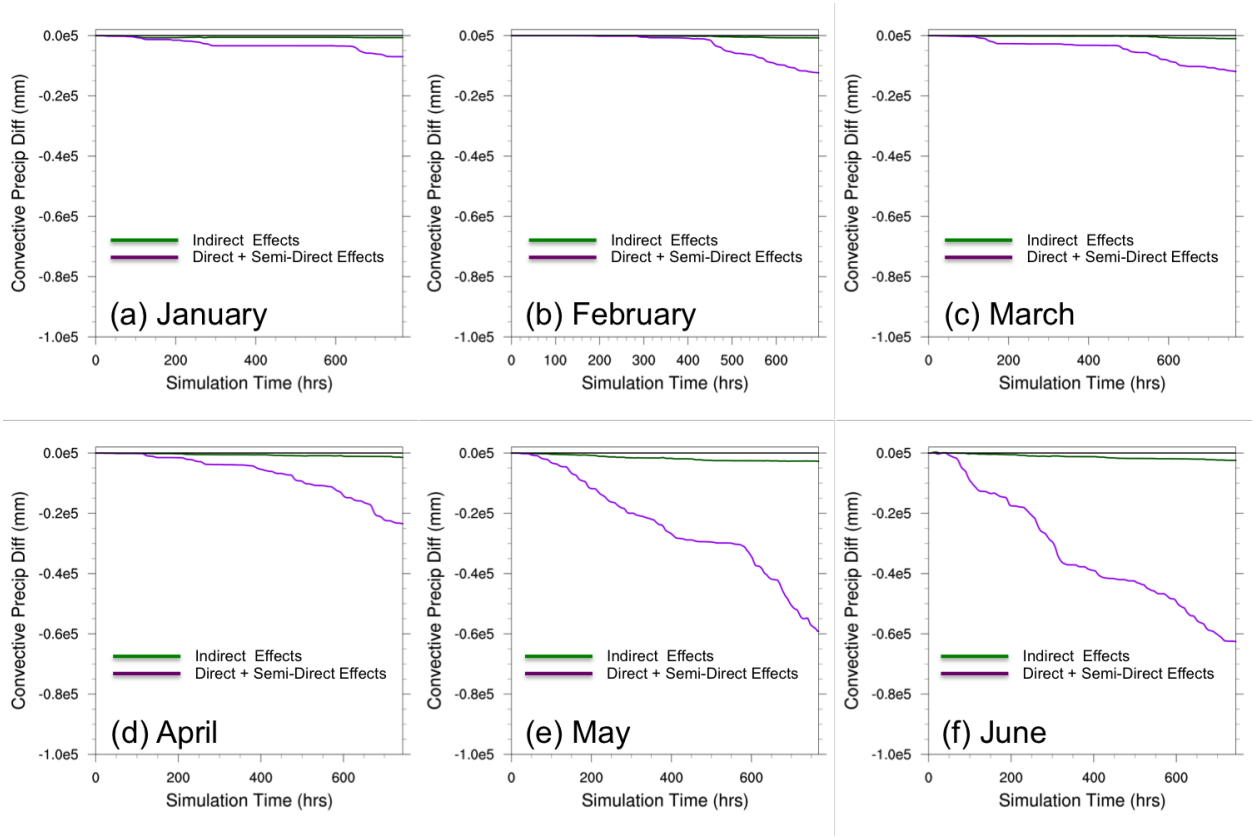

Figure 7.9: Monthly Cases: Domain Averaged Time Series of Black Carbon Effects-Based Convective Precipitation (mm) for January–June. Convective precipitation in the month long simulations from January to June (a–e) show a steady decrease from (a) January through (f) June, much of which comes from the direct and semi-direct effects (purple) of black carbon rather than the indirect effects (green) of black carbon, suggesting the significance of the direct and semi-direct effects of black carbon. The amount of convective precipitation reduction due to the specific black carbon effects is in Table 7.2.

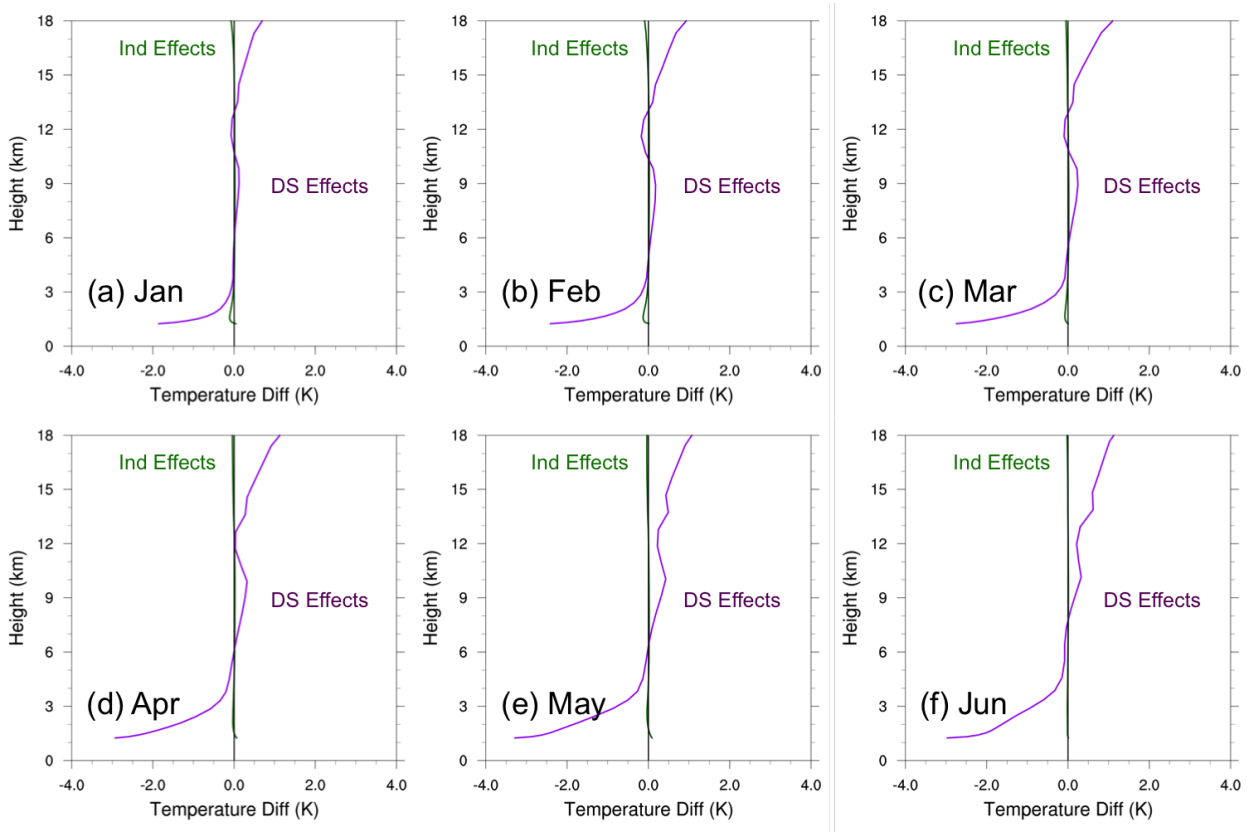

Figure 7.10: Monthly Cases: Domain Averaged Vertical Profile of Black Carbon Effects-Based Temperature (K) for January–June. The domain averaged vertical temperature profiles for (a) January through (f) June show the increasing amount of warming in the upper levels and the strengthening of surface dimming in the lower levels from January to June, due to the direct and semi-direct effects (purple) of black carbon. Temperatures in the lower levels cool as little as 2 K in January and as much as nearly 3.5 K in May. This is the change that the vertical temperature contributes to a stabilizing domain. The indirect effects (green) of black carbon contribute an insignificant amount of change to the overall vertical temperature profile.

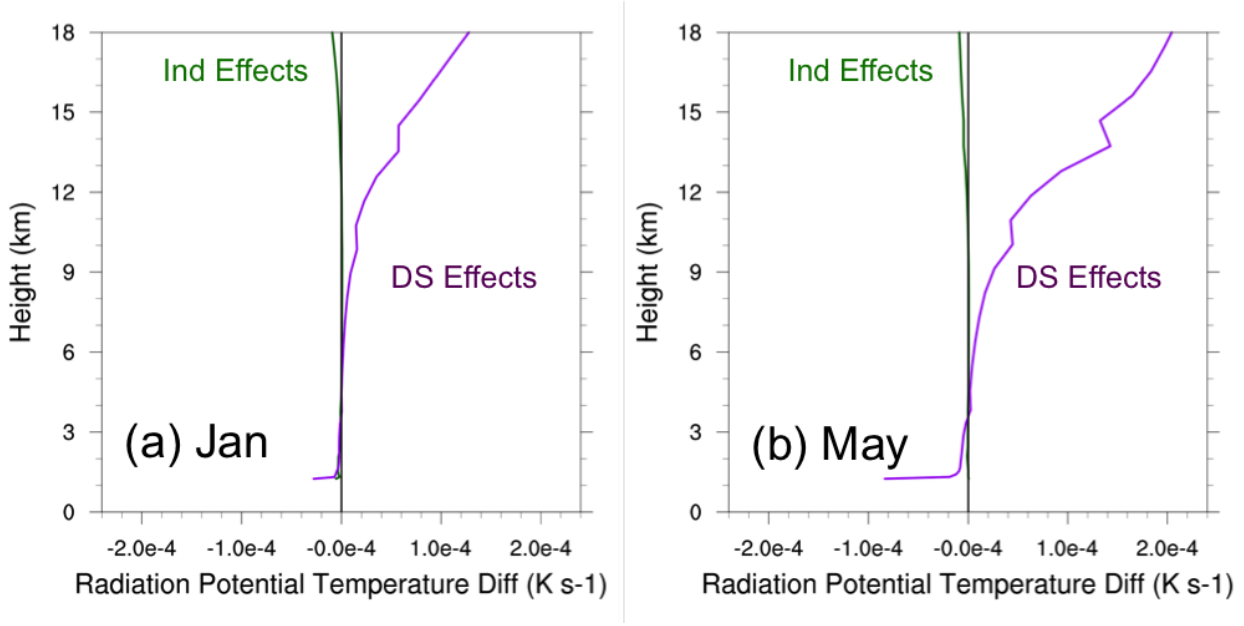

Figure 7.11: Monthly Cases: Domain Averaged Vertical Profile of Black Carbon Effects-Based Radiation Potential Temperature Tendency (K/s^{-1}) for January and May. The domain averaged vertical potential temperature tendency profiles from the radiation scheme for (a) January and (b) May show increased warming of the upper levels and cooling near the surface. This warming is attributed an increase in incoming solar radiation from longer hours as well as reduced obstruction from decreased condensate (Figure 7.5) to allow incoming solar radiation to reach the black carbon lofted and vertically mixed into the atmosphere. The enhanced stability of the radiation potential temperature tendency is due to the direct and semi-direct effects (purple) rather than the indirect effects (green) of black carbon. The increases aloft are nearly twofold and decreases at the surface are nearly threefold from January to May.

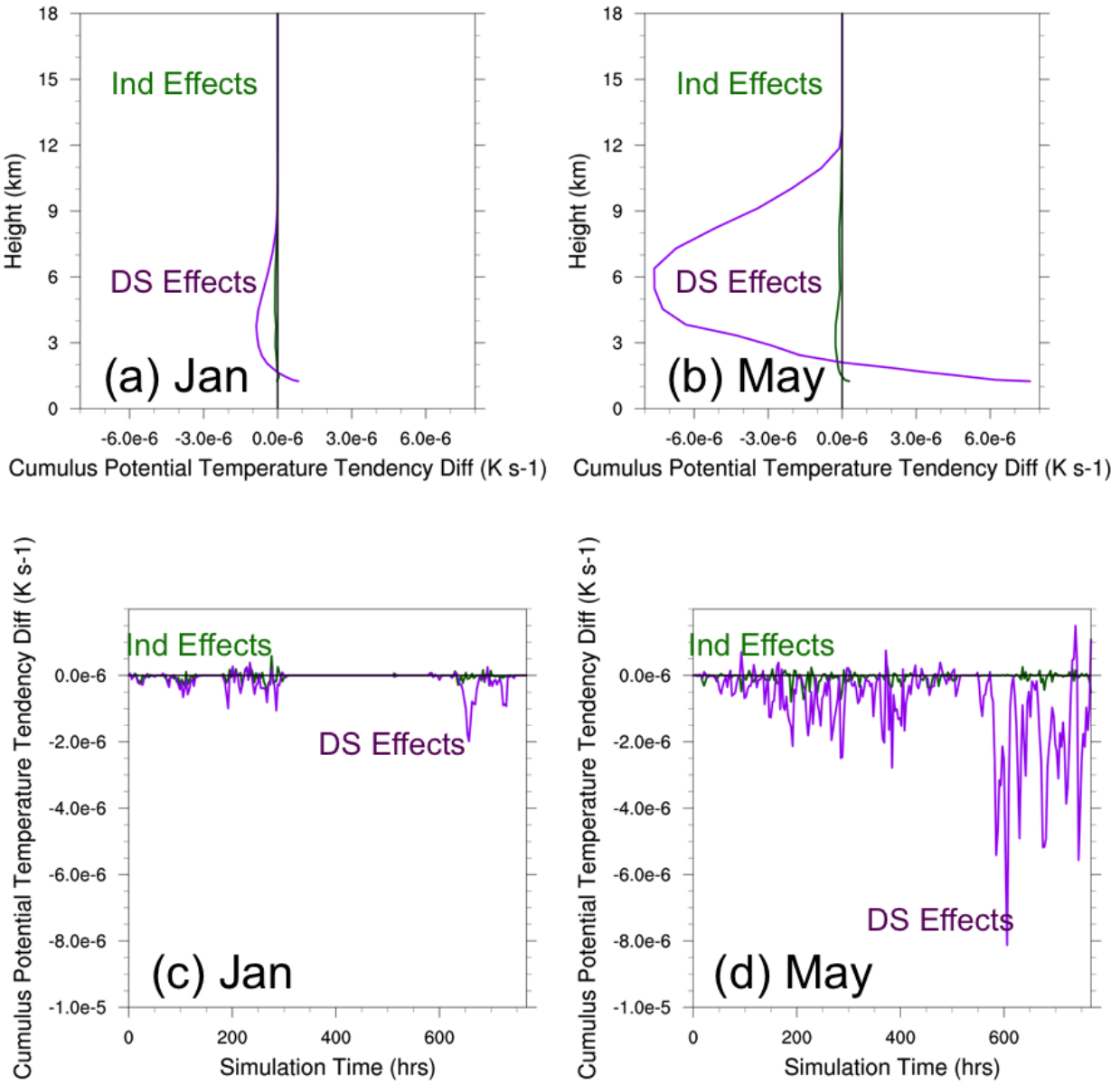

Figure 7.12: Monthly Cases: Domain Averaged Vertical Profile and Time Series of Black Carbon Effects-Based Cumulus Potential Temperature Tendency (K/s^{-1}) for January and May. The domain averaged vertical potential temperature tendency profiles from the cumulus scheme for (a) January and (b) May show a cooling due to the direct and semi-direct effects (purple) of black carbon in both months, with an enhanced cooling in May compared with June. The cooling is greater from the direct and semi-direct effects (purple) compared with the indirect effects (green), and more pronounced in May than in January. There is slight cooling in the cumulus potential temperature tendency from the indirect effects (green) of black carbon. Moreover, as previously mentioned in Section 7.3 and in Figure 7.8, the rapid decline in convective precipitation corresponds closely to the decrease in surface temperature. Similarly, a rapid reduction in convective precipitation can also be identified in the rapid drop to the cumulus potential temperature tendency time series, as atmospheric stability directly ties into the triggering of the convective scheme. (c) This time series of potential temperature tendency from the cumulus parameterization for January and for (d) May. The cooling in this time series matches well with the rapid decrease in convective precipitation. In January, the 648^{th} hour has both a relatively large cooling in cumulus potential temperature tendency which corresponds to the drop in precipitation in Figure 7.9a, and in May at the 15^{th} and 561^{st} hours in Figure 7.9e.

in the lower levels thereby reducing the relative humidity needed for precipitation (Figure 7.15). This is the case for January and more pronounced in May with specific humidity reduction nearly twice as much in May than in January, and relative humidity reduction over four times greater in May than in January. The specific heat decrease could mean the transfer of water vapor to condensate (ice, cloud, rain, snow, graupel mixing ratios), however, we find that this is not case. Each of the hydrometeor types shows a decrease due to the direct and semi-direct effects of black carbon. This suggests that the decrease of specific humidity stems from the surface, meaning the reduction of specific humidity is a result of reduced evaporation. According to (Jensen, 2010), evaporation requires energy, the source of which is mainly from incoming solar radiation. With black carbon absorbing the incoming solar radiation aloft, and reducing it at the lower levels, there is a decreased amount of energy available for evaporation of moisture from the surface. Additionally, with black carbon, there is one order of magnitude of precipitation less in May than in January (Table 7.1,) which could contribute to the reduced evaporation as well.

With a decrease in specific humidity and in relative humidity, it makes sense that there is a cooling of the potential temperature tendency from the microphysics scheme. It cools nearly four times as much in May than in June and extends from 2 km to 9 km in height (Figure 7.14).

Further capping precipitation is the vertical velocity, which is increasingly downward in the lower levels (Figure 7.16), where increased upward vertical velocity would need to be for precipitation (Houze Jr, 1994). Although not conducive to precipitation generation, black carbon's direct and semi-direct effects cause an increased upward vertical velocity, which helps to loft black carbon higher into the atmosphere, further increasing the stability of the atmosphere, and perpetuating a positive feedback cycle for black carbon's direct and semi-direct effects on the atmosphere.

7.5 Discussion

The precipitation behavior due to black carbon inclusion from January to June reaffirms the significant role of the direct and semi-direct effects of black carbon has on stabilizing the atmosphere. Black carbon, whether lofted there by wind and turbulence or lofted there artificially, heats the atmospheric column in the midlevels of the atmosphere, reduces the amount of shortwave radiation able to reach the surface, and causes surfacing cooling (dimming). This stabilization

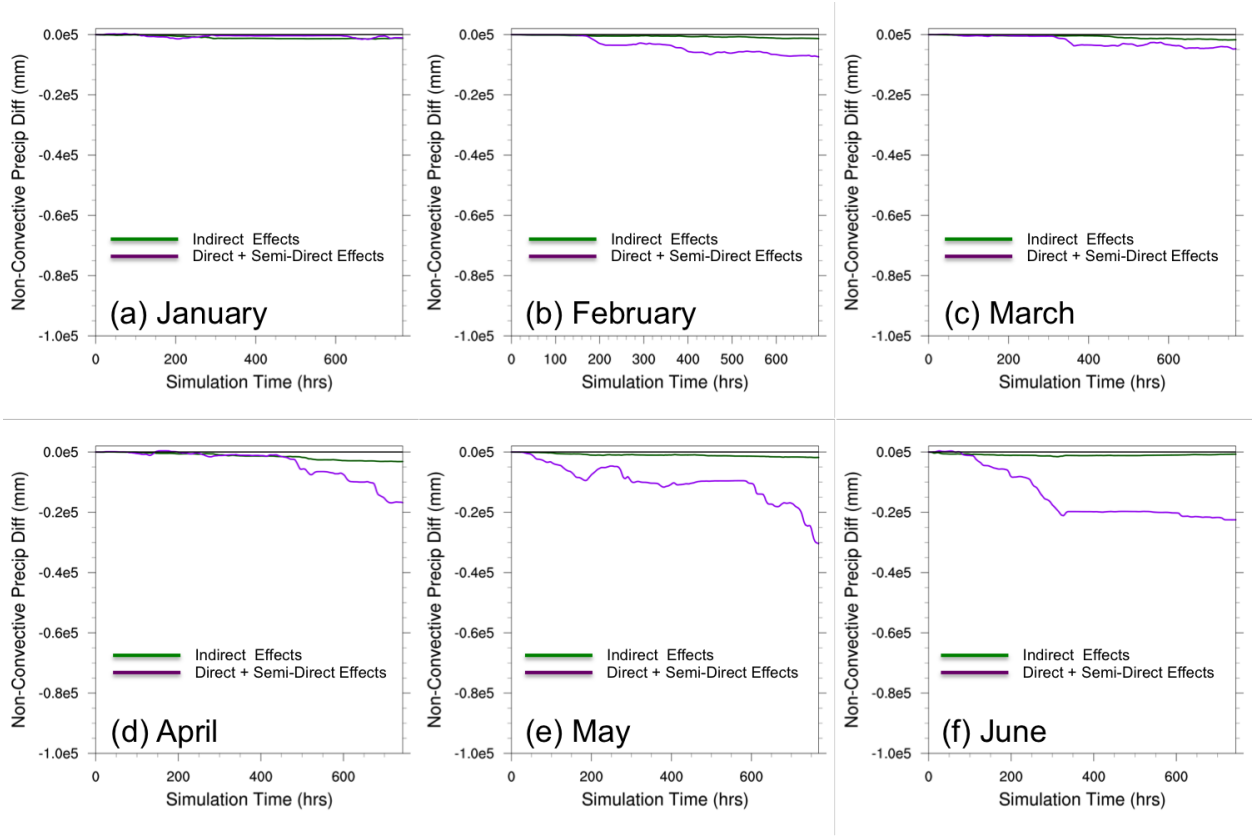

Figure 7.13: Monthly Cases: Domain Averaged Time Series of Black Carbon Effects-Based Non-Convective Precipitation (mm) for January–June. Non-convective precipitation in the month long simulations from January to June (a–e) shows a steady decrease from (a) January through (f) June, much of which comes from the direct and semi-direct effects (purple) of black carbon. The indirect effects (green) of black carbon generate minimal precipitation changes—reductions—from January to June. The ratio of non-convective precipitation decrease compared with convective precipitation decrease is listed in Table 7.2. The non-convective precipitation decrease is not to the extent (up to 72% in April) to that of convective precipitation reduction, as non-convective precipitation does not depend on a trigger mechanism, as the convective scheme requires.

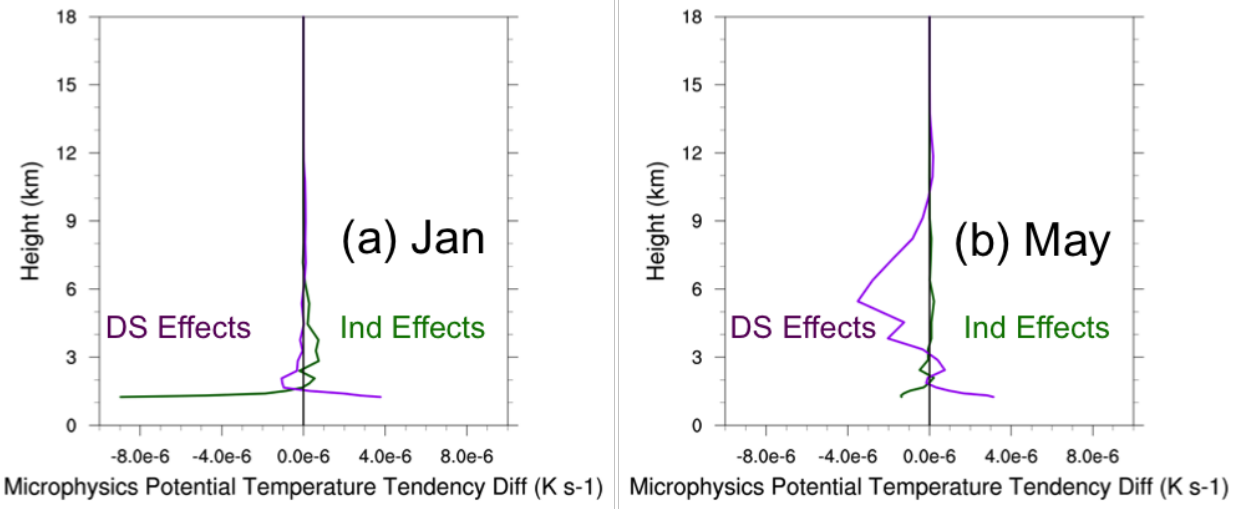

Figure 7.14: Monthly Cases: Domain Averaged Vertical Profile of Black Carbon Effects-Based Microphysics Potential Temperature Tendency (K/s^{-1}) for January and May. The domain averaged vertical potential temperature tendency profiles from the microphysics scheme for (a) January and (b) May are shown here. In January, there is little change to the microphysics potential temperature tendency from both the indirect effects (green) and the direct and semi-direct effects (purple) of black carbon. In May, however, there is substantial cooling in the same parameter from the direct and semi-direct effects (purple) of black carbon, which paves the way for decrease in non-convective precipitation, as shown in Figure 7.13.

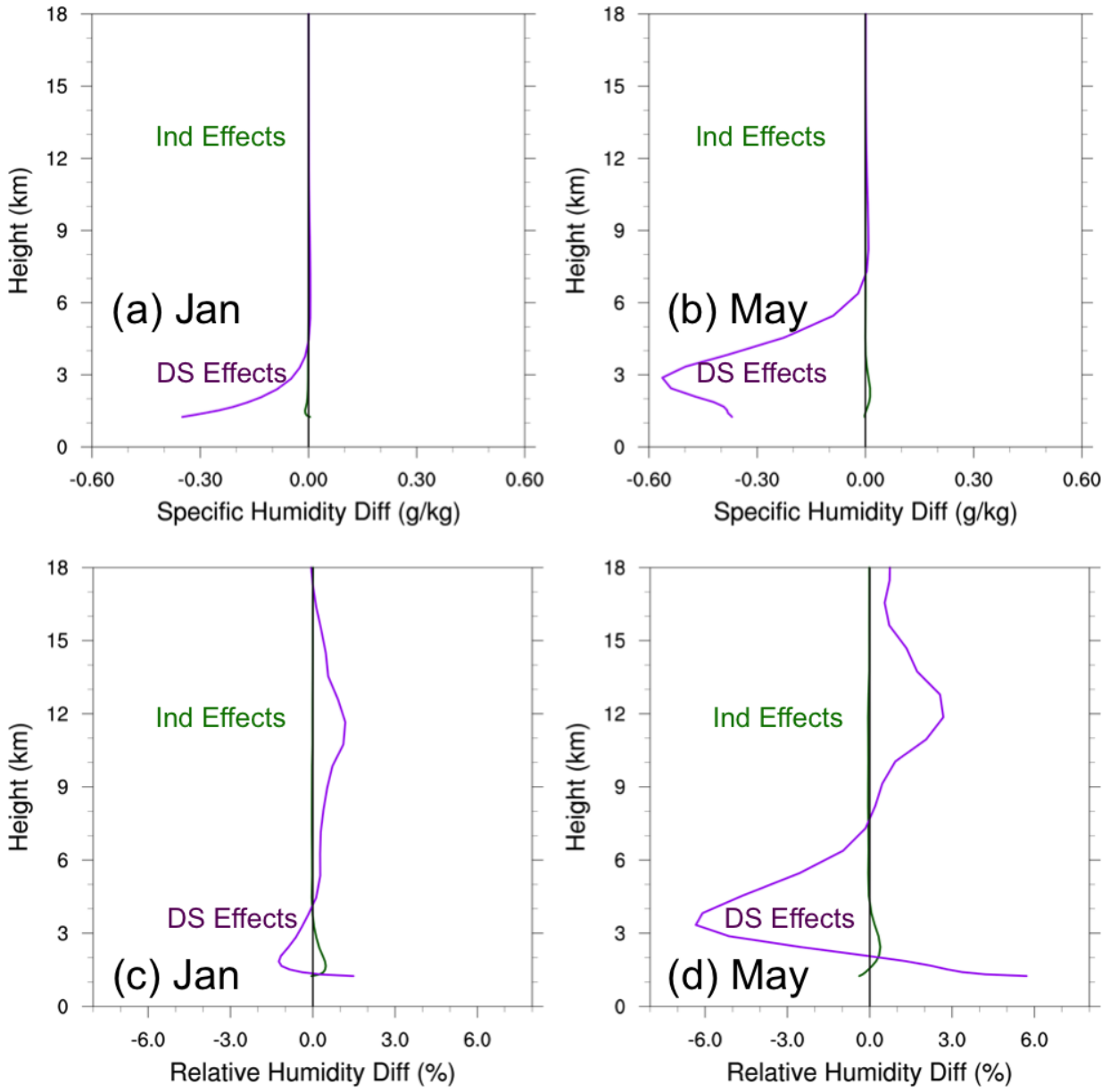

Figure 7.15: Monthly Cases: Domain Averaged Vertical Profile of Black Carbon Effects-Based Specific and Relative Humidity (%) for January and May. (a) The domain averaged specific humidity for (a) January and (b) May are shown here. A decrease in specific humidity means that water vapor can be converted to another hydrometeor, but none of the hydrometeor mixing ratios shows an increase. This suggests that the decrease of specific humidity stems from the surface, meaning the reduction of specific humidity is a result of reduced evaporation, resulting from the cooling near the surface associated with surface dimming from the direct and semi-direct effects (purple) of black carbon. With surface dimming stronger in May than in June (Figures 7.10a and 7.10e). Specific humidity is largely unaffected by the indirect effects (green) of black carbon. The domain averaged relative humidity for (a) January and (b) May are shown here. Overall, the direct and semi-direct effects (purple) of black carbon decrease relative humidity in the lower levels by less than 2% in January and over 6% in May. This decrease in relative humidity is due to decrease in specific humidity, and is enhanced in May compared with January, as it is induced by the direct and semi-direct effects (purple). Relative humidity is largely unaffected by the indirect effects (green) of black carbon. In May, the decrease in relative humidity parallels the cooling of the microphysics potential temperature tendency (Figure 7.14 results in a third of the total precipitation decrease, as shown in Table 7.2.

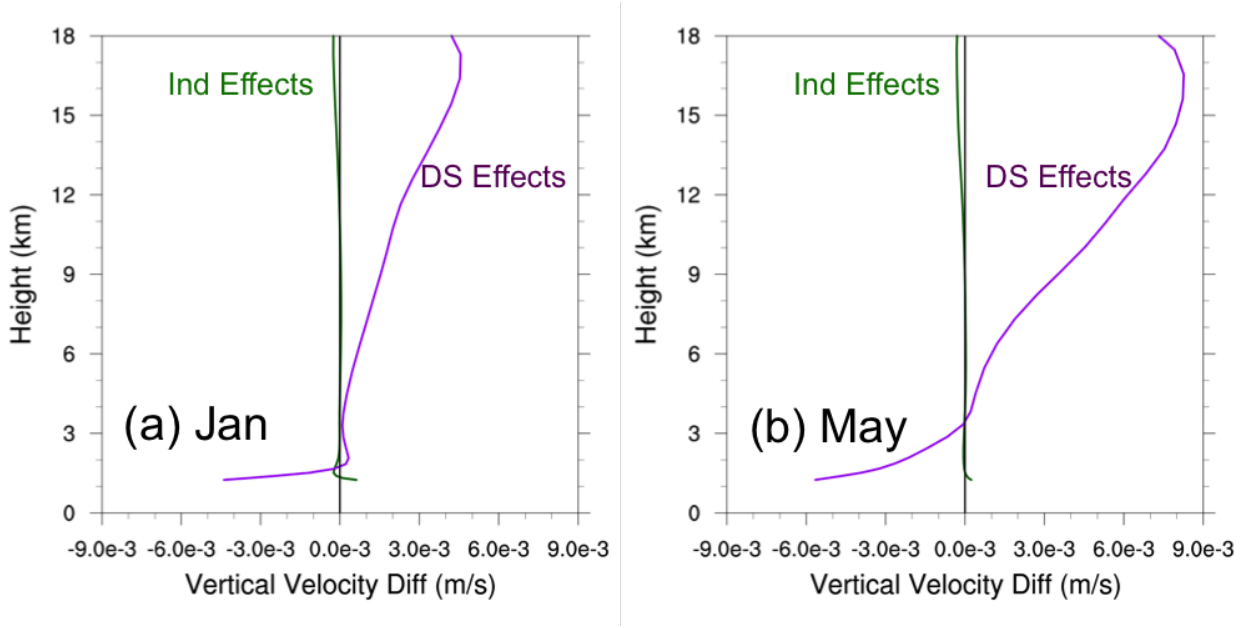

Figure 7.16: Monthly Cases: Domain Averaged Vertical Profile of Black Carbon Effects-Based Vertical Velocity (m/s) for January and May. The domain averaged vertical velocity for (a) January and (b) May are shown here. Both months show a similar pattern, where there is upward vertical motion for much of the atmospheric column and downward vertical motion in the lowest levels due to the direct and semi-direct effects (purple), while the indirect effects (green) of black carbon changes little in vertical velocity. This upward vertical motion is due to the heating aloft, which is conducive to vertical mixing. The increased downward vertical motion is due to the cooling below, which stabilizes the atmosphere, limiting upward vertical motion. The increased downward vertical motion reduces precipitation for both convective and non-convective types.

brings about a reduction in precipitation, particularly convective precipitation.

The six-month experiments also highlight the effect black carbon on non-convective precipitation by its warming aloft and surface dimming. In the case of the 5-day wintertime and summertime rain events, the non-convective precipitation from the indirect effects saw a decrease and an increase in precipitation. The direct and semi-direct effects on non-convective precipitation are second to those of the direct and semi-direct effects from convective precipitation, ranging from 16-72% in ratio. The reduction in non-convective precipitation is due to the decrease in specific relative humidity. The month-long simulations show that these intermittent variations are insignificant, as the month-long trend shows a decrease.

Changes due to the indirect effects are minimal compared with the changes of the direct and semi-direct effects of black carbon. By contrast, the indirect effects change total precipitation by a small amount, as high as 3% in April and as low as 0.85% in January. Another indication that the indirect effects of black carbon are small in this investigation is the effect (or lack thereof) it has on reducing shortwave radiation flux at the surface (SWDOWN). Recall, Twomey et al. (1984) found the indirect effects to cause a higher albedo from the top of the cloud. In comparing the SWDOWN generated by the indirect effects and by the direct and semi-direct effects with the SWDOWN produced by the total effects of black carbon, we find that the direct and semi-direct effects reduces more SWDOWN than the indirect effects Figure 7.17.

However, this may not be the limit of the indirect effects of black carbon. Recall from Section 3.5 that the indirect effects of black carbon are solely generated from the microphysics parameterization, meaning black carbon particles serve as cloud condensation nuclei only in the microphysics scheme and not the cumulus scheme. This means that the cumulus parameterization could potentially create more (and smaller) cloud drops if the cumulus scheme is to ingest cloud droplet number mixing ratio information from the chemistry module. As a consequence, we hypothesize that, coupling the chemistry module with the cumulus scheme, the indirect effects of black carbon would exhibit a larger role in changing the atmosphere, such as increased albedo at the cloud top, strengthened surface dimming, further decrease in evaporation, and consequently, further reduction to precipitation. This would be the case especially because of the large role the direct and semi-direct effects of black carbon have on the cumulus parameterization in its current

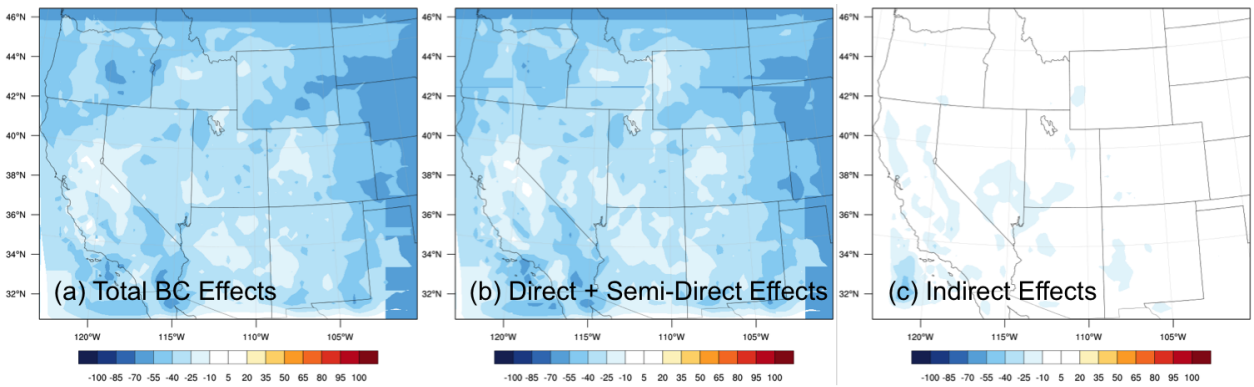

Figure 7.17: Monthly Cases: Month-Long Time Averaged Black Carbon Effects-Based Downward Shortwave Flux at the Surface (W/m^2) for January of (a) total black carbon effects, (b) direct and semi-direct effects, and (c) indirect effects are shown here. The downward shortwave flux at the surface from the total affects of black carbon resemble that of the direct and semi-direct effects, where both exhibit a reduction of shortwave radiation flux at the surface compared with that of the downward shortwave flux from the indirect effects of black carbon. This is counter to Twomey et al. (1984) where the smaller but more plentiful cloud droplets would increase albedo and reflect solar radiation back to the atmosphere, allowing for less shortwave radiation to reach the surface. Although the findings in Twomey et al. (1984) are primarily for the indirect effects, these results suggest that the direct and semi-direct effects of black carbon are stronger than that of the indirect effects of black carbon.

state of assuming a prescribed cloud droplet concentration number.

Chapter 8

Conclusions

8.1 A Summary of Investigation

In order to investigate the direct, semi-direct, and indirect effects of black carbon on precipitation in the western United States, we conducted a three-part study using an atypical black carbon emission data where there is 0.5 μg/kg at every grid point to remove black carbon location dependency and to present to clearest affects of black carbon—horizontal and vertically—in the domain during three periods: 1) a wintertime rain event, 7–11 January 2005; 2) a summertime wet week, 20–24 July 2005; and 3) January to June 2005, each treated as a discrete month. To conduct this investigation, we used WRF-Chem version 3.6.0 with NCEP FNL meteorological data as boundary conditions. The aerosol scheme used is MADE. Physics parameterizations of interest are: FLG for the radiation scheme, Morrison for the microphysics scheme, and GF for the cumulus scheme. The trigger to the GF scheme is instability as determined by the maximum cap strength.

The default FLG parameterization is neither coupled to the chemistry module nor is it coupled to the microphysics scheme. In order to attribute precipitation changes to specific black carbon effect, the total and partial effects of black carbon are needed. As such, we coupled the FLG radiation scheme to both the chemistry module and Morrison microphysics schemes to obtain the total effects of black carbon. We also intentionally uncoupled FLG from the chemistry module while maintaining its coupling to microphysics, and intentionally uncoupled FLG from the microphysics scheme while maintaining its coupling to the chemistry module. Finally, we subtracted the partially coupled schemes from the fully coupled schemes to obtain results for direct and semi-direct effects, and for indirect effects. Although these subtractions indicate that the direct and semi-direct effects,

and the indirect effects of black carbon are linear, they are in fact weakly non-linear.

In the wintertime case, 7–11 January 2005, we find that precipitation decreased by 0.7%, which is within the range of global model studies of black carbon on precipitation. Nevertheless, this reduction in precipitation is mostly due to the direct and semi-direct effects on convective precipitation. In particular, black carbon warms the midlevels of the atmosphere, while cooling the levels below, a phenomenon called surface dimming. We also find that the fastest precipitation decrease matched the timing of the strengthening of the surface temperature decrease, which occurs at approximately the 72-hour point of the 120-hour simulation. We use this event to verify that the coupling and decoupling changes correctly modeled the direct and indirect effects.

In the Summertime Case, 20–24 July 2005, we find a similar precipitation decrease due to the direct and semi-direct effects of black carbon to the wintertime case. In the Summertime Case, however, the precipitation behavior due to the direct and semi-direct effects of black carbon more closely mirrored the precipitation of the total effects of black carbon, at a 40% reduction compared to the wintertime case of 0.7%. Both cases exhibited the same stabilizing trend—warming aloft and cooling below—in the atmosphere, and the pattern of rapid precipitation decrease matching the strengthening of the surface dimming.

Because this case generated a larger difference between simulations with and without black carbon, we also looked at the potential temperature tendencies from the microphysics, radiation, and cumulus schemes. From this examination, we confirm that the surface dimming is from the radiation scheme, and see the effects of a stabilized atmosphere with a cooling in potential temperature tendency from the cumulus scheme.

We also used this case to justify the use of an atypical black carbon emission dataset that essentially mimicked an extremely well-mixed black carbon atmosphere. In comparing NEI black carbon emission data, a uniform black carbon emission at the surface, a uniform black carbon up to 3 km, and a uniform black carbon emission data set, we find a similar pattern in the potential temperature tendencies from the microphysics, radiation, and cumulus schemes, as well as in the temperature profile, where all emissions exhibit a similar pattern of heating aloft and cooling in the lower levels of the atmosphere. Thus the atypical black carbon dataset produces magnified effects without veering from already present trends from the other black carbon emission datasets. As

such, we continued our investigation with a uniform black carbon emission dataset.

Lastly, in the month-long investigation of January to June 2005, we confirm the findings from the wintertime and summertime cases, that black carbon stabilizes the atmospheric column with warming aloft and cooling in the lower levels, that the timing of the strengthening of surface dimming matches that of the most rapid precipitation reduction, and that the majority of the precipitation decrease is from the direct and semi-direct effects. We can also time strong precipitation decreases to the cooling of the potential temperature tendency from the cumulus scheme.

Additionally, the month-long studies reveal the role of the direct and semi-direct effects on non-convective precipitation. Ratios of non-convective precipitation due to direct and semi-directs to convective precipitation of the same effects of black carbon are as high as 72% (April). The smallest ratio is 16% (January). Although the monthly non-convective precipitation reductions due to direct and semi-direct effects are smaller than that of convective precipitation, this finding is striking in that the direct and semi-direct effects that alter microphysics precipitation (non-convective) precipitation via the radiation scheme, when black carbon already has a direct pathway to the microphysics scheme (indirect effect). By contrast, the majority of the precipitation reduction is through the direct and semi-direct effects of black carbon on the convective scheme via the radiation scheme. The reduction in non-convective precipitation is not necessarily due to the strengthened atmospheric stability from black carbon inclusion; its reduction is linked to a decrease in relative humidity and specific humidity in the lower levels with no other reduction of condensate from other hydrometeors. This suggests the reduction of moisture stems from the suppressed evaporation of moisture at the surface due to the surface dimming caused by the black carbon inclusion.

It is in these month-long simulations that we also find a shift in the abilities of the direct and semi-direct effects and the indirect effects to affect change in the atmosphere. In January, there is an increase in the amount of total condensate, largely due to conversion of rain water mixing ratio to cloud water mixing ratio, indicative of the indirect effects. In May, on the other hand, there is a large decrease in condensate. This large decrease in condensate is due to the decrease in snow, rain water, and cloud water mixing ratios, which suggests the semi-direct effect at work.

The overall contribution of the indirect effects is 5-20% of the total precipitation reduction.

We find its role in this investigation to be minimal. However, we reiterate here that the indirect effects in this investigation are only from the microphysics scheme as cloud droplet number concentration is only passed from the chemistry module to Morrison microphysics. In future efforts, we intend to couple the convective parameterization to the chemistry module as well, where we hypothesize that the indirect effects would have a larger contribution to overall atmospheric changes: increased albedo at the cloud top, strengthened surface dimming, further decrease in evaporation, and consequently, further reduction to precipitation, than it does in this investigation.

8.2 The Main Pathway By Which Black Carbon Reduces Precipitation

Figure 8.1 summarizes our conclusions. We have mapped black carbon's effects in two pathways: the direct and semi-direct effects pathway and the indirect effects pathway. The direct and semi-direct effects pathway is the dominant pathway, as it causes the majority of the precipitation changes. The direct and semi-direct of black carbon causes warming aloft and cooling in the lower levels of the atmosphere, creating atmospheric column stability. This strengthened stability reduces the triggering of the convective scheme, reducing convective precipitation, and thereby, contributing to the overall suppression of precipitation. Convective precipitation reduction accounts for approximately 60–75% of the total precipitation reduction. The column stability also can also contribute to the reduction condensate, as it reduces upward vertical motion at the surface. The warming aloft also reduces condensate (semi-direct effect), which, in allowing for black carbon to be subject to incoming solar radiation unhindered, further warms the atmosphere aloft. Cooling in the lower levels reduces the energy needed for evaporation of moisture from the surface, thereby, reducing specific humidity and relative humidity. The reduction in specific humidity and relative humidity lowers the moisture available for non-convective and convective precipitation, reducing non-convective precipitation by approximately 25–40%. The indirect effects also suppress precipitation, by increasing cloud condensate in the form of more, but smaller cloud drops. These smaller cloud drops are less likely to obtain the collision and coalescence efficiencies and fall speeds required to grow into raindrops. The indirect effects also reduce precipitation of 5-20%. The results presented here are similar to that of Shiogama et al. (2010) and Tosca et al. (2010), in that heating aloft reduces evaporation and suppresses convection.

With this research, we ascertain the particular pathways and determine their relative significance by which black carbon affects precipitation for the western United States from an online, coupled meteorology approach. The main *pathway* by which black carbon alters precipitation is increasing atmospheric stability (warming aloft and cooling in the lower levels), which suppresses convective precipitation via the direct and semi-direct effects. Although the actual amount of precipitation reduction varies by meteorology, the smaller reductions, albeit with an atypical black carbon emission dataset, of precipitation changes in the month of January 2005 (4%) and during the heavy precipitation event 7–11 January 2005 (0.7%) are not insignificant. Therefore, with this research, we have also contributed to answering if black carbon has a significant impact in extremely heavy precipitation as prompted in Shiogama et al. (2010).

In this research we find the NEI 2005 emissions did not significantly change precipitation. This is likely due to the aggressive emission regulations that exist for the United States. Emission regulations, however, do not exist or are enforced equally across the globe. In the developing countries that rely on inefficient cook stoves and heating systems, the populations suffer the most due to black carbon emission. Along with respiratory and cardiovascular impacts from black carbon, they may suffer from reduced water resources from suppressed precipitation, as well. In a larger sense, findings from this research serve as a platform for understanding the wider-reaching effects of black carbon on regional precipitation and drought. In particular, in areas where there are no black carbon emission regulations, this would highlight health and potentially significant environmental benefits that could be achieved from a black carbon cap and trade.

8.3 Future Work

Our model captures indirect effects solely from the microphysics parameterization. Future work includes coupling of the cumulus scheme and the chemistry module to capture the total indirect effects. Further research also includes reducing the horizontal resolution such that the simulation only depends on the microphysics parameterization.

Additionally, from the month-long cases, we see that surface dimming helps both to increase the stability of the atmosphere and reduce evaporation near the surface. Further investigation of the surface layer parameterizations is warranted in elucidating the non-convective precipitation

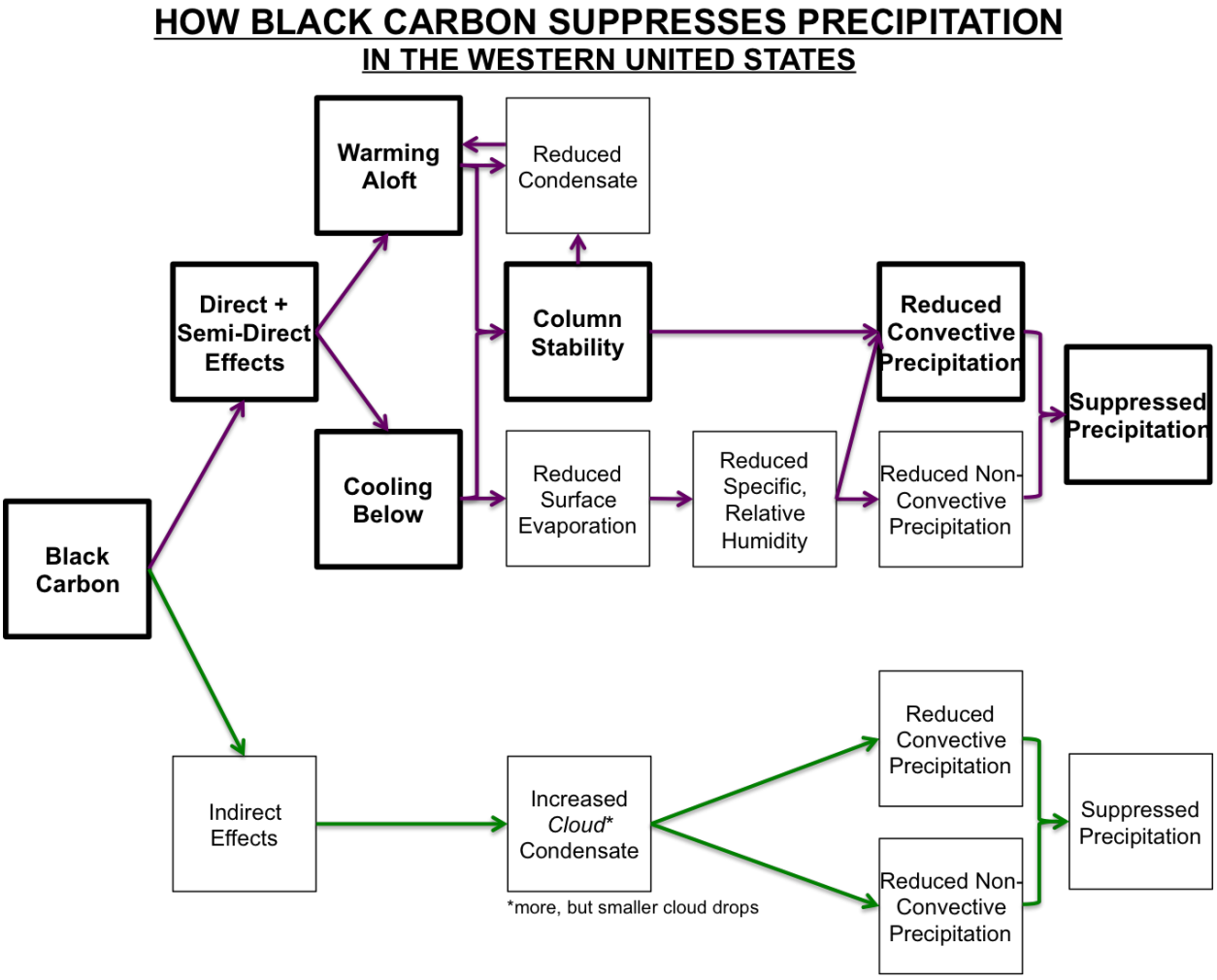

Figure 8.1: Pathways of How Black Carbon Alters Precipitation in the Western United States. Black carbon alters precipitation via two pathways: the direct and semi-direct effects pathway (purple) and the indirect effects pathway (green). The direct and semi-direct effects pathway is the dominant pathway, as it causes the majority of the precipitation changes. The direct and semi-direct of black carbon causes warming aloft and cooling in the lower levels of the atmosphere, creating atmospheric column stability. This strengthened stability reduces the triggering of the convective scheme, reducing convective precipitation, and thereby, contributing to the overall suppression of precipitation. The column stability also can also contribute to the reduction condensate as it reduces upward vertical motion at the surface. The warming aloft also reduces condensate (semi-direct effect), which, in allowing for black carbon to be unhindered to incoming solar radiation, further warms the atmosphere aloft. Cooling in the lower levels reduces the energy needed for evaporation of moisture from the surface, thereby, reducing specific humidity and relative humidity. The reduction in specific humidity and relative humidity lowers the moisture available for non-convective and convective precipitation. The indirect effects also suppress precipitation, which is by increasing cloud condensate in the form of more, but smaller cloud drops. These smaller cloud drops are less likely to obtain the collision and coalescence efficiencies and fall speeds required to grow into raindrops. Highlighted in bold text and boxes is the main pathway by which black carbon reduces precipitation.

change due to black carbon

Moreover, non-linearity, as mentioned in Section 3.6, can also be a limitation, as it could magnify specific black carbon effects. Therefore, further investigation of the black carbon effects on precipitation should include alternate methods in achieving the direct and semi-direct effects, and the indirect effects.

Finally, it would be an added benefit to investigate dry and wet deposition rates of black carbon in heavy and moderate precipitation events, and to relate these rates to black carbon effects-precipitation pathways.

Bibliography

Abdul-Razzak, H., and S. J. Ghan, 2000: A parameterization of aerosol activation: 2. multiple aerosol types. *Journal of Geophysical Research: Atmospheres*, **105 (D5)**, 6837–6844.

Ackerman, A. S., O. B. Toon, D. E. Stevens, A. J. Heymsfield, V. Ramanathan, and E. J. Welton, 2000: Reduction of tropical cloudiness by soot. *Science*, **288 (5468)**, 1042–1047, doi: 10.1126/science.288.5468.1042, URL http://www.sciencemag.org/content/288/5468/1042.abstract.

Ackermann, I. J., H. Hass, M. Memmesheimer, A. Ebel, F. S. Binkowski, and U. Shankar, 1998: Modal aerosol dynamics model for europe: Development and first applications. *Atmospheric Environment*, **32 (17)**, 2981–2999, URL http://www.sciencedirect.com/science/article/pii/S1352231098000065.

Albrecht, B. A., 1989: Aerosols, cloud microphysics, and fractional cloudiness. *Science*, **245 (4923)**, 1227–1230, doi: 10.1126/science.245.4923.1227, URL http://www.sciencemag.org/content/245/4923/1227.abstract.

Andrews, T., P. M. Forster, O. Boucher, N. Bellouin, and A. Jones, 2010: Precipitation, radiative forcing and global temperature change. *Geophysical Research Letters*, **37 (14)**.

Arakawa, A., and W. H. Schubert, 1974: Interaction of a cumulus cloud ensemble with the large-scale environment, part i. *Journal of the Atmospheric Sciences*, **31 (3)**, 674–701.

Baró, R., P. Jiménez-Guerrero, A. Balzarini, G. Curci, R. Forkel, G. Grell, M. Hirtl, L. Honzak, M. Langer, J. L. Pérez, and Coauthors, 2015: Sensitivity analysis of the microphysics scheme in WRF-Chem contributions to AQMEII phase 2. *Atmospheric Environment*, **115**, 620–629.

Bond, T. C., and R. W. Bergstrom, 2006: Light absorption by carbonaceous particles: An investigative review. *Aerosol Science and Technology*, **40 (1)**, 27–67, doi: 10.1080/02786820500421521, URL http://www.tandfonline.com/doi/abs/10.1080/02786820500421521.

Bond, T. C., S. J. Doherty, D. W. Fahey, P. M. Forster, T. Berntsen, B. J. DeAngelo, M. G. Flanner, S. Ghan, B. Kärcher, D. Koch, S. Kinne, Y. Kondo, P. K. Quinn, M. C. Sarofim, M. G. Schultz, M. Schulz, C. Venkataraman, H. Zhang, S. Zhang, N. Bellouin, S. K. Guttikunda, P. K. Hopke, M. Z. Jacobson, J. W. Kaiser, Z. Klimont, U. Lohmann, J. P. Schwarz, D. Shindell, T. Storelvmo, S. G. Warren, and C. S. Zender, 2013: Bounding the role of black carbon in the climate system: A scientific assessment: Black carbon in the climate system. *Journal of Geophysical Research*, **118 (11)**, 5380–5552, doi: 10.1002/jgrd.50171, URL http://doi.wiley.com/10.1002/jgrd.50171.

Brown, J. M., 1979: Mesoscale unsaturated downdrafts driven by rainfall evaporation: A numerical study. *Journal of the Atmospheric Sciences*, **36 (2)**, 313–338.

California Farm Water Coalition, 2014: California Farm Water Coalition. California Farm Water Coalition, URL http://www.farmwater.org, California Farm Water Coalition.

California Nevada River Forecast Center, 2016: Heavy precipitation event southern California January 7-11 2005. Tech. rep., National Oceanic and Atmospheric Administration. URL http://www.cnrfc.noaa.gov/storm_summaries/jan2005storms.php.

Chapman, E. G., W. Gustafson Jr, R. C. Easter, J. C. Barnard, S. J. Ghan, M. S. Pekour, and J. D. Fast, 2009: Coupling aerosol-cloud-radiative processes in the WRF-Chem model: Investigating the radiative impact of elevated point sources. *Atmospheric Chemistry and Physics*, **9 (3)**, 945–964.

Chen, D., Z. Liu, C. Davis, and Y. Gu, 2016: Dust radiative effects on atlantic tropical cyclogenesis using WRF-Chem coupled with and aod data assimilation system. *(in progress)*.

Cotton, W. R., and R. A. Anthes, 1989: *Storm and Cloud Dynamics*. San Diego: Academic, 307–307 pp., doi: 10.1126/science.249.4966.307, URL http://science.sciencemag.org/content/249/4966/307, http://science.sciencemag.org/content/249/4966/307.full.pdf.

Devara, P., and M. Manoj, 2013: Aerosol–cloud–precipitation interactions: A challenging problem in regional environment and climate research. *Particuology*, **11 (1)**, 25–33, doi: 10.1016/j.partic.2012.07.006, URL http://linkinghub.elsevier.com/retrieve/pii/S1674200112002040.

Dyer, A., and B. Hicks, 1970: Flux-gradient relationships in the constant flux layer. *Quarterly Journal of the Royal Meteorological Society*, **96 (410)**, 715–721.

Eastern Research Group, Inc., 2008: Documentation for the 2005 Point Source National Emissions Inventory. Tech. rep., Eastern Research Group, Inc.

Flanner, M. G., C. S. Zender, J. T. Randerson, and P. J. Rasch, 2007: Present-day climate forcing and response from black carbon in snow. *Journal of Geophysical Research*, **112**, doi: 10.1029/2006JD008003, URL http://doi.wiley.com/10.1029/2006JD008003.

Frank, W. M., and C. Cohen, 1985: Properties of tropical cloud ensembles estimated using a cloud model and an observed updraft population. *Journal of the Atmospheric Sciences*, **42 (18)**, 1911–1928.

Fritsch, J., and C. Chappell, 1980: Numerical prediction of convectively driven mesoscale pressure systems. part i: Convective parameterization. *Journal of the Atmospheric Sciences*, **37 (8)**, 1722–1733.

Fu, Q., 1991: Parameterization of radiative processes in vertically nonhomogeneous multiple scattering atmospheres. Ph.D. thesis, Utah University.

Fu, Q., and K. Liou, 1992: On the correlated k-distribution method for radiative transfer in nonhomogeneous atmospheres. *Journal of the Atmospheric Sciences*, **49 (22)**, 2139–2156.

Fu, Q., and K. N. Liou, 1993: Parameterization of the radiative properties of cirrus clouds. *Journal of the Atmospheric Sciences*, **50 (13)**, 2008–2025.

Fu, Q., K. N. Liou, and Y. Gu, 2015: Fu-Liou-Gu radiation parameterization in WRF Version 3.6.0.

Grell, G. A., and D. Dévényi, 2002: A generalized approach to parameterizing convection combining ensemble and data assimilation techniques. *Geophysical Research Letters*, **29 (14)**.

Grell, G. A., and S. R. Freitas, 2014: A scale and aerosol aware stochastic convective parameterization for weather and air quality modeling. *Atmospheric Chemistry and Physics*, **14 (10)**, 5233–5250, doi: 10.5194/acp-14-5233-2014, URL http://www.atmos-chem-phys.net/14/5233/2014/.

Grell, G. A., S. E. Peckham, R. Schmitz, S. A. McKeen, G. Frost, W. C. Skamarock, and B. Eder, 2005: Fully coupled "online" chemistry within the WRF model. *Atmospheric Environment*, **39 (37)**, 6957–6975, doi: 10.1016/j.atmosenv.2005.04.027, URL http://linkinghub.elsevier.com/retrieve/pii/S1352231005003560.

Griffin, D., and K. J. Anchukaitis, 2014: How unusual is the 2012–2014 California drought? *Geophysical Research Letters*, **41 (24)**, 9017–9023, doi: 10.1002/2014GL062433, URL http://dx.doi.org/10.1002/2014GL062433, 2014GL062433.

Gu, Y., K. Liou, W. Chen, and H. Liao, 2010: Direct climate effect of black carbon in China and its impact on dust storms. *Journal of Geophysical Research: Atmospheres*, **115 (D7)**.

Gu, Y., K. Liou, S. Ou, and R. Fovell, 2011: Cirrus cloud simulations using WRF with improved radiation parameterization and increased vertical resolution. *Journal of Geophysical Research: Atmospheres*, **116 (D6)**.

Gu, Y., K. N. Liou, W.-L. Lee, and L. R. Leung, 2012: Simulating 3-d radiative transfer effects over the Sierra Nevada Mountains using WRF. *Atmospheric Chemistry and Physics*, **12 (20)**, 9965–9976, doi: 10.5194/acp-12-9965-2012, URL http://www.atmos-chem-phys.net/12/9965/2012/.

Haby, J., 2016a: Dynamic precip vs convective precip, URL http://www.theweatherprediction.com/habyhints/336/.

Haby, J., 2016b: Skew-T: A look at cap, URL http://www.theweatherprediction.com/habyhints/336/.

Haby, J., 2016c: The thermal low, URL http://www.theweatherprediction.com/habyhints2/367/.

Hong, S.-Y., and J.-O. J. Lim, 2006: The WRF single-moment 6-class microphysics scheme (wsm6). *J. Korean Meteor. Soc*, **42 (2)**, 129–151.

Hong, S.-Y., Y. Noh, and J. Dudhia, 2006: A new vertical diffusion package with an explicit treatment of entrainment processes. *Monthly Weather Review*, **134 (9)**, 2318–2341.

Houze Jr, R. A., 1994: *Cloud dynamics*, Vol. 104. Academic press.

Jacobson, M. Z., 2001: Strong radiative heating due to the mixing state of black carbon in atmospheric aerosols. *Nature*, **409 (6821)**, 695–697, doi: 10.1038/35055518, URL http://dx.doi.org/10.1038/35055518.

Jensen, M. E., 2010: Estimating evaporation from water surfaces. *Evapotranspiration Workshop*, Colorado State University, URL http://ccc.atmos.colostate.edu/ET_Workshop/pdf/11_Jenson.pdf.

Kain, J. S., and J. M. Fritsch, 1993: Convective parameterization for mesoscale models: The kain-fritsch scheme. *The representation of cumulus convection in numerical models*, Springer, 165–170.

Kandler, K., N. Benker, U. Bundke, E. Cuevas, M. Ebert, P. Knippertz, S. Rodríguez, L. Schütz, and S. Weinbruch, 2007: Chemical composition and complex refractive index of Saharan mineral dust at Izaña, Tenerife (Spain) derived by electron microscopy. *Atmospheric Environment*, **41 (37)**, 8058–8074, doi: 10.1016/j.atmosenv.2007.06.047, URL http://linkinghub.elsevier.com/retrieve/pii/S1352231007006061.

Kazil, J., 2014: Aerosol modeling with WRF/chem, URL http://ruc.noaa.gov/wrf/WG11/wrf_tutorial_2014/WRF_CHEM_aerosols.pdf, WRF-Chem Tutorial Summer 2014.

Krishnamurti, T., Y. Ramanathan, H.-L. Pan, R. J. Pasch, and J. Molinari, 1980: Cumulus parameterization and rainfall rates i. *Monthly Weather Review*, **108 (4)**, 465–472.

Kuhns, H., and J. M. Vukovich, 2003: The emissions inventories and SMOKE modeling efforts used to support the BRAVO study. *12th Annual US EPA International Emissions Inventory Conference*, URL http://www.researchgate.net/profile/Hampden_Kuhns/publication/228718673_The_Emission_Inventories_and_SMOKE_Modeling_Efforts_Used_to_Support_the_BRAVO_Study/links/02e7e51a696210a367000000.pdf.

Lagzi, I., R. Meszaros, G. Gelybo, and A. Leelossy, 2013: *Atmospheric Chemistry*. Eotvos Lorand University, URL http://elte.prompt.hu/sites/default/files/tananyagok/atmospheric/index.html.

Lauer, S., 2011: Sierra Nevada water facts. URL www.watereducation.org.

Lee, W.-L., K. N. Liou, and A. Hall, 2011: Parameterization of solar fluxes over mountain surfaces for application to climate models. *Journal of Geophysical Research*, **116**, doi: 10.1029/2010JD014722, URL http://doi.wiley.com/10.1029/2010JD014722.

Lin, R.-G. I., 2015: 63 trillion gallons of groundwater lost in drought, study finds. *Los Angeles Times*, URL http://www.latimes.com/local/lanow/la-me-ln-63-trillion-gallons-of-groundwater-lost-in-drought-study-finds-20140821-story.html.

Lin, Y.-L., R. D. Farley, and H. D. Orville, 1983: Bulk parameterization of the snow field in a cloud model. *Journal of Climate and Applied Meteorology*, **22 (6)**, 1065–1092.

Liou, K.-N., Q. Fu, and T. P. Ackerman, 1988: A simple formulation of the delta-four-stream approximation for radiative transfer parameterizations. *Journal of the atmospheric sciences*, **45 (13)**, 1940–1948.

Liou, K. N., Y. Gu, L. R. Leung, W. L. Lee, and R. G. Fovell, 2013: A WRF simulation of the impact of 3-d radiative transfer on surface hydrology over the Rocky Mountains and Sierra Nevada. *Atmospheric Chemistry and Physics*, **13 (23)**, 11 709–11 721, doi: 10.5194/acp-13-11709-2013, URL http://www.atmos-chem-phys.net/13/11709/2013/.

Liou, K.-N., and S.-C. Ou, 1989: The role of cloud microphysical processes in climate: An assessment from a one-dimensional perspective. *Journal of Geophysical Research: Atmospheres (1984–2012)*, **94**, 8599–8607, URL http://onlinelibrary.wiley.com/doi/10.1029/JD094iD06p08599/full.

Liu, P., Y. Zhang, and S. T. Martin, 2013: Complex refractive indices of thin films of secondary organic materials by spectroscopic ellipsometry from 220 to 1200 nm. *Environmental Science & Technology*, **47 (23)**, 13 594–13 601, doi: 10.1021/es403411e, URL http://pubs.acs.org/doi/abs/10.1021/es403411e.

Liu, X., and J. E. Penner, 2005: Ice nucleation parameterization for global models. *Meteorologische Zeitschrift*, **14 (4)**, 499–514.

Lohmann, U., and J. Feichter, 2001: Can the direct and semi-direct aerosol effect compete with the indirect effect on a global scale? *Geophysical Research Letters*, **28 (1)**, 159–161, doi: 10.1029/2000GL012051, URL http://dx.doi.org/10.1029/2000GL012051.

Medrano, M., 2008: Impact of cloud microphysics on the development of trailing stratiform precipitation in a simulated squall line: Comparison of one-and two-moment schemes, Morrison H., Thompson G., Tatarskii, V., URL https://www.rsmas.miami.edu/users/mulate-medrano/docs/spring2009/MPO-531/Morrison-etal-2008.pdf, Physical Meteorology MPO 531, University of Miami.

Ming, Y., V. Ramaswamy, and G. Persad, 2010: Two opposing effects of absorbing aerosols on global-mean precipitation: Effects of absorbing aerosols on precipitation. *Geophysical Research Letters*, **37 (13)**, n/a–n/a, doi: 10.1029/2010GL042895, URL http://doi.wiley.com/10.1029/2010GL042895.

Morrison, H., 2010: An overview of cloud and precipitation microphysics and its parameterization in models, WRF Workshop.

Morrison, H., 2014: Morrison microphysics two moment parameterization WRF Version 3.6 Code. Tech. rep., National Center for Atmospheric Research (MMM-NCAR).

Morrison, H., G. Thompson, and V. Tatarskii, 2009: Impact of cloud microphysics on the development of trailing stratiform precipitation in a simulated squall line: Comparison of one-and two-moment schemes. *Monthly Weather Review*, **137 (3)**, 991–1007.

National Centers for Environmental Prediction, National Weather Service, NOAA, U.S. Department of Commerce, 2000: NCEP FNL Operational Model Global Tropospheric Analyses, continuing from July 1999. Research Data Archive at the National Center for Atmospheric Research, Computational and Information Systems Laboratory, Boulder CO, URL http://dx.doi.org/10.5065/D6M043C6.

National Geodetic Survey, 1995: Whitney. Tech. rep., National Geodetic Survey. URL http://www.ngs.noaa.gov/cgi-bin/ds_mark.prl?PidBox=GT1811.

NOAA National Centers for Environmental Information, 2016: NOAA National Operational Model Archive and Distribution System. URL http://nomads.ncdc.noaa.gov, Department of Commerce.

Paulson, C. A., 1970: The mathematical representation of wind speed and temperature profiles in the unstable atmospheric surface layer. *Journal of Applied Meteorology*, **9 (6)**, 857–861.

Peckham, S., 2012: Anthropogenic emissions, URL http://ruc.noaa.gov/wrf/WG11/anthropogenic.htm, weather Research and Forecasting (WRF) Model Working Group 11: Atmospheric Chemistry.

Peckham, S. E., G. A. Grell, S. A. McKeen, M. Barth, G. Pfister, C. Wiedinmyer, J. D. Fast, W. I. Gustafson, S. J. Ghan, R. Zaveri, and Coauthors, 2014: *WRF/Chem Version 3.6 User's Guide*. US Department of Commerce, National Oceanic and Atmospheric Administration, Oceanic and Atmospheric Research Laboratories, Global Systems Division.

Pendergrass, A. G., and D. L. Hartmann, 2012: Global-mean precipitation and black carbon in AR4 simulations: Black carbon and precipitation in a1b. *Geophysical Research Letters*, **39 (1)**, n/a–n/a, doi: 10.1029/2011GL050067, URL http://doi.wiley.com/10.1029/2011GL050067.

Peralta, R. J., C. Nardell, B. Cairns, E. E. Russell, L. D. Travis, M. I. Mishchenko, B. A. Fafaul, and R. J. Hooker, 2007: Aerosol polarimetry sensor for the glory mission. *International Symposium on Multispectral Image Processing and Pattern Recognition*, International Society for Optics and Photonics, 67 865L–67 865L.

Petters, M., and S. Kreidenweis, 2007: A single parameter representation of hygroscopic growth and cloud condensation nucleus activity. *Atmospheric Chemistry and Physics*, **7 (8)**, 1961–1971.

Ramanathan, V., and G. Carmichael, 2008: Global and regional climate changes due to black carbon. *Nature Geosci*, **1 (4)**, 221–227, doi: 10.1038/ngeo156, URL http://dx.doi.org/10.1038/ngeo156.

Roberts, D. L., 2004: Climate sensitivity to black carbon aerosol from fossil fuel combustion. *Journal of Geophysical Research*, **109**, doi: 10.1029/2004JD004676, URL http://doi.wiley.com/10.1029/2004JD004676.

Rotstayn, L. D., W. Cai, M. R. Dix, G. D. Farquhar, Y. Feng, P. Ginoux, M. Herzog, A. Ito, J. E. Penner, M. L. Roderick, and M. Wang, 2007: Have Australian rainfall and cloudiness increased due to the remote effects of asian anthropogenic aerosols? *Journal of Geophysical Research*, **112**, doi: 10.1029/2006JD007712, URL http://doi.wiley.com/10.1029/2006JD007712.

Samset, B., G. Myhre, M. Schulz, Y. Balkanski, S. Bauer, T. Berntsen, H. Bian, N. Bellouin, T. Diehl, R. C. Easter, and Coauthors, 2013: Black carbon vertical profiles strongly affect its radiative forcing uncertainty. *Atmospheric Chemistry and Physics*, **13 (5)**, 2423.

Sasser, E., 2011: *Report to Congress on Black Carbon*. US Environmental Protection Agency, Office of Air Quality Planning and Standards.

Shiogama, H., S. Emori, K. Takahashi, T. Nagashima, T. Ogura, T. Nozawa, and T. Takemura, 2010: Emission scenario dependency of precipitation on global warming in the MIROC3.2 model. *Journal of Climate*, **23 (9)**, 2404–2417, doi: 10.1175/2009JCLI3428.1, URL http://journals.ametsoc.org/doi/abs/10.1175/2009JCLI3428.1.

Skamarock, W., J. Klemp, J. Dudhia, D. Gill, D. Barker, M. Duda, X. Huang, W. Wang, and J. Powers, 2008: A description of the Advanced Research WRF Version 3, NCAR technical note, Mesoscale and Microscale Meteorology Division. Tech. rep., NCAR/TN-475+ STR.

Stensrud, D. J., 2009: *Parameterization schemes: keys to understanding numerical weather prediction models*. Cambridge University Press.

Tosca, M., J. Randerson, C. Zender, M. Flanner, and P. J. Rasch, 2010: Do biomass burning aerosols intensify drought in equatorial Asia during El Niño? *Atmospheric Chemistry and Physics*, **10 (8)**, 3515–3528.

Tseng, H.-L., K. N. Liou, Y. Gu, L. Wu, and R. Fovell, 2014: Investigation of black carbon effects on precipitation over the western united states using the new chemistry-coupled FLG radiation scheme in WRF-Chem, American Geophysical Union Fall Meeting 2015.

Twomey, S. A., M. Piepgrass, and T. Wolfe, 1984: An assessment of the impact of pollution on global cloud albedo. *Tellus B*, **36 (5)**, 356–366.

UNISYS Weather, 2016: UNISYS image and map archive. URL http://weather.unisys.com/archive/, UNISYS Weather.

United States Naval Observatory, 2016: Duration of daylight for 2005. URL http://aa.usno.navy.mil/cgi-bin/aa_durtablew.pl?form=1&year=2005&task=-1&state=CA&place=los+angeles.

Wang, C., D. Kim, A. M. L. Ekman, M. C. Barth, and P. J. Rasch, 2009: Impact of anthropogenic aerosols on Indian summer monsoon. *Geophysical Research Letters*, **36 (21)**, doi: 10.1029/2009GL040114, URL http://doi.wiley.com/10.1029/2009GL040114.

Wang, W., C. Bruyere, M. Duda, M. Duda, D. Gill, M. Kavulich, K. Keene, H.-C. Lin, J. Michalakes, S. Rizvi, and X. Zhang, 2014: User's Guide for Advanced Research WRF (ARW) Modeling System Version 3. *Mesoscale and Microscale Meteorology Division–National Center for Atmospheric Research (MMM-NCAR)*.

Wesely, M., 1989: Parameterization of surface resistances to gaseous dry deposition in regional-scale numerical models. *Atmospheric Environment (1967)*, **23 (6)**, 1293–1304.

Zaveri, R. A., R. C. Easter, J. D. Fast, and L. K. Peters, 2008: Model for simulating aerosol interactions and chemistry (MOSAIC). *Journal of Geophysical Research: Atmospheres*, **113 (D13)**.